

1 **A new species of longirostrine plioplatecarpine mosasaur (Squamata: Mosasauridae)**
2 **from the Late Cretaceous of Morocco, with a re-evaluation of the problematic taxon**
3 ***'Platecarpus' ptychodon***

4 Catherine R. C. Strong^{a*}, Michael W. Caldwell^{a,b}, Takuya Konishi^c, and Alessandro Palci^{d,e}

5 ^a*Department of Biological Sciences, University of Alberta, Edmonton, Canada, T6G 2E9;*

6 ^b*Department of Earth and Atmospheric Sciences, University of Alberta, Edmonton, Canada,*

7 *T6G 2E9; ^cDepartment of Biological Sciences, University of Cincinnati, Cincinnati, U.S.A.,*

8 *45221-0006; ^dEarth Sciences Section, South Australian Museum, Adelaide, Australia, 5000;*

9 ^e*College of Science and Engineering, Flinders University, Adelaide, Australia, 5042*

10 * Corresponding author. Email: crstrong@ualberta.ca

11

12

13

14

15

16

17

18

19

20

21

1 **Abstract**

2

3 The Upper Cretaceous phosphates of Morocco preserve one of the world's most
4 diverse assemblages of mosasaurs, reflecting the adaptive radiation of this clade during the
5 Maastrichtian Stage. We herein describe a new mosasaur from these deposits. Although the
6 teeth of this specimen resemble those of '*Platecarpus*' *ptychodon*, suggesting referral to this
7 species, we re-examine and ultimately reject the fundamental validity of '*P.*' *ptychodon* due
8 to the non-diagnostic nature of its holotype and original diagnosis. We instead designate the
9 new specimen as the holotype of a new genus and species, *Gavialimimus almaghribensis*,
10 gen. et sp. nov. *G. almaghribensis* is characterized by a highly elongate snout, highly
11 retracted nares, and large supratemporal fenestrae, among other features. Phylogenetic
12 analysis under multiple parsimony-based methods reveals novel substructure within the
13 subfamily Plioplatecarpinae, consistently recovering a clade uniting the new species with
14 *Selmasaurus* and the enigmatic *Goronyosaurus*. Synapomorphies of this clade include a
15 highly constricted parietal, with *Selmasaurus* and *Gavialimimus* being further united by a
16 broadly excavated medial surface of the quadrate suprastapedial process. The cranial
17 morphology of *G. almaghribensis* also provides new insight into several aspects of mosasaur
18 evolution and comparative anatomy, including adaptive radiation and niche partitioning in
19 Moroccan marine palaeoecosystems.

20

21 **Keywords:** adaptive radiation; functional morphology; niche partitioning; palaeoecology;
22 taxonomic revision; vertebrate palaeontology

23

1 **Introduction**

2

3 Determining the phylogenetic relationships among extinct taxa is essential for
4 understanding broad evolutionary processes such as adaptive radiation. Despite this
5 importance, the evolutionary history of many major clades, such as mosasaurs, remains
6 unresolved (Wright & Shannon 1988; LeBlanc *et al.* 2012; Simões *et al.* 2017b). Mosasaurs
7 were a dominant group of marine reptiles during the Late Cretaceous (100.5–66.0 Ma), noted
8 for their worldwide adaptive radiation during the latter stages of this period (Everhart 2005).

9 This diversification into various body forms and predatory specializations is
10 particularly apparent in the Upper Cretaceous deposits of northwestern Africa. Both the
11 Maastrichtian phosphates of Morocco and the Iullemeden Basin of the Dukamaje
12 Formation in Nigeria and Niger record extensive mosasaur assemblages (Lingham-Soliar
13 1991, 1998; Bardet *et al.* 2015; Bardet *et al.* 2018). The Moroccan phosphates preserve
14 remarkably high taxonomic and morphological diversity, containing at least seven genera
15 comprising species such as the halisaurine *Halisaurus arambourgi* Bardet & Pereda
16 Superbiola, 2005, and the mosasaurines *Eremiasaurus heterodontus* LeBlanc, Caldwell &
17 Bardet, 2012 and *Globidens simplex* LeBlanc, Mohr & Caldwell, 2019 (Bardet *et al.* 2005;
18 LeBlanc *et al.* 2012; Bardet *et al.* 2015; Bardet *et al.* 2018; LeBlanc *et al.* 2019). The
19 Dukamaje Formation preserves a similar level of diversity, with seven genera spanning the
20 Plioplatecarpinae, Halisaurinae, and Mosasaurinae; most notable among these taxa is the
21 enigmatic *Goronyosaurus nigeriensis* (Swinton, 1930), a poorly known species of uncertain
22 phylogenetic placement (Azzaroli *et al.* 1975; Soliar 1988). These deposits together
23 exemplify the remarkable capacity for evolutionary radiation present in mosasaurs.

24 Our study builds on current knowledge of this diversity via the description and
25 analysis of a new mosasaur specimen (MHN.M.KHG.1231) from Morocco. The teeth of this

1 specimen resemble those of '*Platecarpus*' *ptychodon* Arambourg, 1952, suggesting referral to
2 this species. However, the holotype and diagnosis of '*P.*' *ptychodon* exhibit critical flaws
3 forcing a re-evaluation – and ultimately a rejection – of its taxonomic validity. Morphological
4 and phylogenetic analyses of this specimen instead support referral to a new genus and
5 species, closely related to *Selmasaurus* Wright & Shannon, 1988, a genus of plioplatecarpine
6 mosasaur currently known only from the Santonian (86.3–83.6 Ma) and early Campanian
7 (83.6–80.6 Ma) of Kansas and Alabama (Wright & Shannon 1988; Polcyn & Everhart 2008;
8 Ogg *et al.* 2012). Specifically, the distribution of *Selmasaurus russelli* Wright & Shannon,
9 1988 within the Eutaw Formation (upper Santonian) in Alabama and within the unnamed
10 lower member of the Mooreville Chalk Formation (lower Campanian) in Kansas results in an
11 overall temporal range of 85–81.5 Ma (Wright & Shannon 1988; Kiernan 2002; Liu 2007;
12 Konishi 2008; Ogg *et al.* 2012). *Selmasaurus johnsoni* Polcyn & Everhart, 2008 occurs in
13 Kansas within the Smoky Hill Chalk Member of the Niobrara Formation, in biostratigraphic
14 units corresponding to the lower Santonian (86.3–85 Ma) (Polcyn & Everhart 2008; Ogg *et*
15 *al.* 2012).

16 We herein present a detailed osteological description of MHNM.KHG.1231, followed
17 by phylogenetic analyses of mosasauroid relationships incorporating this new specimen. We
18 then assess the evolutionary implications of these phylogenetic results for the new specimen
19 and associated taxa, including discussions of functional morphology and palaeoecology.
20 Ultimately, this specimen provides insight into the striking diversity – both morphological
21 and ecological – of the Late Cretaceous palaeoecosystems in which these mosasaurs lived, as
22 well as the phylogenetic framework underlying this diversity.

23 **Geological context**

24 MHNM.KHG.1231 originates from the Maastrichtian phosphate deposits of Morocco.
25 These deposits are a major component of the Mediterranean Tethyan Phosphogenic Province,

1 a belt of phosphates that extends around the Mediterranean Sea, from North Africa to the
2 Middle East (Lucas & Prévôt-Lucas 1996). These deposits span the Upper Cretaceous
3 (Maastrichtian) to the middle Eocene (Lutetian) and outcrop in five major basins: the Oulad
4 Abdoun, Ganntour, Meskala, Sous, and Oued Eddahab (Bardet *et al.* 2010; LeBlanc *et al.*
5 2012; Fig. 1A).

6 Historically, establishing stratigraphic correlations within and among these phosphatic
7 basins has been difficult for many reasons, most significantly the drastic local lateral facies
8 changes and the low abundance of microvertebrate and invertebrate fossils typically used for
9 biostratigraphic correlations (Bardet *et al.* 2010; LeBlanc *et al.* 2012). Arambourg was the
10 first to perform a methodical biostratigraphic analysis for these deposits, focussing his efforts
11 on the Oulad Abdoun and Ganntour basins (Arambourg 1952; Bardet *et al.* 2010). Using
12 unique assemblages of vertebrate remains (mainly fishes and reptiles), Arambourg
13 established three main stratigraphic levels of phosphates in each basin, referring to them as
14 ‘couches’, or ‘beds’ in English (Arambourg 1952; Bardet *et al.* 2010). These beds span the
15 Maastrichtian (Couche III) to the Ypresian (Couche I) (LeBlanc *et al.* 2012). The
16 Maastrichtian component (Couche III) of the Oulad Abdoun basin contains three major
17 subdivisions: a basal limestone bonebed, an intermediate grey phosphatic layer (Lower
18 Couche III), and an upper layer of fossiliferous, yellow phosphates of upper Maastrichtian
19 age (Upper Couche III) (LeBlanc *et al.* 2012; Fig. 1B). These layers are interspersed with
20 marly and calcareous beds (Bardet *et al.* 2015).

21 MHNM.KHG.1231 was discovered in a Moroccan phosphate mine, corresponding to
22 the aforementioned Couche III. This provenance is further supported by the sediments and
23 microfossils associated with this specimen. Teeth from the selachian taxa *Serratolamna*
24 *serrata* (Agassiz, 1843) and *Squalicorax pristodontus* (Agassiz, 1843) were present in the
25 matrix surrounding MHNM.KHG.1231 (C.S., pers. obs.), consistent with Couche III

1 (Maastrichtian) of the Oulad Abdoun basin (Arambourg 1952; Fig. 1). Furthermore, the soft,
2 yellow, phosphatic matrix itself unequivocally matches the description of Upper Couche III
3 (LeBlanc *et al.* 2012).

4

5 *[Insert Figure 1 here as a double-column (173 mm width) figure]*

6

7 **Material and methods**

8

9 **Specimen and figures**

10 The holotype specimen is accessioned in the collections of the Museum of Natural
11 History of Marrakech at Cadi Ayyad University in Morocco as MHNM.KHG.1231 and has
12 been on loan to the University of Alberta Laboratory for Vertebrate Palaeontology (UALVP),
13 where it was studied. This specimen consists of: an articulated skull, complete except for the
14 chondrocranium (Figs 2–5); partial left and right mandibles (Figs 6, 7); a partial right
15 quadrate (Fig. 8); and other disarticulated cranial (pterygoids) and postcranial (humerus and
16 vertebrae) material (Fig. 9). Specimens were photographed using a Canon PowerShot 340HS
17 digital camera. Images were traced and figured in Adobe Photoshop CC 2019 and 2020 and
18 Adobe Illustrator 2020.

19

20 *[Insert Figures 2 & 3 here, each as a double-column (173 mm width) figure]*

21

22 **Dataset selection**

23 The two datasets used for this analysis (see Supplementary Material, S1–S4) were
24 modified from the two character matrices of Simões *et al.* (2017b). Both of these source
25 matrices include 44 mosasauroid taxa and are based on the same fundamental characters,

1 though implement different coding schemes. The source matrix applying multistate character
2 coding contained 125 characters before modification, whereas the source matrix applying
3 contingent character coding contained 131 characters (Simões *et al.* 2017b). These matrices
4 were chosen because they comprise the most recent large-scale mosasauroid phylogeny and
5 contain numerous species from every major mosasaur group. This thorough taxon sampling is
6 ideal, as it tests the phylogenetic placement of MHNM.KHG.1231 relative to all mosasaurs
7 (rather than just a select subfamily), thus eliminating ingroup choice as a potential source of
8 bias.

9 Because these source datasets use both multistate and contingent coding schemes in
10 both unweighted and implied weighting maximum parsimony analyses, they therefore allow
11 the phylogenetic position of MHNM.KHG.1231 to be tested and compared under various
12 conditions and methods. Contingent coding schemes are useful for comparison to other
13 mosasauroid phylogenies because most previous phylogenies have been generated using this
14 scheme (e.g., Palci *et al.* 2013; Jiménez-Huidobro *et al.* 2016; Simões *et al.* 2017b).
15 However, multistate coding schemes are more logically sound, as they evaluate dependent
16 characters in a single transformational series, rather than parsing them into separate
17 characters (Simões *et al.* 2017a; Simões *et al.* 2017b). Similarly, unweighted maximum
18 parsimony analysis is the approach most commonly used in mosasauroid phylogenetics
19 (Simões *et al.* 2017b), though implied weighting has been proposed as a more accurate
20 method of phylogenetic reconstruction because it down-weights the impact of homoplasy in
21 tree construction (Goloboff 1993; Goloboff *et al.* 2008a; Simões *et al.* 2017b). Given this
22 diversity of phylogenetic methods, the chosen source datasets therefore enable a range of
23 analyses and comparisons concerning the phylogenetic position of MHNM.KHG.1231 and
24 related taxa. Performing and reporting these analyses also accounts for algorithm choice as a
25 potential source of methodological bias or error.

1 Furthermore, the inclusion of multiple dolichosaur and aigialosaur species in these
2 source matrices – with *Adriosaurus suessi* Seeley, 1881 being designated as the official
3 outgroup – ensures that the outgroup is closely related to the ingroup (Mosasauridae), as
4 opposed to the traditional usage of Varanidae as an outgroup. These datasets are therefore
5 preferred over other mosasauroid matrices, in which the outgroup is typically an artificial
6 operational taxonomic unit (OTU) generated using a compilation of varanid lizard character
7 states (Simões *et al.* 2017b). Using a theoretical unit as an outgroup can cause bias in
8 character polarization, as character polarity for the ingroup is often designated based on
9 previous assumptions of character evolution rather than on the actual character states
10 observed in a tangible outgroup taxon (Simões *et al.* 2017b). The use of varanids or a
11 varanid-based artificial OTU is also problematic because varanids are more distantly related
12 to mosasaurs than dolichosaurs or aigialosaurs are, thus increasing the possibility that
13 independent character evolution along the outgroup and ingroup branches has changed the
14 outgroup state from the true ancestral state (Simões *et al.* 2017b). Given these issues, using
15 an actual (i.e., non-theoretical), closely-related taxon such as *A. suessi* as the outgroup is
16 preferred, as this approach addresses the aforementioned inaccuracies that can result from
17 outgroup choice.

18 **Dataset modifications**

19 Three taxa were added to the source matrices: MHNM.KHG.1231 as a new species
20 (see below), *Goronyosaurus nigeriensis*, and *Selmasaurus russelli*. These latter two taxa were
21 included because they each exhibit certain morphological similarities to MHNM.KHG.1231
22 (e.g., snout elongation and deep interdental pits for *G. nigeriensis*; similar medial excavation
23 of the suprastapedial process of the quadrate for *S. russelli*), suggesting the potential for a
24 close evolutionary relationship worth being tested phylogenetically. Both of these taxa were
25 scored directly. Published descriptions were used to complement these direct observations,

1 but were not used as the sole basis for scoring any particular character; if a feature was
2 described in the manuscript but could not be directly observed by us, it was scored as ‘?’,
3 rather than relying on written descriptions. Although this approach may have reduced the
4 number of characters that could be scored, it was employed in order to ensure soundness of
5 methodology.

6 Certain characters within the source matrices were also modified. Character 51/55
7 (basioccipital tubera shape) in the multistate and contingent source matrices, respectively,
8 was deleted from this analysis on the basis of poor character construction. This character’s
9 states (tubera not anteroposteriorly elongate [0], or anteroposteriorly elongate with rugose
10 ventrolateral surfaces [1]) conflate different features – elongation and rugosity – thus
11 exemplifying problematic character type I A.6 as outlined by Simões *et al.* (2017a). Character
12 74/79 (tooth replacement mode) in the multistate and contingent source matrices was also
13 deleted on the basis of poor character construction, as its character states (replacement teeth
14 form in shallow excavations [0], or in subdental crypts [1]) simply refer to different stages of
15 tooth replacement (e.g., see Caldwell 2007) and therefore carry no phylogenetic signal. A
16 new character (Character 124/130: quadrate mid-shaft lateral deflection; absent [0], or present
17 [1]) was added to both the multistate and contingent datasets. This is a modified version of
18 character 95 in Konishi & Caldwell (2011) and was included because the quadrate shaft
19 deflection to which it refers is a synapomorphy of *Selmasaurus*.

20 The state for character 12/13 (frontal olfactory canal embrasure) in the modified
21 multistate and contingent datasets was changed from ‘1’ (canal almost or completely
22 enclosed ventrally by descending processes) to ‘0’ (canal not embraced ventrally by
23 descending processes) for *Selmasaurus johnsoni* in light of re-interpretation of this character
24 and its condition in *S. johnsoni* and *S. russelli*. The character states for multistate character 26
25 (prefrontal-postorbitofrontal contact) were originally mis-labelled as ‘0’, ‘0’, and ‘1’ in the

1 source character list; this typographic error was corrected to ‘0’, ‘1’, ‘2’ in the modified
2 dataset. For character 54/59 (dentary medial parapet), a new character state (state 3: medial
3 parapet taller than lateral wall of bone) was added to the original states (parapet positioned at
4 base of tooth roots [0], or parapet elevated and strap-like, enclosing about half of height of
5 tooth attachment in shallow channel [1], or parapet equal in height to lateral wall of bone [2]).
6 This new state accounts for additional variation present in MHNM.KHG.1231 and some
7 individuals of *Plioplatecarpus* (cf. Konishi & Caldwell 2011:Ch. 54[2]).

8 **Phylogenetic analysis**

9 **Unweighted maximum parsimony.** Unweighted maximum parsimony analysis was
10 performed for both the multistate and contingent character matrices using TNT v.1.5
11 (Goloboff *et al.* 2008b; Goloboff & Catalano 2016) via a heuristic ‘traditional search’ using
12 the tree bisection and reconnection (TBR) algorithm with 1000 random-addition-sequence
13 replicates. This method is consistent with that used by Simões *et al.* (2017b).

14 **Implied weighting maximum parsimony.** In these analyses, trees were generated from both
15 the multistate and contingent matrices using an implied weighting function of $k = 3.0$, as per
16 the methods of Simões *et al.* (2017b). Values of $k = 7.0$ and $k = 11.0$ were also used to test
17 the effect of stringency of the concavity function on the resultant topology. All other settings
18 and methods were retained from the unweighted maximum parsimony analysis.

19 **Character mapping.** Synapomorphies were mapped onto all most-parsimonious-trees
20 (MPTs) in TNT v.1.5 (Goloboff *et al.* 2008b; Goloboff & Catalano 2016). Character history
21 was traced in Mesquite v.3.51, with ancestral states reconstructed using parsimony
22 (Maddison & Maddison 2018). Trees were visualized in Mesquite v.3.51 (Maddison &
23 Maddison 2018) and prepared for figures using Adobe Illustrator 2020.

24 **Institutional abbreviations**

1 **BMNH**, Natural History Museum (formerly the British Museum [Natural History]), London,
2 England; **CMN**, Canadian Museum of Nature, Ottawa, Canada; **FHSM**, Sternberg Museum
3 of Natural History, Fort Hays State University, Hays, Kansas; **IGF**, Institute of Geology and
4 Paleontology of the University of Florence, Florence, Italy; **IRSNB**, Institut Royal des
5 Sciences Naturelles de Belgique, Brussels, Belgium; **MHNM**, Museum of Natural History of
6 Marrakech at Cadi Ayyad University, Marrakech, Morocco; **MNHN**, Muséum National
7 d'Histoire Naturelle, Paris, France; **UALVP**, University of Alberta Laboratory for Vertebrate
8 Palaeontology, Edmonton, Canada; **YPM**, Yale Peabody Museum.

9

10 **Systematic palaeontology**

11

12

Reptilia Linnaeus, 1758

13

Squamata Oppel, 1811

14

Mososauridae Gervais, 1852

15

Plioplatecarpinae (Dollo, 1884) Williston, 1897b

16

Gavialimimus gen. nov.

17

(Figs 2–9)

18

19 **Type species.** *Gavialimimus almaghribensis*, sp. nov.

20 **Diagnosis.** As for the type and only species.

21 **Derivation of name.** Meaning ‘gharial mimic’, from the Gallicised Hindi root ‘*gavial*’ and
22 the Greek root ‘*mimus*’, the genus name refers to morphological convergence between the
23 holotype specimen and the extant gharial (*Gavialis gangeticus*), primarily regarding their
24 distinctive longirostry and interlocking teeth.

25 **Occurrence.** As for the type and only species.

26

1 *Gavialimimus almaghribensis* sp. nov.

2 (Figs 2–9)

3 **Holotype.** MHNM.KHG.1231: articulated skull, including the premaxilla, maxillae,
4 prefrontals, frontal, parietal, postorbitofrontals, squamosals, vomers, and palatines; isolated
5 left and right dentaries; articulated right posterior mandibular unit; isolated pterygoids; partial
6 right quadrate; and four isolated vertebrae, one caudal, two cervical, and one indeterminate.

7 **Diagnosis.** Plioplatecarpine mosasaur species bearing the following autapomorphies: snout
8 highly elongate, with openings for the external nares small and highly retracted;
9 supratemporal fenestrae large, nearly as long as the entire frontal including the anterior
10 frontal processes; dentary medial parapet taller than lateral wall of dentary; Meckelian groove
11 of the dentary terminating anteriorly at the sixth tooth position; parietal markedly constricted,
12 resulting in a triangular parietal table with a distinct midsagittal crest posteriorly; prefrontal
13 extending posteriorly nearly to level of frontoparietal suture. Also distinguished by a unique
14 combination of the following features: marginal teeth not medially striated; interdental pits
15 deep, present along most of the length of the marginal tooth rows; pineal foramen elongate
16 and in slight contact with the frontoparietal suture; postorbitofrontal wide in dorsal view,
17 equal to roughly half the width of the frontal, and lacking a transverse dorsal ridge;
18 zygosphenes and zygantra absent; humerus ectepicondyle present. Differs from *Selmasaurus*
19 *johnsoni* in the following respects: premaxillary predental rostrum absent; postorbitofrontal in
20 contact with prefrontal; maxillary-premaxillary suture terminating posteriorly between the
21 eighth and ninth maxillary teeth. Differs from *Selmasaurus russelli* in the following respects:
22 posterior parietal shelf absent. Differs from *Goronyosaurus nigeriensis* in the following
23 respects: ectopterygoid processes of pterygoid not forked; maxilla terminating just posterior
24 to anterior border of orbit, as opposed to extending beyond posterior margin of orbit;
25 premaxillary teeth not caniniform.

1 **Derivation of name.** The specific epithet is a romanized version of the Arabic name for
2 Morocco, paired with the Latin suffix ‘-ensis’, thus denoting the country of origin of the
3 holotype.

4 **Occurrence.** Upper Couche III (upper Maastrichtian) of the Oulad Abdoun basin in northern
5 Morocco.

7 **Description and comparisons**

9 **General**

10 MHNM.KHG.1231 consists of an articulated skull (mostly complete except for the
11 chondrocranium) (Figs 2–5), left and right dentaries (Figs 6, 7A–B), right posterior
12 mandibular unit (Fig. 7C–F), a partial right quadrate (Fig. 8), isolated right and left
13 pterygoids (Fig. 9A–D), four isolated vertebrae (Fig. 9C–F), and the right humerus (Fig. 9G).
14 Most of these elements were recovered in three major blocks: one containing the skull, one
15 containing the left dentary and partial quadrate, and one containing the right dentary. The
16 other elements were small enough to be recovered individually from the *in situ* matrix
17 surrounding the three main blocks. Several isolated teeth (UALVP 57049) matching the
18 morphology of those present in the jaw bones were also recovered from the matrix
19 surrounding the *in situ* elements.

20 The preorbital region of the skull comprises almost two-thirds of the total length of
21 the skull (Figs 2, 3). This striking elongation of the snout is an uncommon occurrence among
22 mosasaurs, with *Ectenosaurus clidastoides* (Merriam, 1894) and, to a lesser extent,
23 *Plotosaurus bennisoni* (Camp, 1942) and *Goronyosaurus nigeriensis* being the only
24 mosasaurs exhibiting a comparable condition.

25 Although the skull is articulated, taphonomic deformation has displaced some of the

1 bones from their natural positions. The entire skull is slanted to its right. Most significantly,
2 the palate and skull roof are collapsed onto each other, with the palate being offset from the
3 skull roof such that the right internal naris is aligned with the left external naris. The right
4 maxilla is also collapsed underneath the skull, such that it underlies the right external naris.

5 **Skull**

6 **Premaxilla.** In MHNM.KHG.1231, the premaxilla is preserved largely in natural position,
7 though the internarial bar is broken slightly posterior to its midpoint (Fig. 2). The premaxilla
8 is smoothly rounded anteriorly, terminating just beyond the anteriormost premaxillary tooth
9 and thus lacking a rostrum (Figs 2, 3, 4A, 6A). The dorsal surface of the premaxilla is
10 smooth, possessing neither a sulcate texture nor a dorsal crest (Fig. 2B). Foramina marking
11 the exits of the ophthalmic ramus (V1 branch) of the trigeminal nerve are loosely dispersed
12 on either side of the dorsal midline (Russell 1967; Fig. 2). Although most mosasaurs exhibit
13 six or seven such foramina on each side of the premaxilla, MHNM.KHG.1231 possesses
14 approximately 10; this comparatively high number is similar to the state present in
15 *Goronyosaurus nigeriensis* (Lingham-Soliar 1991).

16 The premaxilla articulates with the maxilla via a long suture that is posteriorly
17 displaced due to deformation of the skull. Based on our interpretation of the skull, this suture
18 likely would have extended to between the eighth and ninth maxillary tooth positions, at
19 which point the bones separate to surround the anterior extent of the openings for the external
20 nares (Fig. 2). The internarial bar forms the anteromedial border of the external nares,
21 extending to the posterior extent of the external narial openings, where it articulates on either
22 side with the paired anterior processes of the frontal (Fig. 2). The internarial bar is mostly
23 uniform in width, being slightly narrower than half the width of the rostrum and tapering
24 slightly toward its posterior terminus.

25 The external nares themselves are unique in being highly retracted, extending

1 posteriorly almost to the level of the orbits and being restricted to the posterior 25% of the
2 preorbital region (Fig. 2); similar external narial retraction has been noted in *Goronyosaurus*
3 (*Azzaroli et al.* 1972; Soliar 1988).

4 The ventral surface of the premaxilla – including the junction of the internarial bar
5 and dentigerous portion of the premaxilla – is largely obscured by the vomers (Figs 3, 4A–B).
6 However, the vomerine process of the premaxilla is visible as a median ridge between the
7 second pair of premaxillary teeth, separated from the roots of the teeth on either side by a
8 shallow groove (Figs 3, 4A). Posteriorly, this ridge articulates with the vomers, though the
9 exact suture is difficult to discern; anteriorly, it terminates just rostral to the second pair of
10 premaxillary teeth. A slight groove separates the anterior pair of premaxillary teeth (Fig. 4A).

11

12 [*Insert Figure 4 here as a full-page (232 mm x 173 mm) figure*]

13

14 **Maxilla.** The maxillae terminate posteriorly at the anterior border of the orbits (Figs 2, 3, 4C,
15 5). They are fairly uniform in height along their extent, though taper anteriorly following the
16 curve of the maxillary-premaxillary suture (Fig. 2). The left maxilla is broken – either
17 pathologically or taphonomically – at the level of the eighth maxillary tooth (Fig. 2). Several
18 large foramina are present along the ventral border of the lateral surface of the maxilla, above
19 roughly every other tooth position. Several smaller foramina are scattered over the rest of the
20 lateral surface, being mostly concentrated toward the anterior of the maxilla (Fig 2). These
21 foramina mark the exits of the maxillary (V2) branch of the trigeminal nerve (Russell 1967).

22

23 The maxilla articulates with the prefrontal via a straight suture that extends
24 posterolaterally from the posterolateral edge of the external naris to the anterodorsal edge of
25 the orbit (Figs 2, 5C). Thus, the maxilla forms most of the lateral border of the external naris,
with the prefrontal surrounding the posterior and posterolateral edges of the external nares

1 (Fig. 2).

2 The posterior terminus of the maxilla extends beyond the posteriormost maxillary
3 tooth for a distance roughly equivalent to one alveolus length (Figs 3, 4C). The posterior
4 extent of the lateral border of the left maxilla is marked by several large indentations or pits
5 (Figs 2, 5C). However, as these pits are absent on the right maxilla, they are likely the result
6 of taphonomic deformation.

7 The maxillae each bear 12 tooth positions (Fig. 2); the morphology of these teeth is
8 described in Description – Dentition. The maxillary tooth row is slightly inset from the
9 smoothly rounded ventrolateral border of the maxilla (Figs 3, 4B–C). The lingual shelf of the
10 maxilla is best visible posteriorly on the left maxilla (Fig. 4C) and anteriorly on the right
11 maxilla (Fig. 4B). It extends along the medial border of the maxillary tooth row and is quite
12 pronounced, especially posteriorly, causing the tooth row to effectively occupy a one-sided
13 trough (Figs 3, 4B–C). Although the lingual shelf is about 1.8 cm wide at its widest point
14 posteriorly and remains quite pronounced along most of its length, it does become thinner
15 anteriorly, with its thinnest width of 0.1 cm occurring medial to the third maxillary tooth.
16 Anterior to this point, the lingual shelf is no longer visible, though it is unclear whether this
17 absence is biological or simply the result of being obscured by matrix.

18

19 *[Insert Figure 5 here as a full-page (173 mm x 232 mm) figure]*

20

21 **Dentition.** Two pairs of teeth are present on the premaxilla (Figs 2, 3, 4A). The anterior pair
22 is moderately recurved, with the teeth showing slight wear on their tips (Figs 4A, 6A). The
23 right anterior tooth is slightly more prognathous than its left counterpart (Figs 3, 4A, 6A),
24 likely the result of taphonomic deformation to the associated alveolus (see below; Fig. 6A).
25 This displacement may also have been facilitated by the lack of fusion between this tooth and

1 its alveolus (see below; Fig. 6A). The second premaxillary tooth is absent on the left side of
2 the premaxilla and taphonomically distorted on the right side; however, based on the
3 dimensions of the alveolus and the remnants of the tooth that are present, this tooth was likely
4 of similar size to the anteriormost premaxillary tooth (Figs 3, 4A). As such, this specimen
5 lacks the prominent caniniform premaxillary dentition characteristic of *Goronyosaurus*
6 (Lingham-Soliar 2002).

7 There are 12 tooth positions on the maxilla (Figs 2, 3) and at least 10 tooth positions
8 on the dentary (Fig. 7A–B). All of the marginal teeth are strongly fluted, bicarinate, and lack
9 serrations (Fig. 6). The teeth are widely spaced, indicating strong interdigitation of the tooth
10 rows when occluded. As in *Goronyosaurus*, deep interdental pits are present along the
11 premaxillary, maxillary, and dentary tooth rows to accommodate this interdigitation
12 (Lingham-Soliar 1991; Figs 3, 4, 6). These interdental pits can be distinguished from the
13 replacement tooth pits because they are located lateral to the tooth row, whereas the
14 replacement teeth form posteromedial to the tooth roots (Figs 3, 6). The interdental pits are
15 deepest anteriorly on the jaws and get progressively shallower until finally disappearing
16 posterior to the seventh dentary (Figs 6F, 7A) and at least the fifth maxillary tooth positions
17 (Figs 3, 4B). The interdental pits may extend beyond the fifth tooth position on the maxilla,
18 but this location is obscured by the displaced humerus. This shallowing is related to
19 progressive changes in the dimensions of the teeth: the premaxillary and anterior maxillary
20 teeth are long and distinctly recurved whereas the more posterior maxillary teeth are
21 progressively shorter, stouter, and less recurved (Figs 3, 4, 6). This moderate heterodonty
22 allows the posterior teeth to interlock without interdental pits.

23 The tooth bases are oval in cross-section, and are posteriorly elongated toward the
24 posterior extent of the maxillary tooth row (Figs 3, 4, 6). The teeth also exhibit progressive
25 changes in the degree of wear. The premaxillary and anterior maxillary and dentary teeth are

1 barely worn (Figs 4A, 6), whereas the posterior maxillary teeth exhibit much more
2 pronounced wear (Figs 4B–C, 6C). In the tenth and eleventh left maxillary teeth, this wear
3 extends from the tip of the tooth crown along the tooth's mesial carina.

4 The marginal tooth roots are broadly exposed along their respective tooth rows,
5 constituting between one-third and one-half of the height of the overall tooth (Figs 2B, 3B, 4,
6 6). Taphonomic damage to the alveolus of the right anterior premaxillary tooth has caused the
7 root of this tooth to be further exposed beyond the level of the maxillary tooth row, revealing
8 the root to be elongate and curved underneath the interdental pit between the right
9 premaxillary teeth (Figs 3B, 4A, 6A). Similar breakage at the fourth tooth position on the left
10 dentary reveals similar curvature of the tooth root underneath the interdental pit posterior to
11 this tooth position, with the exposed root being at least twice the length of the tooth crown
12 (Fig. 7A). The presence of this root curvature at both the first premaxillary and fourth dentary
13 tooth positions therefore indicates that this curvature is present and pronounced at least
14 anteriorly on the marginal tooth rows, though whether it continues into the posterior extent of
15 the tooth rows remains uncertain. Similar curvature is also present in the tooth roots of
16 *Prognathodon solvayi* Dollo, 1889a (C.S., pers. obs.).

17 Three replacement teeth are visible on the marginal jaw elements: one in the early
18 stages of development occurs in association with the eleventh tooth on the left maxilla (Figs
19 3A, 6C); another replacement tooth at a slightly more advanced stage, indicated by its slightly
20 larger size, occurs in association with the third tooth on the right maxilla (Figs 3A, 6B); and a
21 final replacement tooth at a much more advanced developmental stage – indicated by its
22 much larger size – occurs in association with the seventh tooth position on the left dentary
23 (Figs 6F, 7A). The two smaller replacement teeth occur in shallow pits directly posteromedial
24 to their respective tooth positions (Fig. 6B–C), whereas the largest replacement tooth is
25 present in a crypt underneath the functional tooth (Fig. 6F). As in the functional teeth, none

1 of the replacement teeth are serrated. However, these replacement teeth differ from the
2 functional teeth in having smooth faces, thus lacking the plicae present on the fully
3 developed, functional teeth.

4 Different stages of post-eruption tooth development are also visible along the left
5 dentary tooth row, reflecting the progressive fusion that occurs throughout this late-stage
6 tooth development. The roots of the second, fourth, and sixth teeth are separate from their
7 surrounding alveoli, with each alveolus forming a rim around the associated tooth root (Figs
8 6F, 7A). The third tooth root is partially fused to the bone, such that the aforementioned rim
9 is less pronounced; instead, the junction between the tooth root and the alveolus is marked by
10 a slight groove encircling the root (Figs 6D, 7A). The fifth tooth is completely fused to its
11 alveolus, with the root being smoothly confluent with the surrounding dentary bone (Figs 6E,
12 7A). Similar developmental stages are evident along the upper marginal tooth row: the right
13 first premaxillary and first maxillary teeth are unfused to their respective tooth-bearing
14 elements (Fig. 6A); the right second premaxillary and second, third, tenth and eleventh
15 maxillary teeth are partially fused (Fig.6B); and the right fifth maxillary tooth is completely
16 fused to the maxilla. Various empty alveoli are present along all marginal tooth-bearing
17 elements (Figs 3, 4, 6, 7).

18

19 *[Insert Figure 6 here as a double-column (173 mm width) figure]*

20 *[Insert Figure 7 here as a full-page (232 mm x 173 mm) figure]*

21

22 **Prefrontal.** The prefrontal articulates laterally with the maxilla, medially with the frontal,
23 and posteriorly with the postorbitofrontal, and is slightly curved to form the anterodorsal
24 border of the orbit (Figs 2, 5). The suture with the maxilla is described in Description –
25 Maxilla.

1 The anterior border of the prefrontal is smoothly and tightly curved, with two
2 processes – one medial and one lateral – that surround the posterior and posterolateral border
3 of the external naris (Fig. 2). The lateral process is much longer than the medial one, such
4 that the prefrontal fully surrounds the posterolateral margin of the external naris but only
5 barely rounds the posteromedial portion before articulating with the frontal. This condition is
6 consistent with the lack of anterolateral processes of the frontal in MHNM.KHG.1231 and in
7 *Selmasaurus*, as discussed in Description – Frontal below; i.e., rather than the frontal bearing
8 anterolateral processes which surround the posterolateral borders of the external nares, it is
9 the prefrontal which embays the external narial openings (Fig. 2).

10 The prefrontal articulates with the frontal via a straight suture that extends from the
11 posteromedial corner of the external naris to the posterolateral corner of the frontal, another
12 unusual feature among mosasaurs, where in dorsal aspect the prefrontal typically terminates
13 posteriorly at the mid-length of the frontal supraorbital border (Figs 2, 5; see Russell
14 1967:fig. 4; and Bell 1997:fig. 6 for comparison). The posterior terminus of the prefrontal is
15 deeply notched, with diverging medial and lateral processes that articulate with the
16 anteriorly-projecting main body of the postorbitofrontal (Figs 2, 3, 4C, 5). The lateral process
17 extends to the midpoint of the orbit, thus forming the anterolateral border of the orbit, with
18 the medial process being slightly longer (Figs 2, 3, 5C). This articulation of the prefrontal
19 with the postorbitofrontal excludes the frontal from the orbital margin. Similar to the
20 condition in *Plotosaurus* (see LeBlanc *et al.* 2013:figs 2, 6), the prefrontal and
21 postorbitofrontal exhibit extensive contact along the ventrolateral, lateral, and dorsolateral
22 borders of the orbit (Fig. 5). This pronounced articulation, previously considered unique to
23 *Plotosaurus* among mosasaurs, contributes to reduced kinesis between the muzzle and
24 posterior skull (LeBlanc *et al.* 2013).

1 **Lacrimal.** In many non-ophidian squamates, a lacrimal is present between the prefrontal and
2 maxilla (see Konishi *et al.* 2016 for proposed location in mosasaurs). However, because this
3 area of the skull is taphonomically distorted in MHNM.KHG.1231 (Figs 2, 5C), the presence
4 of the lacrimal cannot be assessed in this specimen.

5 **Frontal.** The frontal is a triangular bone articulating anteriorly with the internarial bar of the
6 premaxilla, laterally with the prefrontal, posterolaterally with the postorbitofrontal, and
7 posteriorly with the parietal (Figs 2, 5). In MHNM.KHG.1231, the frontal possesses a single
8 pair of long anterior projections, about half the length of the main body of the frontal, that
9 surround the posterior extent of the internarial bar and thus border the external nares
10 posteromedially (Fig. 2). These processes bear short but sharp ridges concentrated on the
11 medial half of their respective dorsal surfaces (Fig. 2). Though the posteriormost portion of
12 the premaxillary internarial bar is broken, the tight V-shaped notch formed by the frontal's
13 anterior processes indicates that the internarial bar would have invaded the frontal to a point
14 roughly in line with the posterior extent of the openings for the external nares (Fig. 2B).

15 Uniquely shared with *Ectenosaurus* and *Selmasaurus* among russellosaurines,
16 MHNM.KHG.1231 lacks a pair of frontal anterolateral processes, thus precluding the frontal
17 from forming the posterolateral corner of the naris (compare Fig. 2 to Russell 1967:figs 83,
18 86; Wright & Shannon 1988:fig. 1; Holmes 1996:fig. 2A; Konishi & Caldwell 2007:fig. 5A;
19 and Polcyn & Everhart 2008:fig. 3).

20 Though the dorsal surface of the frontal is quite deeply fractured, the sutures between
21 the frontal and surrounding bones are still clear and the ventral surface is much more intact.
22 The frontal is tightly joined to the parietal via a complex and interdigitating suture (Figs 2, 3,
23 4C, 5), similar to the condition described in *Goronyosaurus nigeriensis* (Lingham-Soliar
24 1999) and *Selmasaurus russelli* (Wright & Shannon 1988) and also present, albeit to a lesser
25 extent, in *Ectenosaurus* (C.S., pers. obs., FHSM VP-401). The junction between the frontal

1 and prefrontal is similarly tightly articulated, though lacks clear interdigitation (Figs 2, 3, 4C,
2 5). The posterolateral corners of the frontal each bear an ala overlying the postorbitofrontal
3 between its anterior and medial processes and forming the main junction between the frontal
4 and postorbitofrontal (Figs 2, 5B–C). These alae are particularly long and narrow, resembling
5 the condition in *Goronyosaurus* and *Phosphorosaurus ponpetelegans* Konishi, Caldwell,
6 Nishimura, Sakurai & Tanoue, 2016, but differing from most other mosasaurs, including
7 closely related taxa such as *Selmasaurus* (C.S., pers. obs.; see also Azzaroli *et al.* 1972;
8 Soliar 1988; Wright & Shannon 1988; Konishi *et al.* 2016 for comparison to the
9 aforementioned taxa).

10 Ventrally, the frontal is underlain posterolaterally by the postorbitofrontals (Figs 3,
11 4C, 5A). These overlap the frontal alae so that the posterolateral corners of the frontal's
12 ventral surface are laterally concave (Figs 3, 4C, 5A) rather than triangularly projecting as the
13 alae are dorsally (Figs 2, 5B–C). Highly unusually for mosasaurs, the prefrontal extends
14 nearly as far posteriorly as to the frontoparietal suture (Figs 2, 3, 4C, 5; see also Description –
15 Prefrontal above). The posteromedian flanges of the frontal project posteriorly in ventral
16 view to a level about one-third along the length of the pineal foramen (Figs 3, 5A). These
17 flanges articulate medially with the parietal and so do not directly border the pineal foramen
18 (Figs 3, 5A). The only contact between the frontal and the pineal foramen occurs where the
19 anterior terminus of the pineal foramen contacts the midpoint of the posterior border of the
20 frontal (Figs 3, 4C, 5A).

21 Anterior to the pineal foramen, the frontal bears a pronounced, roughly triangular boss
22 on its ventral surface that tapers anteriorly to join the olfactory canal (Figs 3, 4C, 5A). The
23 edges of the tabular boss form a sharp ridge, whereas the central portion of the boss is slightly
24 concave and is at about the same level as the frontal's main ventral surface (Figs 4C, 5A).
25 The olfactory canal continues anteriorly along the ventral midline of the frontal, though is

1 only visible for about 1 cm before being obscured by the displaced palatal bones (Figs 3, 4C,
2 5A). The posterior portion of the canal is completely surrounded by bone, such that it appears
3 on the frontal's ventral surface as a narrow rectangular tube extending from the anterior
4 portion of the aforementioned boss (Figs 4C, 5A); however, as only this posteriormost extent
5 is visible, it is uncertain whether this ventral enclosure continues along the rest of the canal or
6 not. Lateral to the anterior half of the tabular boss and the posterior portion of the olfactory
7 tract, narrow and smoothly concave depressions preserve the location of the cerebral
8 hemispheres *sensu* Russell (1967) or, alternatively, the articulation surface for the
9 orbitosphenoids *sensu* Konishi & Caldwell (2011) (Figs 3, 4C, 5A). These depressions are
10 approximately 0.5–0.6 cm in width and 3.2 cm in length, though may extend further
11 anteriorly under the superimposed palatal bones.

12 **Parietal.** The parietal is an elongate element that forms the medial and anteromedial borders
13 of the supratemporal fenestrae. The anterior portion of the parietal forms a flattened table
14 approximately 7 cm wide and almost 4 cm long, articulating with the frontal anteriorly and
15 the postorbitofrontal laterally (Figs 2, 3, 5B). The pineal foramen barely contacts the
16 frontoparietal suture anteriorly on this roughly triangular table (Figs 2, 3, 4C, 5A–B). This
17 foramen is large and elongate, measuring 2.4 cm long and 0.6 cm wide. Dorsally, its edges
18 are smoothly rounded (Figs 2B, 5B), whereas the ventral opening of this foramen is
19 surrounded by a high, sharp, oval ridge (Figs 3, 4C, 5A) akin to the condition in *Mosasaurus*
20 spp. (see e.g., Konishi *et al.* 2014:fig. 4C for comparison) and at least one specimen of
21 *Ectenosaurus* sp. (T.K., pers. obs., YPM 4674). This ridge projects sharply from the level of
22 the rest of the parietal, reaches its peak about 1 cm from the pineal foramen's border, and
23 curves down smoothly into the foramen itself (Figs 4C, 5A). Anteriorly, this ridge is
24 confluent with the raised tabular boss on the ventral midline of the frontal (Figs 4C, 5A).
25 Posteriorly, the sides of the ridge on either side of the pineal foramen converge to form a

1 groove that extends the length of the parietal's ventral midline, terminating where the parietal
2 diverges posteriorly to form the suspensorial rami (Figs 3A, 4C, 5A). This groove is laterally
3 offset near the anterior origin of the parietal descending processes, though this discontinuity
4 is likely the result of taphonomy, as evidenced by the other breaks and grooves visible on the
5 parietal.

6 The majority of the parietal consists of a narrow, elongate median body forming the
7 medial borders of the supratemporal fenestrae (Figs 2, 3). This portion of the parietal is
8 extremely constricted, a condition otherwise noted only in *Goronyosaurus* and *Selmasaurus*
9 (Wright & Shannon 1988; Polcyn & Everhart 2008). Dorsally, an overhanging lateral shelf is
10 present on each side of the parietal table posterolateral to the pineal foramen (Figs 2, 5B).
11 This shelf extends diagonally from the center of each side of the flattened anterior parietal to
12 a point about one-fifth of the way along the lateral surface of the constricted body of the
13 parietal (Fig. 2). This is in distinct contrast to the typical mosasaur condition: in other
14 mosasaurs, these overhanging crests typically extend to the suspensorial rami of the parietal,
15 causing almost the entire dorsal surface of the parietal to be distinctly flattened. In
16 MHNM.KHG.1231, by comparison, these crests are greatly shortened, restricting the parietal
17 table to the anterior one-third of the parietal.

18 Due to its marked constriction, the rest of the parietal forms a midsagittal crest. As
19 noted above, this marked parietal constriction is also present in *Selmasaurus russelli* (see
20 Wright & Shannon 1988:fig. 1) and *S. johnsoni* (see Polcyn & Everhart 2008:fig. 3);
21 however, the condition in MHNM.KHG.1231 is more pronounced than in these species,
22 resulting in a triangular, rather than subrectangular, parietal table and a posterior midsagittal,
23 rather than parasagittal, crest(s) (Fig. 2). As mentioned, the parietal of *Goronyosaurus* shows
24 similar constriction; however, it is too incomplete to fully assess the state of the sagittal crest
25 or table.

1 Ventrally, the parietal bears two broadly crescentic descending flanges that descend at
2 an angle from either side of the parietal's posterior body, forming the medial wall of the
3 supratemporal fenestrae (Figs 2, 3). These flanges extend from the anteromedial corner of the
4 supratemporal fenestrae to a point about 4 cm anterior to the divergence of the parietal into
5 the suspensorial rami. In life they would have articulated with the prootics, though in
6 MHNM.KHG.1231 these bones, as well as other elements of the chondrocranium, are not
7 preserved. These descending flanges are about 0.5–0.6 cm thick, tapering ventrally to a width
8 of about 0.1 cm.

9 In mosasaurs, the posterior portion of the parietal is typically comprised of the
10 suspensorial rami, though in MHNM.KHG.1231 these structures are broken such that only
11 the most proximal portion of each ramus is preserved (Figs 2, 3). From what remains of the
12 posterior parietal, it is evident that the rami diverge horizontally at about 30° to the sagittal
13 midline. Proximally, the rami are relatively similar in height and width, though soon after
14 their divergence become dorsoventrally depressed so as to be wider than they are tall, as is
15 typical of non-halisaurine mosasaurs (e.g., Konishi *et al.* 2016).

16 **Postorbitofrontal.** The postorbitofrontal articulates anteriorly with the prefrontal,
17 anteromedially with the frontal, medially with the parietal, and posteroventrally with the
18 squamosal (Figs 2, 3, 4C, 5). Anteriorly, the main body of the postorbitofrontal extends to
19 form the posterior half of the dorsal orbital border, articulating with the notched posterior
20 terminus of the prefrontal just anterior to the midpoint of the orbit (Figs 4C, 5). The
21 prefrontal-postorbitofrontal suture thus delineates an anteriorly-facing wedge of the
22 postorbitofrontal surrounded on either side by posteriorly-projecting medial and lateral
23 processes of the prefrontal. A similarly extensive articulation of the postorbitofrontal and
24 prefrontal has been described in *Plotosaurus* as an adaptation for reduced cranial kinesis
25 (LeBlanc *et al.* 2013).

1 The postorbitofrontal's medial process to the parietal forms the anterolateral border of
2 the supratemporal fenestra. Dorsally, this medial process is overlapped by the
3 posterolaterally-projecting frontal ala (Figs 2, 5B). The dorsal suture between the frontal ala
4 and the postorbitofrontal is complex and interdigitating, in contrast to the more linear sutures
5 connecting the postorbitofrontal to the prefrontal (Figs 2, 5B–C). Ventrally, the
6 postorbitofrontal meets the parietal in a laterally concave suture marked by a distinct groove
7 in the ventral skull roof (Figs 3, 4C, 5A).

8 At the junction between its anterior, medial, and posterior processes, the
9 postorbitofrontal bears a descending process that in life would have articulated with the jugal
10 (Russell 1967; Figs 3, 4C, 5A). This process is anteroposteriorly compressed and tapers to a
11 smoothly rounded ventrolateral border.

12 Posteriorly, the postorbitofrontal bears a long, thin process that articulates with the
13 dorsal surface of the squamosal (Figs 2, 3, 5C). Whereas the anterior and medial processes of
14 the postorbitofrontal are dorsoventrally depressed, this squamosal process is laterally
15 compressed. The junction of this process with the main body of the postorbitofrontal forms
16 the anterolateral corner of the supratemporal fenestra and occurs at approximately a right
17 angle (Fig. 2). This corner is obtuse in another plioplatecarpine *Platecarpus tympaniticus*
18 Cope, 1869 (e.g., Konishi & Caldwell 2009:fig. 5D), with *Selmasaurus* showing an
19 intermediate condition (e.g., Wright & Shannon 1988:fig. 1). The squamosal process extends
20 nearly to the posterior extent of the squamosal, becoming progressively thinner as it
21 approaches its posterior terminus (Figs 2, 3). A notch at the ventral junction of the
22 postorbitofrontal's squamosal and jugal processes articulates with the pointed anterior
23 terminus of the squamosal (Fig. 3).

24 **Squamosal.** The squamosal is a laterally compressed, rod-like bone that articulates dorsally
25 with the squamosal process of the postorbitofrontal (Figs 2, 3, 5C). In MHNM.KHG.1231,

1 the left squamosal is broken near its anterior extent and is twisted such that its dorsal surface
2 now lies medially (Fig. 2). The dorsal border of the squamosal is gently inclined, such that
3 the squamosal shaft is 2.8 cm high at its posterior terminus and tapers downward anteriorly to
4 a height of 1.1 cm, terminating anteriorly in a wedge that inserts between the
5 postorbitofrontal's jugal and squamosal processes (Figs 3, 5C).

6 The posterior terminus of the squamosal forms a ventromedially-expanded head (Fig.
7 3) that in life would have articulated medially with the supratemporal and parietal and
8 ventrally with the quadrate. The dorsal surface of the squamosal head is continuous with the
9 dorsal surface of the squamosal shaft (Fig. 2), whereas the ventral portion of the body
10 expands below the level of the ventral shaft (Fig. 3). The internal face of the squamosal head
11 is teardrop-shaped and medially concave, forming a facet for the posterior portion of the
12 supratemporal (Fig. 3). The squamosal head bears a flat facet anteroventrally that would have
13 articulated with the dorsal surface of the quadrate, possibly along the suprastapedial process
14 (Fig. 3).

15 The squamosal bone and the squamosal process of the postorbitofrontal together form
16 the lateral border of the supratemporal fenestra. The junction of the squamosal shaft and
17 squamosal head forms the posterolateral corner of this fenestra, as the squamosal head
18 expands ventromedially from the shaft. The dorsal articulation between the squamosal and
19 postorbitofrontal extends nearly the full length of the squamosal, terminating at the
20 approximate dorsal midpoint of the squamosal head (Fig. 2).

21 **Quadrate.** A partial right quadrate was recovered from the matrix surrounding the right
22 dentary (Fig. 8). Very little of the quadrate is preserved, with this fragment representing the
23 dorsal-most portion of the quadrate shaft and most of the suprastapedial process. The medial
24 surface of the suprastapedial process bears a broad excavation, causing the suprastapedial
25 process to be constricted dorsally (Fig. 8B–C). This condition is limited to

1 MHNM.KHG.1231, *Ectenosaurus*, and *Selmasaurus* among the Plioplatecarpinae (Konishi
2 2008). Dorsal constriction of the suprastapedial process has been recognized in previous
3 studies as a trait typical of mosasaurines (e.g., see Bell 1997:char. 45); however, given the
4 results of our and previous phylogenetic analyses (e.g., Bell 1997; Caldwell *et al.* 2008;
5 Jiménez-Huidobro & Caldwell 2019), we discard the possibility that the condition in
6 mosasaurines could be homologous with that observed in *Gavialimimus* as unparsimonious.
7 (For further discussion of this condition, see description and scoring of characters 38 and 42
8 in our multistate [§S1] and contingent [§S2] character lists, respectively.)

9 The dorsal surface of the suprastapedial process is generally consistent in width,
10 measuring about 1.3 cm wide along most of its length, though does flare outward distally and
11 taper proximally (Fig. 8C). This ventral flaring is mostly medial with minor lateral expansion,
12 likely reflecting medial deflection of the distal terminus of the suprastapedial process
13 combined with a minimal degree of distal expansion of this process. However, the distalmost
14 portion of the suprastapedial process was sheared off during excavation of the specimen (see
15 unfinished surface in Fig. 8D), so its exact morphology is unclear. The proximal tapering of
16 this quadrate fragment represents the small preserved remnant of the quadrate shaft. This
17 portion of the quadrate is exceptionally narrow, which if anatomically accurate would be
18 quite unique among mosasaurs; however, the highly fragmentary nature of this element
19 makes confident interpretation of the quadrate shaft morphology in its entirety impossible.

20 The alar concavity on the lateral surface is smooth and flat, curving tightly
21 dorsolaterally to give rise to the quadrate ala around its rim (Fig. 8A). The quadrate ala is
22 mostly broken off, though what is preserved is quite thin. The dorsal extent of the stapedial
23 notch is present and is smoothly and tightly curved, measuring about 0.8 cm in width (Fig.
24 8A–B, D). The stapedial pit overlies the stapedial notch anteromedially at the junction
25 between the suprastapedial process and the quadrate shaft (Fig. 8B, D). It is a relatively

1 narrow oval, measuring approximately 1.2 cm and 0.6 cm along its long and short axes,
2 respectively. Its long axis is oriented parallel to the anterodorsal border of the stapedial notch
3 (Fig. 8D).

4 Several of the features noted above are similar to the quadrate morphology of
5 *Selmasaurus*. For example, a medially excavated suprastapedial process and corresponding
6 narrow dorsal surface are also present in the holotypes of *S. russelli* and *S. johnsoni* and in
7 quadrates referred to *Selmasaurus* sp. (C.S., pers. obs.; see also Konishi 2008; Polcyn &
8 Everhart 2008:fig. 6). In *Selmasaurus*, the suprastapedial and infrastapedial processes are in
9 broad contact (Konishi 2008), with both processes being medially deflected. This medial
10 deflection also occurs in the suprastapedial process of MHNM.KHG.1231; however, the
11 infrastapedial process is not preserved and so this contact is impossible to assess.
12 Furthermore, in *Selmasaurus*, the suprastapedial process simply tapers to a blunt terminus,
13 without the distal expansion that appears to be present in MHNM.KHG.1231. A
14 synapomorphy of the genus *Selmasaurus* is the presence of a distinct lateral deflection
15 midway along the length of the quadrate shaft, a condition also present in *Taniwhasaurus*
16 *antarcticus* (Novas, Fernández, Gasparini, Lirio, Nuñez & Puerta, 2002) and certain species
17 of *Plioplatecarpus* (e.g., *Plioplatecarpus houzeaui* Dollo, 1889b) (C.S., pers. obs.; see also
18 Konishi 2008; Fernandez & Martin 2009). Again, the incomplete nature of the quadrate of
19 MHNM.KHG.1231 makes this feature impossible to assess in this specimen. Therefore,
20 although what little is left of the quadrate in MHNM.KHG.1231 is broadly similar to the
21 morphology of *Selmasaurus*, the degree of incompleteness of this specimen limits the extent
22 of comparisons that can be made and synapomorphies evaluated.

23

24 **[Insert Figure 8 here as a single-column (82 mm width) figure]**

25

1 **Vomer.** The vomers in MHNM.KHG.1231 are long, splint-like bones that extend from the
2 midpoint of the main body of the palatine to the posterior extent of the premaxilla, lying
3 medially to and in close contact with the lingual shelves of the maxillae for most of their
4 length, thus forming a nearly solid bony palate (Figs 3, 4).

5 The vomer-palatine suture is well-preserved. The posterior terminus of the vomer
6 articulates with the anteromedial corner of the main palatine body (Figs 3A, 4C). The lateral
7 border of the vomer then curves medially to form the rounded posteromedial corner of the
8 internal naris (Figs 3, 4C). From this point onward, the lateral margin of the vomer extends
9 straight anteriorly toward its contact with the premaxilla (Figs 3, 4A–B). Medially, the
10 vomers articulate with each other along their entire length, forming a straight anteroposterior
11 suture along the midline of the palate (Figs 3, 4). As the snout thins anteriorly, so too do the
12 vomers, becoming narrower and less distinguishable from each other as they approach their
13 anterior articulation with the vomerine processes of the premaxilla (Figs 3, 4A). The ventral
14 oblique crest of the left vomer extends farther ventrally than that of the right vomer, due to
15 displacement of the palate.

16 Anterior to the disarticulated humerus – which obscures part of the posterior palate –
17 a small splint of bone is present lateral to the right vomer (Figs 3, 4B). This splint lies medial
18 to the fourth, fifth, and sixth tooth positions on the right maxilla. This bone may represent
19 part of the right septomaxilla; alternatively, it may simply be a broken portion of the right
20 vomer. Due to taphonomic distortion of the palate, especially at its anterior extent, it is not
21 possible to definitively discount either of these options.

22 **Palatine.** Due to taphonomic compression of the skull in MHNM.KHG.1231, the skull roof
23 is in direct contact with the palate. The palate is also offset laterally, such that the palatal
24 midline is to the left of the skull roof midline and the right internal naris is in line with the left
25 external naris (Figs 3, 4). The palatal bones themselves are quite well-preserved, including

1 preservation of the articulation between the palatines and vomers (Figs 3, 4C), a contact
2 rarely preserved in mosasaurs (Russell 1967).

3 The palatine in MHNM.KHG.1231 consists of a roughly triangular main body bearing
4 a process projecting anteriorly from the anterolateral corner of its ventral surface (Figs 3, 4C).
5 The vomero-palatine contact creates a diagonal suture running posteromedially from the
6 internal naris to the midpoint of the medial border of the palatine (Fig. 4C). Posterior to this
7 suture, the medial border of the palatine runs almost straight posteriorly (Figs 3, 4C). The
8 palatines possess only a narrow contact with one another medially (Fig. 4C). This separation
9 may be the result of taphonomic distortion, but may alternatively represent where the
10 pterygoids, here not preserved *in situ*, would have articulated medially to the palatines [e.g.,
11 as in *Plesioplatecarpus planifrons* (Cope, 1874), as figured in Konishi & Caldwell (2007):fig.
12 3].

13 As in most mosasaur specimens, the palatine-pterygoid articulation is not preserved
14 (Russell 1967; Konishi & Caldwell 2007). The posterior extent of each palatine is broken,
15 such that the posterior border is transversally straight on the right palatine and curved on the
16 left palatine (Figs 3, 4C).

17 The palatine articulates laterally with the maxilla via an unusually long suture, at least
18 four alveoli long based on the right side, due in part to a long anterolateral process (see
19 below). Posteriorly, the maxilla-palatine contact is directed anteromedially at about 45° in
20 ventral view (Fig. 4C). Anterior to this, the palatine bears a process projecting directly
21 anteriorly and articulating with a groove on the medial surface of the posterior maxilla (Figs
22 3, 4C). This process is about half the length of the main body of the palatine, terminating just
23 anterior to the eleventh maxillary tooth position and forming the posterolateral border of the
24 internal naris (Fig. 4C). The anterior border of the palatine is tightly curved to form the
25 oblong posterior border of the internal naris (Fig. 4C). The ventral surface of the palatine

1 slopes gently dorsally as it anteriorly approaches the internal naris.

2 Due to the taphonomic distortion of the skull roof and palate, as well as the placement
3 of a disarticulated humerus midway along the palate, the anterior extent of the internal nares
4 is unclear. However, based on the left internal naris – the more intact of the internal nares in
5 MHNM.KHG.1231 – the internal nares are teardrop-shaped, tapering anteromedially and
6 extending to at least the ninth maxillary tooth position (Fig. 3). Posteriorly, the internal nares
7 terminate between the eleventh and twelfth maxillary tooth positions (Figs 3, 4C), whereas
8 this posterior termination typically occurs more anteriorly along the tooth row in other
9 mosasaurs. This is particularly true in short-snouted plioplatecarpines such as
10 *Plioplatecarpus primaevus* Russell, 1967 (see Holmes 1996:fig. 2) and *Platecarpus*
11 *tympaniticus* (see Russell 1967:fig. 84). This more anterior termination also occurs in long-
12 snouted taxa such as early-diverging mosasaurines (e.g., BMNH R2946, C.S., pers. obs.). In
13 this latter specimen, the internal nares terminate posteriorly near the thirteenth of its 16–18
14 maxillary teeth and are therefore comparatively more anteriorly placed than those of
15 MHNM.KHG.1231. The internal nares in MHNM.KHG.1231 are thus somewhat retracted
16 compared to other mosasaurs.

17 **Pterygoid.** Both pterygoids are partially preserved in MHNM.KHG.1231 (Fig. 9A–D). The
18 anterior and posterior termini of both pterygoids are broken, such that the pterygoids both
19 terminate anteriorly midway along the tooth row on the main pterygoid body and posteriorly
20 just beyond the divergence between the basisphenoid process and quadrate ramus. The
21 ectopterygoid process is also preserved on both pterygoids (Fig. 9A–D). Both pterygoids are
22 noticeably fractured, with the right pterygoid also being partially obscured laterally and
23 dorsally by two vertebrae (Fig. 9C–D).

24 The main body of the pterygoid tapers to a thin, flat flange that projects laterally from
25 the pterygoid tooth row, causing the tooth row to be medially offset from the pterygoid

1 midline (Fig. 9A–B). Dorsally, the main body extends to form a narrow, rounded ridge that
2 sits directly above the tooth row (Fig. 9B).

3 The ectopterygoid process projects generally transversally, though taphonomic
4 distortion and differences in preservation between the left (Fig. 9A–B) and right (Fig. 9C–D)
5 pterygoids cause subtle differences in morphology and orientation of the respective
6 ectopterygoid processes. The ectopterygoid process tapers anterolaterally, also bearing a
7 posterodistal projection angled posteromedially toward the proximal end of the quadrate
8 ramus of the pterygoid. The posterior border of the ectopterygoid process meets the pterygoid
9 body posterolateral to the posterior terminus of the pterygoid tooth row (Fig. 9A, C). This
10 condition resembles that of *Goronyosaurus nigeriensis*, the holotype of *Platecarpus*
11 *somenensis* Thévenin, 1896, and *Selmasaurus johnsoni* (but unknown in *S. russelli*), in which
12 the base of the ectopterygoid process is also unusually broad (T.K., pers. obs.; see also Soliar
13 1988:fig. 5; Polcyn & Everhart 2008:fig. 4). The former two species also possess a
14 posterodistal projection of the ectopterygoid process, as described above for
15 MHNM.KHG.1231. This projection contacts the quadrate ramus of the pterygoid in *G.*
16 *nigeriensis* but not in *P. somenensis*. This process also appears to contact the quadrate ramus
17 in the left pterygoid of MHNM.KHG.1231 (Fig. 9A–B); however, this contact is likely
18 taphonomic, as the distalmost tip of this projection is deeply broken on the left pterygoid,
19 giving rise to an artificial contact between these processes. The true anatomical configuration
20 would therefore likely resemble that of *P. somenensis*, with the posterodistal projection of the
21 ectopterygoid process approaching but not contacting the quadrate ramus, as seen in the right
22 pterygoid of MHNM.KHG.1231 (Fig. 9D).

23 The basisphenoid process and quadrate ramus begin to diverge slightly posterior to
24 the pterygoid tooth row. This divergence is visible dorsally, as the dorsally-rounded surfaces
25 of these processes extend posteriorly from the main pterygoid body, forming ridges that

1 border a progressively deepening sulcus (Fig. 9B, D). About 5 cm posterior to the
2 posteriormost pterygoid tooth – a distance equivalent to approximately three pterygoid tooth
3 positions – this sulcus gives way to a complete divergence between these processes. The
4 basisphenoid process projects directly posteriorly from the main pterygoid body, with the
5 quadrate ramus projecting laterally at a 45° angle (Fig. 9B, D). The dorsal surface of the
6 basisphenoid process is smoothly rounded, whereas the quadrate ramus bears a thin groove
7 lateral to its dorsal midline. The ventral surface of the quadrate ramus is uniformly smooth,
8 whereas the basisphenoid process bears a narrow, rounded ridge along the medial border of
9 its ventral surface.

10 The pterygoid tooth row preserves six tooth positions (Fig. 9A, C). A separate
11 fragment of the anterior pterygoid tooth row is present in a block containing two vertebrae
12 (Fig. 9E–F), though it is uncertain to which pterygoid this fragment belongs. Only four
13 pterygoid tooth crowns are preserved: two on the separated fragment and two on the right
14 pterygoid at the fifth- and sixth-posteriormost tooth positions (Fig. 9C, E). These teeth exhibit
15 narrow plicae, similar to the marginal dentition. The pterygoid teeth are much more recurved
16 and much smaller than the marginal teeth, an expected condition for plioplatecarpines among
17 russellosaurines. The tooth row itself is straight; the anteriormost teeth preserved on the right
18 pterygoid project ventromedially from the tooth row, but this is clearly the result of
19 taphonomy (Fig. 9C). On the left pterygoid, breakage of the thin flange lateral to the tooth
20 row gives the appearance of the anterior part of the tooth row rising above the level of the
21 ventral surface (Fig. 9A); however, the posterior extent of both the left and right pterygoid
22 tooth rows is unbroken and shows the tooth row to be level with the ventral surface formed
23 by the diverging processes.

24

25

[Insert Figure 9 here as a full-page (173 mm x 232 mm) figure]

1
2
3
4
5
6
7
8
9
10
11
12
13
14
15
16
17
18
19
20
21
22
23
24
25

Mandible

Dentary. Both the left and right dentaries are heavily fractured posteriorly, with several less severe fractures throughout (Fig. 7A–B). The posterior portion of the left dentary is also separated from the rest of the dentary by a large break (Fig. 7A), though whether this break is due to predation or to breakage during excavation of the specimen is indeterminable.

The ventral border of the dentary is horizontal along most of its length, though curves dorsally at the anteriormost tooth position to form the anterior terminus of the dentary, and curves ventrally posterior to the tenth tooth position (Fig. 7A). The ventral border of the dentary is tightly rounded and is thicker anteriorly than posteriorly. The dorsal border of the dentary is flattened to accommodate the tooth row and interdental pits (Fig. 7A). The morphology of the teeth and associated features is described in Description – Dentition.

Medial to the tooth row, the medial parapet of the dentary rises vertically so as to be taller than the lateral surface of the dentary (Figs 6D–F, 7A), a condition otherwise only known to occur in *Plioplatecarpus* (see Konishi & Caldwell 2011). The medial parapet increases in height posteriorly, progressing from covering the ventral one-third of the exposed portion of the dentary tooth roots anteriorly to covering about one-half of the exposed roots of the posterior dentary teeth (Fig. 7A). Replacement tooth pits occur lateral to the medial parapet and posteromedial to their respective tooth positions (Figs 6D–F, 7A).

The lateral surface of the dentary is almost entirely flat, though bulges slightly outward at its anteriormost extent under the first and second tooth positions (Fig. 7A). The height of the dentary increases along its length, such that the height of the posterior terminus is about threefold that of the anterior terminus (Fig. 7A–B). The lateral surface of the dentary bears several foramina marking the exits of the mandibular (V3) branch of the trigeminal nerve (cranial nerve V) (Russell 1967; Fig. 7A). These foramina are the same size as those on

1 the premaxilla and maxilla (Fig. 2). They form three loose anteroposterior rows along the
2 lateral surface of the anterior dentary, below the first four dentary tooth positions (Fig. 7A).

3 The medial surface of the dentary is mostly flat, though bears a deep excavation
4 marking the Meckelian groove (Fig. 7B). This groove runs along the ventral half of the
5 dentary's medial surface, with its anterior terminus under the sixth-antiermost tooth
6 position. The Meckelian groove in MHNM.KHG.1231 thus extends markedly less anteriorly
7 compared to other mosasaurs, in which this groove typically extends almost all the way to the
8 anterior terminus of the dentary [e.g., *Platecarpus tympaniticus*: Russell (1967):fig. 29;
9 *Selmasaurus johnsoni*: Polcyn & Everhart (2008):fig. 7S]. This posteriorly retracted position
10 of the anterior terminus of the Meckelian groove therefore represents an autapomorphy of
11 this species. The Meckelian groove is tallest posteriorly, tapering from a height of 4.7 cm at
12 its posterior terminus to a height of 0.8 cm at its anterior terminus (Fig. 7B). The dorsal
13 margin of the Meckelian groove is horizontal and uniformly inset from the main plane of the
14 medial surface of the dentary (Fig. 7B). In contrast, the ventral margin is inset along the
15 anteriormost one-third of its length, though posterior to this, the Meckelian groove opens
16 directly onto the ventral margin of the dentary (Fig. 7B).

17 **Angular.** The right angular is preserved in articulation with the rest of the right posterior
18 mandibular unit (Fig. 7C–F). The anterior terminus of the angular is broken, so the
19 morphology of the splenial-angular articulating surface is unknown. The angular is much
20 more exposed laterally (Fig. 7C–D) than it is medially (Fig. 7E–F). Laterally, the dorsal
21 border of the angular is parallel to its ventral border and is slightly ventrally concave (Fig.
22 7C–D). In contrast, in medial view the angular tapers sharply posteriorly to form a long, thin
23 sliver of bone that underlies the articular-prearticular (Fig. 7E–F). The angular extends
24 posteriorly much farther than is typical of mosasaurs [e.g., *Platecarpus tympaniticus*: Russell
25 (1967):fig. 29], terminating below the glenoid fossa, just anterior to a posteroventral flange

1 on the articular that likely represents a crushed and distorted retroarticular process (Fig. 7E–
2 F).

3 **Surangular.** The surangular is quite fragmented, especially anteriorly (Fig. 7C–F). The
4 dorsal border of the surangular is straight with a slight posterodorsal bump marking the
5 anterodorsal portion of the glenoid fossa. In lateral view the surangular becomes taller
6 anteriorly, consistent with the anterior dorsoventral expansion of the overall posterior
7 mandibular unit (Fig. 7C–D). Posteriorly, the surangular meets the articular at the middle of
8 the glenoid fossa (Fig. 7E–F). The medial surface of the surangular is slightly thickened near
9 its posterodorsal corner, delimiting the anteromedial border of the glenoid fossa. The suture
10 between the surangular and articular-prearticular is marked by a deep groove on the medial
11 surface of the posterior mandibular unit (Fig. 7E–F); such a groove is lacking on the lateral
12 surface, with the sutures between the surangular and surrounding elements being much less
13 pronounced (Fig. 7C–D).

14 **Articular-Prearticular.** The anterior extent of the prearticular is long and narrow,
15 underlying most of the surangular (Fig. 7E–F). The surangular-prearticular suture is strongly
16 grooved medially, representing the adductor fossa, though taphonomically compressed (Fig.
17 7F). The prearticular bears a pronounced ridge ventral to the anterior half of this suture, with
18 the surangular bearing a similar – though less pronounced – ridge on its ventral border at the
19 same position (Fig. 7F). Posteriorly, the dorsal border of the prearticular curves
20 posterodorsally at a 50° angle relative to its flat anterodorsal border as it gives way to the
21 articular (Fig. 7E–F). The surangular-articular suture terminates dorsally within the glenoid
22 fossa (Fig. 7C–F). This suture is marked by a medial thickening of the articular at the
23 posterior border of the glenoid fossa, causing the posteroventral corner of the surangular to be
24 inset relative to the articular (Fig. 7F). The dorsal border of the articular is relatively straight
25 and dips at a slight posteroventral angle. The posterior extent of the articular is relatively

1 complete except for a displaced flange preserved at its posteroventral corner, possibly
2 representing a taphonomically deformed and displaced retroarticular process (Fig. 7C–F).

3 **Postcranial**

4 **Vertebrae.** Three complete though disarticulated and distorted vertebrae are preserved, as
5 well as one highly crushed vertebral centrum (Fig. 9C–F). The synapophyses of each vertebra
6 project horizontally at a slight posterior angle, though the exact angle varies among the
7 vertebrae due to taphonomic distortion (Fig. 9C–F). The articular facet of each
8 synapophysis is a depressed oval distinctly shorter than the centrum height, suggesting a
9 position in the anterior to intermediate cervical region (Russell 1967). Two of the vertebrae
10 possess prominent hypapophyses (Fig. 9C, vertebra on the left; Fig. 9E), consistent with this
11 possible anterior cervical position. However, the other vertebra (Fig. 9D, vertebra on the left)
12 instead possesses a pair of haemapophyses, one intact and the other mostly sheared off (Fig.
13 9D). The presence of these haemapophyses, in conjunction with the narrower, taller, and less
14 concave and convex (i.e., flatter) vertebral centrum, suggests that this is a caudal vertebra.

15 The neural spine of each vertebra is slightly more than twice the height of the
16 centrum, though all are broken at their dorsal extent (Fig. 9C–F). Each neural spine projects
17 from the centrum at about a 20° posterodorsal angle. The pre- and postzygapophyses are
18 particularly well preserved in one of the vertebrae (Fig. 9E–F). On this vertebra, the
19 prezygapophysis projects at a slight anterolateral and upturned angle from the lateral border
20 of the neural arch (Fig. 9E). The postzygapophyses are smaller than the prezygapophyses,
21 forming circular tubers that project laterally from the base of the neural spine just dorsal to
22 the neural arch (Fig. 9E–F). The articular facet of each postzygapophysis is directed
23 ventrolaterally (Fig. 9E–F). A small depression is present under one of the postzygapophyses,
24 potentially representing a zyganchium (Fig. 9F). However, the lack of zygosphenes on any of
25 the vertebrae, as well as the breakage of the neural spine of this vertebra, suggest that this

1 feature is the result of taphonomic distortion; it is more likely that this specimen lacks
2 zygantra and zygosphenes.

3 **Humerus.** The right humerus, in extensor view, is preserved on the underside of the palate
4 (Figs 3, 4B, 9G). Due to the fragility of the palate, the humerus was not removed. Breakage
5 and abrasion to the humerus obscure the position of muscle attachment scars. The length and
6 distal width of the humerus are essentially equal, with the length measuring 8.6 cm and the
7 distal width measuring 9.0 cm (Fig. 9G). The distal end of the humerus is expanded relative
8 to the proximal end, similar to the condition in *Platecarpus* (Russell 1967; Fig. 9G). Both the
9 entepicondyle and ectepicondyle are present (Fig. 9G). Though both processes are broken,
10 the portions that are preserved indicate that the ectepicondyle was likely larger and more
11 laterally prominent than the entepicondyle. Both processes extend from the distal border of
12 the humerus to about midway along the humerus shaft. The shaft itself is smoothly concave
13 along its preaxial and postaxial borders (Fig. 9G). The extensor surface of the shaft is gently
14 constricted along its longitudinal axis, resulting in a slight ridge extending along this surface
15 from the proximal to distal ends of the humerus (Fig. 9G). This long ridge is not typical of
16 plioplatecarpines, though the thin cracks bordering this ridge suggest that it may be
17 taphonomically exaggerated in MHNM.KHG.1231 (Fig. 9G). The proximal end of the
18 humerus is mediolaterally deeper than the comparatively compressed distal end. The
19 proximal end exhibits a spongy texture, indicating the presence of a cartilage cap, similar to
20 the condition in *Platecarpus* and *Tylosaurus* (Russell 1967). As such, specific features such
21 as the postglenoid process and the glenoid condyle are not preserved.

22

23 **Phylogenetic Analysis**

24

25 **Multistate coding scheme – Unweighted maximum parsimony analysis (Mu-UMP)**

1 Unweighted maximum parsimony analysis of the dataset using a multistate coding
2 scheme recovered 26 most parsimonious trees (MPTs) of 464 steps (consistency index [CI] =
3 0.34913793, retention index [RI] = 0.70304818). A strict consensus tree was generated from
4 these optimal trees (Fig. S5A). For improved resolution, a 50% majority rule consensus tree
5 was also generated (Fig. S5B).

6 **Multistate coding scheme – Implied weighting maximum parsimony analysis (Mu-**
7 **IWMP)**

8 Implied weighting maximum parsimony analysis of the dataset using a multistate
9 coding scheme and a k -value of 3.0 recovered one MPT of 468 steps (fit = 46.630811, CI =
10 0.34615385, RI = 0.69911504) (Fig. 10A). Implied weighting analyses using k -values of 7.0
11 (Fig. 7B) and 11.0 (Fig. 7C) each recovered one MPT of 465 steps (CI = 0.3483871, RI =
12 0.7020649), with fit values of 28.187371 and 20.361057, respectively. This analytical
13 approach produced the trees with the highest resolution (i.e., a single MPT for each k -value).
14 Each k -value also recovered the same topology within Mosasauridae, except within the
15 Mosasaurinae.

16 **Contingent coding scheme – Unweighted maximum parsimony analysis (Co-UMP)**

17 Unweighted maximum parsimony analysis of the dataset using a contingent coding
18 scheme recovered 112 MPTs of 468 steps (CI = 0.34615385, RI = 0.70520231). Strict
19 consensus and 50% majority rule consensus trees were generated from these optimal trees
20 (Fig. S6).

21 **Contingent coding scheme – Implied weighting maximum parsimony analysis (Co-**
22 **IWMP)**

23 Implied weighting maximum parsimony analysis of the dataset using a contingent
24 coding scheme and a k -value of 3.0 recovered two MPTs of 472 steps (fit = 48.300075, CI =
25 0.34322034, RI = 0.70134875). A strict consensus tree was generated from these optimal

1 trees (Fig. S7A). Analysis using a k -value of 7.0 (Fig. S7B) recovered one MPT of 468 steps
2 (fit = 29.016181, CI = 0.34615385, RI = 0.70520231). Analysis using a k -value of 11.0
3 recovered two MPTs of 468 steps (fit = 20.889202, CI = 0.34615385, RI = 0.70520231),
4 from which a strict consensus tree was generated (Fig. S7C).

5

6 **[Insert Figure 10 here as a full-page (173 mm x 232 mm) figure]**

7

8 **Topology**

9 All of the phylogenies recovered generally similar topologies, with the major
10 differences among them resulting from variation in resolution. A detailed comparison of the
11 various phylogenies is provided in the Supplementary Material (§S8). We herein focus on the
12 phylogenetic relationships within the Plioplatecarpinae (Fig. 10D), as this is the subfamily in
13 which MHNM.KHG.1231 was consistently recovered in all analyses (Figs 10, S5–7).

14 The Plioplatecarpinae exhibited a highly variable topology across different analyses,
15 with polytomies greatly reducing internal resolution in the Mu-UMP consensus trees (Fig.
16 S5) and essentially collapsing this clade in the Co-UMP strict consensus tree (Fig. S6A). That
17 being said, certain aspects of its internal topology were fairly consistent across the different
18 analytical conditions. The clade (*Latoplatecarpus* (*Plioplatecarpus*, *Platecarpus*
19 *tympaniticus*)) was recovered in every analysis, contra Konishi & Caldwell (2011) (Figs 10,
20 S5–7). In the Mu-IWMP (Fig. 10), Co-UMP majority rule consensus (Fig. S6B), and Co-
21 IWMP (Fig. S7) trees – i.e., all of the trees in which the Plioplatecarpinae were monophyletic
22 and fully resolved – *Ectenosaurus* was the earliest-diverging taxon, followed by
23 *Plesioplatecarpus planifrons*. In the Mu-IWMP trees (Fig. 10), this was followed by
24 (*Latoplatecarpus* (*Plioplatecarpus*, *P. tympaniticus*)), then *Angolasaurus* as the sister group
25 to a clade consisting of (*Goronyosaurus* (*Selmasaurus johnsoni* (*S. russelli*,

1 MHNM.KHG.1231)); in the contingent trees (Figs S6B, S7), the positions of
2 (*Latoplatecarpus* (*Plioplatecarpus*, *P. tympaniticus*)) and *Angolasaurus* were switched.

3 This *Goronyosaurus*–*Selmasaurus*–MHNM.KHG.1231 clade is of particular interest
4 for this study, as MHNM.KHG.1231 represents the species of interest, *Gavialimimus*
5 *almaghribensis*, gen. et sp. nov. This clade is supported by the following synapomorphies:
6 highly constricted parietal; sides of the frontal in front of the orbits relatively straight. It was
7 recovered in 93% of the MPTs in the Co-UMP majority rule consensus tree (Fig. S6B) and in
8 all of the IWMP trees (Figs 10, S7). Polytomies collapsed this clade in the Mu-UMP and Co-
9 UMP strict consensus tree (Figs S5A, S6A). Interestingly, the Mu-UMP majority rule
10 consensus tree (Fig. S5B) recovered *G. nigeriensis* as sister to (*Latoplatecarpus*
11 (*Plioplatecarpus*, *Platecarpus tympaniticus*)).

12 *Gavialimimus almaghribensis* was recovered as the sister to *Selmasaurus russelli* in
13 100% of the MPTs in the Mu-UMP majority rule consensus tree (Fig. S5B) and 91% of the
14 MPTs in the Co-UMP majority rule consensus tree (Fig. S6B). This sister-group relationship
15 was also recovered in the Mu-IWMP trees (Fig. 10) and Co-IWMP trees (Fig. S7). *G.*
16 *almaghribensis* and *Selmasaurus* share several synapomorphies from the multistate and
17 contingent datasets, comprising: parietal table elongate, triangular to subrectangular, and
18 highly medially constricted, with a distinct mid- or parasagittal crest anterior to the
19 divergence of the suspensorial rami (character 18/20 in the multistate and contingent
20 character lists, respectively); frontal not invaded by posterior end of nares (character 9/10);
21 and lack of a frontal midline dorsal keel (character 10/11). These taxa also share a distinct
22 broad excavation of the medial surface of the quadrate suprastapedial process (Konishi 2008;
23 Fig. 8). *G. almaghribensis* further shares the following synapomorphies with *S. russelli*:
24 pineal foramen ventral opening surrounded by a rounded, elongate ridge (character 21/23);
25 and pineal foramen large (character 19/21). Note that, although this latter character state does

1 occur in most other plioplatecarpines, it does not occur in *S. johnsoni*, thus distinguishing *S.*
2 *russelli* and *G. almaghribensis* from *S. johnsoni*.

3

4 **Discussion**

5

6 **Rejection of ‘*Platecarpus*’ *ptychodon***

7 The diagnosis for ‘*Platecarpus*’ *ptychodon* is as follows (translated from Arambourg
8 1952):

9 “*Platecarpus* (?) with teeth that are relatively low and broad at the base of the crown,
10 slightly compressed with wide edges and no serrations along the symphyseal and
11 commissural borders; the lingual and labial faces are ornamented with numerous
12 irregular vertical plicae extending 2/3 of the tooth’s height from the neck.”

13 The teeth of MHNM.KHG.1231 match this diagnosis, suggesting referral of this specimen to
14 ‘*P.*’ *ptychodon*. However, although the teeth of ‘*P.*’ *ptychodon* were considered by
15 Arambourg (1952) – and thus by subsequent workers (e.g., Bardet *et al.* 2000; Bardet *et al.*
16 2018) – to be highly diagnostic, their putatively unique features are also present in the teeth
17 of other mosasaur species, such as *Platecarpus somenensis* (Fig. 11). Given that this latter
18 species was named in 1896, well before the creation of ‘*P.*’ *ptychodon* in 1952, ‘*P.*’
19 *ptychodon* is therefore not a valid species, as its diagnosis and holotype, represented by a
20 single isolated tooth (Fig. 11A), are insufficient in distinguishing it from the already-
21 established *P. somenensis* (Fig. 11G–I).

22 The teeth of ‘*Platecarpus*’ *ptychodon* also resemble those of *Prognathodon solvayi*
23 (Fig. 11J–L), *Tylosaurus ivoensis* (Persson, 1963) (see Lindgren & Siverson 2002:fig. 4),
24 *Taniwhasaurus* (see Caldwell *et al.* 2008:fig. 5), and some specimens of *Mosasaurus*
25 *lemonnieri* Dollo, 1889b (Fig. 11M–O). However, a feature distinguishing the teeth of ‘*P.*’

1 *ptychodon* from the mosasaurines *Prognathodon solvayi* and *Mosasaurus lemonnieri* is the
2 presence of slight crenulations or serrations in the enamel along the carinae of mosasaurine
3 teeth, best visible in histological thin section. Importantly, though, these crenulations are
4 largely limited to the replacement teeth in mosasaurines, being worn down very quickly in
5 functional teeth (A. LeBlanc., pers. comm.). Therefore, even this feature is unreliable as the
6 sole basis for distinguishing taxa such as those listed above. *M. lemonnieri* and *Pr. solvayi*
7 thus also exemplify already-established species with which the holotype of '*P.*' *ptychodon*
8 may be confounded. Furthermore, no plioplatecarpine – including '*P.*' *ptychodon* and
9 *Platecarpus somenensis* – has been observed to possess these crenulations (Bell 1997; A.
10 LeBlanc, pers. comm.). As such, '*P.*' *ptychodon* remains indistinguishable from
11 plioplatecarpines such as *P. somenensis* regarding both histological and coarser-scale
12 morphology.

13 Indeed, although *Mosasaurus lemonnieri*, *Platecarpus somenensis*, *Prognathodon*
14 *solvayi*, *Tylosaurus ivoensis*, *Taniwhasaurus*, and MHNM.KHG.1231 are clearly different
15 taxa, their teeth overlap so greatly in morphology that the '*Platecarpus*' *ptychodon* type
16 material and similar isolated teeth often cannot be referred to a single species; this tooth
17 morphology is ultimately entirely non-diagnostic (Fig. 11). As cautioned by various authors
18 (e.g., Massare 1987; LeBlanc *et al.* 2012), tooth morphology in general is highly susceptible
19 to convergence; as such, diagnosing a taxon based solely on such a homoplastic feature is a
20 fundamentally unreliable taxonomic approach. '*P.*' *ptychodon* is thus a *nomen dubium*, as its
21 type material is indeterminate and lacks any autapomorphic features distinguishing it from
22 already-named species [see ICZN 4e, Glossary and Article 75.5 (International Commission
23 on Zoological Nomenclature 1999); see also e.g., Coombs (1990) and Modesto (1996) for
24 similar designations of other taxa as *nomina dubia* based on non-diagnostic type material]. As
25 a consequence of this invalidity, all specimens that have since been referred to '*P.*' *ptychodon*

1 no longer bear this designation and therefore must be re-examined for correct referral to a
2 valid species. Ultimately, because '*P.*' *ptychodon* is not a valid species, MHNM.KHG.1231 is
3 free to be assigned as the holotype of a new taxon.

4

5 **[Insert Figure 11 here as a single-column (82 mm x 232 mm) figure]**

6

7 **Phylogenetic relationships of *Gavialimimus almaghribensis***

8 Before discussing the phylogenetic relationships of *Gavialimimus almaghribensis*, it
9 is important to first assess the various analytical approaches presented above. From a
10 theoretical viewpoint, we prefer implied weighting to unweighted parsimony analyses
11 because of the ability of implied weighting analyses to reduce the impact of homoplasy on
12 phylogenetic reconstruction (Goloboff 1993; Goloboff *et al.* 2008a; Simões *et al.* 2017b). We
13 also prefer multistate character coding schemes, rather than contingent schemes, because of
14 their treatment of dependent characters as a single transformational series (Simões *et al.*
15 2017a; Simões *et al.* 2017b). This theoretical background was ultimately supported by our
16 results: of all the analyses presented above, the Mu-IWMP analyses (Fig. 10) produced the
17 trees with the highest resolution and among the lowest number of steps (465, second only to
18 the Mu-UMP trees with 464 steps). For these methodological and empirical reasons, this is
19 our preferred analysis (Fig. 10).

20 The recovered *Goronyosaurus–Selmasaurus*–MHNM.KHG.1231 clade also warrants
21 further discussion. As noted above in Phylogenetic Analysis – Topology, the latter two
22 genera share several synapomorphies, raising the possibility that MHNM.KHG.1231 should
23 be assigned to *Selmasaurus* rather than a new genus. However, because of the many
24 autapomorphies of MHNM.KHG.1231, doing so would result in quite a high degree of
25 intrageneric variation within *Selmasaurus*. MHNM.KHG.1231 also differs temporally from

1 *Selmasaurus*, occurring in the upper Maastrichtian at least 9 million years after the upper
2 Santonian–lower Campanian distribution of *S. russelli* (Wright & Shannon 1988; Kiernan
3 2002; Liu 2007; Konishi 2008; Ogg *et al.* 2012) and at least 13 million years after the lower
4 Santonian range of *S. johnsoni* (Polcyn & Everhart 2008; Ogg *et al.* 2012). For these reasons,
5 although MHNM.KHG.1231 is in many ways morphologically similar to *Selmasaurus* and
6 was recovered herein as nested within this genus, we have concluded that it is sufficiently
7 different in various aspects to warrant the establishment of a new genus.

8 Furthermore, both *Goronyosaurus* and *Selmasaurus* are known from only a few
9 specimens, a level of incompleteness which makes assessing possible synapomorphies with
10 MHNM.KHG.1231 difficult (see below). As more specimens of these taxa are discovered
11 and more of their anatomy becomes known, it is quite possible that the exact phylogenetic
12 relationships hypothesized herein for this clade may change. Specifically, although
13 MHNM.KHG.1231 nests within *Selmasaurus* in the current analysis (Fig. 10), future
14 phylogenies may recover a different topology. This is especially likely given the overall
15 uncertainty surrounding mosasaur phylogenetics (e.g., Simões *et al.* 2017b); indeed, even
16 across our analyses, different methodological approaches produced disparate phylogenies,
17 including within the Plioplatecarpinae (Figs 10, S5–7). Therefore, although our assignment of
18 MHNM.KHG.1231 to a new genus renders *Selmasaurus* paraphyletic under the current
19 phylogeny (Fig. 10), we do not consider this a major concern, nor a valid impetus for
20 modifying the taxonomic status of MHNM.KHG.1231 or of either existing *Selmasaurus*
21 species.

22 *Goronyosaurus* was recovered as basal to *Selmasaurus* within this *Goronyosaurus*–
23 *Selmasaurus*–*Gavialimimus* clade; however, it does share certain features with *Gavialimimus*
24 *almaghribensis*, including highly retracted external nares, a distinctly elongated snout, deep
25 interdental pits, and a high number of premaxillary foramina (C.S., pers. obs; see also

1 Azzaroli *et al.* 1972; Soliar 1988; Lingham-Soliar 1991). These features are unknown in *S.*
2 *russelli*, as the related elements are not preserved in specimens of this taxon. However, these
3 elements are preserved in *S. johnsoni*, revealing the aforementioned features to be absent in
4 this latter species. This is potentially indicative of a closer relationship between
5 *Goronyosaurus* and *Ga. almaghribensis* than recovered in this phylogenetic analysis.

6 However, this possible affiliation remains equivocal. For example, interdental pits
7 were described by Lingham-Soliar (1991) as the defining characteristic of the genus
8 *Goronyosaurus*, but have since been noted to varying extents in several mosasaurines and
9 were listed by LeBlanc *et al.* (2012) as a diagnostic feature of the Mosasaurini; as such, this
10 characteristic by itself does not inherently necessitate referral of *Ga. almaghribensis* as a
11 close relative of *Goronyosaurus*. Furthermore, although snout elongation and external narial
12 retraction are diagnostic of both *Goronyosaurus* and *Ga. almaghribensis*, they are not
13 necessarily synapomorphic for these taxa. Both of these features result from the modification
14 of several constituent elements, such as the premaxilla, maxillae, vomers, palatines, frontal,
15 and prefrontals. As such, although the gross morphology of these taxa may be similar, the
16 underlying components and modifications giving rise to that morphology may not be
17 homologous (Caldwell *et al.* 1995; Caldwell 2012; Simões *et al.* 2017a). As a hypothetical
18 example, snout elongation could incorporate elongation of the vomers in one taxon but
19 elongation of the vomerine processes of the palatines in the other taxon. In order to properly
20 assess the phylogenetic significance of this similarity, these overall conditions cannot be
21 treated in terms of gross morphology; rather, the homology of each separate component of
22 these integrated structures must be assessed independently (Caldwell *et al.* 1995; Caldwell
23 2012; Simões *et al.* 2017a). However, the poor quality of preservation of the only known
24 articulated *Goronyosaurus* skull (IGF 14750) severely hinders our ability to make such
25 precise anatomical comparisons, leaving the potential homology of these conditions

1 equivocal.

2 Indeed, the interrelationships among *Goronyosaurus*, *Selmasaurus*, and *Gavialimimus*
3 *almaghribensis* are further complicated by the fragmentary nature of existing *Selmasaurus*
4 material. For example, because snout elongation and narial retraction are not preserved in the
5 holotype of *S. russelli*, it is difficult to determine whether these features are unique to
6 *Goronyosaurus* and *Ga. almaghribensis* only or are more broadly characteristic of this
7 overall clade. Of note, however, the degree of narial retraction can be assessed in the
8 holotype of *S. johnsoni*, whose naris begins very anteriorly above the level of the third
9 maxillary tooth (T.K., pers. obs.). Based on this observation, at least the overall condition of
10 narial retraction appears unique to *Goronyosaurus* and *Ga. almaghribensis* based on currently
11 available specimens; importantly, though, the above arguments regarding homology
12 assessments for complex morphologies still apply to this condition, and the condition in *S.*
13 *russelli* remains unknown. Similarly, because the posterior portion of the parietal of *G.*
14 *nigeriensis* is not sufficiently preserved in any currently available specimens, it is uncertain
15 whether the parietal constriction present in *G. nigeriensis* matches the condition described by
16 character 18/20 above and uniting *Ga. almaghribensis* and *Selmasaurus*; i.e., parietal
17 constriction in general is a synapomorphy of the *Goronyosaurus–Selmasaurus–Gavialimimus*
18 clade, but the specific condition of the parietal as conveyed by our dataset is restricted to the
19 latter two genera.

20 A final intriguing feature involves the ectopterygoid process of the pterygoid. As
21 noted above (see Description – Pterygoid), this process has an unusually broad base in
22 *Selmasaurus johnsoni*, *Goronyosaurus nigeriensis*, the holotype of *Platecarpus somenensis*,
23 and *Gavialimimus almaghribensis*. Furthermore, the latter three taxa possess a posterodistal
24 projection on this process, which contacts the quadrate ramus of the pterygoid in *G.*
25 *nigeriensis* but not the latter two taxa. The presence of this projection again suggests a

1 possible closer relationship between *Goronyosaurus* and *Ga. almaghribensis* than recovered
2 herein, with the similarity of this feature in *P. somenensis* bringing yet another poorly-known
3 taxon into the mix. However, a rigorous assessment of this condition would require detailed
4 re-analysis of both the *Goronyosaurus* and *P. somenensis* holotype material, which falls
5 outside the scope of this study. Furthermore, the *Goronyosaurus* type material is quite poorly
6 preserved as previously noted, with much of the subsequently referred material possibly
7 being chimaeric in nature.

8 Unfortunately, the aforementioned uncertainties regarding the anatomy and
9 phylogeny of these taxa can only be remedied with the discovery of more complete
10 specimens. In all, although *Goronyosaurus* and *Gavialimimus almaghribensis* do share
11 several intriguing cranial similarities, these similarities do not provide conclusive evidence of
12 a closer evolutionary relationship between these taxa than that recovered in this study's
13 phylogenetic analyses, and at this point do not necessitate referral of MHNM.KHG.1231 to
14 the genus *Goronyosaurus*. However, the presence of such similarities – including some
15 shared with the equally enigmatic *Platecarpus somenensis* – underlines the need for further
16 research into the relationships and morphologies of these taxa.

17 **Palaeoecology and functional morphology**

18 Massare (1987) divided Mesozoic marine reptiles into seven gradational predatory
19 guilds based on tooth morphology, emphasizing shape of the tooth apex, type of tooth wear,
20 presence of carinae or cutting edges, and shape and size of the tooth crown. These guilds
21 unite taxa based on primary prey preference, regardless of phylogenetic placement. The three
22 'end member' guilds are: 'Pierce I', consisting of taxa with long, slender, pointed teeth used
23 to pierce soft-bodied prey items; 'Cut', containing taxa with robust, pointed, carinated teeth
24 used to rip the flesh of large marine vertebrates; and 'Crush', consisting of taxa with robust,
25 blunt teeth used to crush thick-shelled invertebrates (Massare 1987; Fig. 12). The other

1 guilds, which bridge these end-point morphotypes, are ‘Pierce II’, ‘Smash’, ‘Crunch’, and
2 ‘General’ (Massare 1987; Fig. 12).

3 In a palaeoecological analysis of niche partitioning within the Maastrichtian
4 phosphates of Morocco, Bardet *et al.* (2015) modified this system, adding a new guild,
5 ‘Crush-Cut’ (Fig. 12). These authors included ‘*Platecarpus*’ *ptychodon* in their analysis
6 (Bardet *et al.* 2015). Although we reject this species as a *nomen dubium* (see preceding
7 discussion), the teeth used by Bardet *et al.* (2015) in their analysis are morphologically
8 equivalent to those of *Gavialimimus almaghribensis* (see preceding discussion and Fig. 11).
9 As such, these authors’ conclusions regarding the ‘*P.*’ *ptychodon* morphotype can be
10 extrapolated to *Gavialimimus*, as they should be also to the other taxa depicted in Figure 11.
11 Though these authors assigned ‘*P.*’ *ptychodon* to a combination of the ‘Pierce II’ and ‘Cut’
12 guilds, reflecting a diet of cephalopods and fishes (Bardet *et al.* 2015), new information from
13 the *G. almaghribensis* holotype allows refinement of this interpretation.

14 The narrow, highly elongate snout and interlocking teeth of *Gavialimimus*
15 *almaghribensis* are convergent with the condition in gharials, a distinctive taxon of
16 longirostrine crocodylians. In gharials, this morphotype reflects predation on rapidly moving
17 fish, with the interlocking teeth entrapping highly agile prey and the narrow snout reducing
18 drag and displacement of water as the head swings laterally and the jaws snap shut (McHenry
19 *et al.* 2006; Pierce *et al.* 2008; Cuff & Rayfield 2013; McCurry *et al.* 2017). Several aspects
20 of the cranial morphology of *Gavialimimus* also converge upon that of the derived
21 mosasaurine *Plotosaurus*, such as the elongate snout (though this longirostry is far more
22 pronounced in *Gavialimimus*), interlocking teeth, and reduced cranial kinesis, especially
23 along extensively articulating frontoparietal and prefrontal-postorbitofrontal sutures (LeBlanc
24 *et al.* 2013). A recent functional analysis of the skull of *Plotosaurus* interpreted these
25 adaptations as evidence of predatory specialization on small, rapid prey, thus contributing

1 toward niche partitioning in the Maastrichtian of California (LeBlanc *et al.* 2013). Finally,
2 although the specific function of the fluted tooth morphology present in *Gavialimimus*
3 remains uncertain, similar fluting occurs convergently in several other mosasaur taxa (Fig.
4 11) and in several piscivorous snakes, such as *Acrochordus* and homalopsids (Vaeth *et al.*
5 1985). The widespread presence of tooth fluting across these taxa suggests that this feature
6 may represent an adaptation for piscivory. Altogether, these convergences with gharials and
7 other piscivorous squamates therefore suggest similar piscivory specialized on rapid, evasive
8 fish.

9 This diet would likely have been composed primarily of teleosts, which underwent an
10 extensive radiation during the late Mesozoic enabled in large part by their more efficient and
11 rapid swimming compared to earlier fishes (Schaeffer 1969; Massare 1988). The radiation of
12 mosasaurs as a whole during the Late Cretaceous has been tied to their ability to predate upon
13 teleosts more effectively than pursuit predators such as ichthyosaurs could (Massare 1988).
14 The unique adaptations of *Gavialimimus* relative to other mosasaurs therefore suggest a
15 scenario of predation-based niche partitioning, with this morphology reflecting a particularly
16 specialized form of piscivory in *Gavialimimus* under this hypothesis.

17 In terms of feeding guilds, this interpretation of predatory behaviour in *Gavialimimus*
18 *almaghribensis* adds detail to the findings of Bardet *et al.* (2015). Although these authors
19 assigned the morphologically-equivalent teeth of '*Platecarpus*' *ptychodon* to the 'Pierce II'–
20 'Cut' guilds, Massare (1987) describes the 'Cut' morphoguild as reflecting predation upon
21 large marine vertebrates, a diet that would cause significant breakage and wear to the teeth
22 (Massare 1987). This wear would logically occur along the entire tooth row, which is not the
23 case in *G. almaghribensis*. Instead, this specimen displays very minimal tooth wear anteriorly
24 on the tooth row (Fig. 6A–B), with this wear only becoming prominent on the posterior teeth
25 (Figs 4B–C, 6C). This minimal anterior tooth wear is more consistent with the 'Pierce I' or

1 'Pierce II' feeding guilds. Rather than being an indication of specific diet, the progressive
2 increase in wear posteriorly is largely an expected consequence of adductor muscle
3 attachment on the posterior mandible and resultant distribution of force along the jaws while
4 biting (e.g., see Callison 1967; Russell 1967). Extensive tooth replacement would also be
5 necessary to cope with the considerable breakage described by Massare (1987) for members
6 of the 'Cut' guild; in *G. almaghribensis*, however, tooth replacement is quite minimal, with
7 replacement teeth visible at only three positions on the maxillae and dentaries (Figs 3, 6, 7).
8 Finally, although the teeth of *G. almaghribensis* do possess carinae, which Massare (1987)
9 uses to characterize the 'Cut' guild, these cutting edges could reasonably have aided in
10 capturing and killing evasive prey and therefore are not automatically indicative of
11 membership in the 'Cut' guild.

12 Re-interpretation of cranial features also present in *Goronyosaurus* further supports
13 removal from the 'Cut' guild. In a biomechanical analysis of the skull of *Goronyosaurus*,
14 Lingham-Soliar (1999) discussed two possible feeding methods for this taxon based on
15 cranial morphology: predation upon small and evasive organisms, or predation upon larger
16 prey items involving the need for processing prior to ingestion. The prognathous condition of
17 the dentary teeth was used as evidence for the former mode, though the majority of cranial
18 adaptations were interpreted as support for the latter. Lingham-Soliar (1999) concluded that
19 this taxon's deep interdental pits and lack of cranial kinesis would have strengthened the skull
20 and enabled tight interlocking of the jaws. Combined with the elongate snout and extensive
21 area for muscle attachment in the posterior skull, these features were interpreted as
22 adaptations for predation on large aquatic vertebrates, comparable to the 'Cut' guild (Massare
23 1987; Lingham-Soliar 1999). These adaptations also occur in *Gavialimimus almaghribensis*,
24 such as the large supratemporal fenestrae which would have accommodated massive jaw
25 adductor musculature (Figs 2, 3), as well as the interlocking frontoparietal suture (Figs 2, 3,

1 5) which would have prevented or minimized movement along this mesokinetic axis (Wright
2 & Shannon 1988; Lingham-Soliar 1999; LeBlanc *et al.* 2013). However, the strong
3 convergence between *G. almaghribensis* and extant gharials suggests re-interpretation of
4 these adaptations.

5 Instead of being used to predate upon large vertebrates, these modifications for
6 powerful closure and interlocking of the jaws are also consistent with a predation style reliant
7 upon rapidly closing the jaws and grasping evasive prey items (see also LeBlanc *et al.* 2013).
8 As suggested by Lingham-Soliar (1999) for *Goronyosaurus*, the recurved and slightly
9 prognathous anterior teeth of *Gavialimimus* could have contributed to this specialized
10 piscivory by directing prey into the mouth (Massare 1987; Lingham-Soliar 1999), where the
11 posterior marginal teeth could then grasp this prey. Finally, as noted above, a similar
12 connection between cranial akinesis and predatory specialization upon small, evasive prey is
13 hypothesized to occur in the long-snouted mosasaurine *Plotosaurus* (LeBlanc *et al.* 2013).
14 These adaptations in *G. almaghribensis* are therefore consistent with a gharial-like
15 specialization on smaller, highly agile aquatic prey.

16 Altogether, the cranial adaptations and dental features of *Gavialimimus*
17 *almaghribensis* reflect membership in the ‘Pierce II’ guild, closer to the ‘Pierce I’ apex than
18 the ‘Cut’ apex (Fig. 12). Although this places *G. almaghribensis* in a similar position to
19 *Halisaurus arambourgi*, the preorbital region of the skull of *G. almaghribensis* represents
20 almost two-thirds of the total skull length (Figs 2, 3), compared to only 50% in *H.*
21 *arambourgi* (Bardet *et al.* 2015). As well, *H. arambourgi* is a halisaurine, for which Konishi
22 *et al.* (2016) reported well-developed binocular vision possibly linked to nocturnal foraging
23 upon small, bioluminescent animals such as 10-armed cephalopods. Unlike in halisaurines,
24 the orbits of *G. almaghribensis* are neither forward facing nor large, therefore not conducive
25 to binocular vision. Thus, based on its extensive snout elongation, alongside its other cranial

1 adaptations, *G. almaghribensis* altogether exhibits increased specialization for piscivory,
2 most likely during the daytime. This proposed ecological niche specialization would make *G.*
3 *almaghribensis* unique among Moroccan mosasaurs, if not mosasaurs as a whole. Under this
4 hypothesis, these adaptations would therefore have allowed *G. almaghribensis* to exploit prey
5 items with reduced or minimal competition from sympatric mosasaur species, enabling its
6 survival in such a diverse ecosystem (Fig. 13).

7
8 **[Insert Figure 12 here as a single-column (82 mm width) figure]**

9

10 **Narial retraction**

11 Pronounced retraction of the openings for the external nares is listed herein as a
12 diagnostic feature of *Gavialimimus almaghribensis*. We interpret this condition as ‘true’
13 narial retraction, in contrast to the traditional concept of ‘posteriorly retracted external nares’
14 as a synapomorphy linking mosasauroids and varanoids (e.g., Rieppel *et al.* 2007; Conrad
15 2008; Conrad *et al.* 2008; Conrad *et al.* 2011). This distinction is important, as this traditional
16 view of ‘narial retraction’ is pervasive in the squamate literature (e.g., the global squamate
17 dataset of Conrad 2008, and all phylogenies derived therefrom) and has long played a key
18 role in shaping perceptions of mosasaur evolution and phylogenetics (Caldwell 2012).
19 However, as discussed below, it is deeply flawed as a primary homology concept (see also
20 Caldwell *et al.* 1995; Caldwell 2012). This clarification is particularly timely in light of
21 recent discussions of character construction (e.g., Simões *et al.* 2017a) and applications of
22 these guidelines in revising morphological phylogenetic datasets (e.g., Simões *et al.* 2018;
23 Garberoglio *et al.* 2019). As a longirostrine organism exemplifying ‘true’ narial retraction,
24 *Gavialimimus* therefore provides novel insight into and clarification of this anatomical
25 condition.

1 The hypothesized homology of the openings for the external nares in varanoids with
2 those in mosasauroids is flawed in numerous aspects. Although the overall fenestration of the
3 snout may be superficially similar, this condition is achieved in these two groups via different
4 modifications to the shape and topology of the surrounding bones (Caldwell *et al.* 1995; see
5 Caldwell 2012 for a detailed discussion of this issue). Employing the test of similarity for
6 primary homology (Rieppel & Kearney 2002), posterior expansion of the narial fenestrae in
7 varanoids and mosasauroids is therefore not homologous and does not unite these taxa.
8 Furthermore, the external nares themselves in varanoids are not in fact retracted compared to
9 the condition in other lizards. Instead, the soft-tissue external narial openings remain at an
10 anteriorly terminal position in varanoids (as in other lizards), with only the bony fenestrae
11 being posteriorly extended (Caldwell 2012). Although not terminal, slit-like soft-tissue
12 external nares also occur anteriorly inside the anteriormost, expanded section of the bony
13 fenestrae in *Platecarpus tympaniticus*, a condition that again does not exemplify retraction of
14 the nares and which could have been widespread among all mosasaurs except those few with
15 ‘true’ narial retraction (Lindgren *et al.* 2010; Caldwell 2012).

16 In contrast to this erroneous conceptualization of the external narial openings in
17 typical varanoids and mosasauroids, the condition in *Gavialimimus almaghribensis* is distinct
18 in portraying true retraction of the openings for the external nares relative to the tip of the
19 snout. The bony snout fenestrae terminate anteriorly around the eighth maxillary tooth
20 position, limiting this fenestration to only the posteriormost 25% of the preorbital region of
21 the skull (Fig. 2). The only non-platecarpine taxa that potentially exhibit an analogous
22 narial retraction would be halisaurines, in which the premaxillary-maxillary suture is longer
23 than the length of the entire external naris, which is hence closer to the frontal than to the
24 snout tip (e.g., Konishi *et al.* 2016:fig. 18).

1 In comparison, in other mosasaurs the bony openings for the external nares either
2 comprise a much greater proportion of the preorbital skull region and/or terminate anteriorly
3 much closer to the snout [e.g., *Platecarpus tympaniticus*: see Konishi *et al.* (2012):fig. 3;
4 *Prognathodon overtoni* (Williston, 1897a): see Konishi *et al.* (2011):fig. 2; *Tylosaurus*
5 *bernardi* (Dollo, 1885): see Jiménez-Huidobro & Caldwell (2016):fig. 1]. Even in other
6 mosasaurs exhibiting snout elongation, the bony openings for the external nares are distinct
7 from the condition in *Gavialimimus almaghribensis*. For example, these openings extend
8 over most of the preorbital region of the skull in *Plotosaurus bennisoni* (e.g., see LeBlanc *et*
9 *al.* 2013:fig. 2). In *Ectenosaurus clidastoides* – the mosasaur most comparable to
10 *Gavialimimus* in terms of pronounced snout elongation – these openings are small, similar to
11 the condition in *Gavialimimus*, but are positioned much closer to the tip of the snout (e.g., see
12 Russell 1967:fig. 86). Finally, although the external narial openings appear to be small and
13 retracted in *Goronyosaurus nigeriensis*, as in *Gavialimimus*, the poor condition of the *G.*
14 *nigeriensis* holotype skull somewhat obscures this comparison (C.S., pers. obs.; see also
15 Azzaroli *et al.* 1972; Soliar 1988).

16 Therefore, even if the soft-tissue narial openings were located at the anterior termini
17 of the bony fenestrae in *Gavialimimus almaghribensis*, as in varanoids, the fenestrae
18 themselves are retracted enough that this position would still be distinctly posterior relative to
19 the typical condition in varanoids and presumably mosasaurs, save halisaurines. As such, *Ga.*
20 *almaghribensis* provides a rare example of true retraction of the external nares, in contrast to
21 the traditional but inaccurate conceptualization of external narial retraction in mosasaurs and
22 varanoids.

23

24 **[Insert Figure 13 here as a double-column (173 mm width) figure]**

25

1 **Conclusions**

2

3 The Maastrichtian phosphates of Morocco record an incredibly diverse assemblage of
4 numerous mosasaur genera from many subfamilies (Bardet *et al.* 2015; Bardet *et al.* 2018).

5 This study builds on our knowledge of this diversity via the description and analysis of a new

6 mosasaur specimen (MHNM.KHG.1231) from Morocco, consisting of relatively complete

7 cranial and isolated postcranial material (Figs 2–9). Although the teeth of this specimen

8 initially suggest referral to *'Platecarpus' ptychodon*, closer examination of this species and

9 others exhibiting similar tooth morphology (Fig. 11) reveals the diagnosis of *'P. ptychodon*

10 to be fundamentally flawed, leading to the rejection of this species as a *nomen dubium*.

11 Phylogenetic analysis under multiple parsimony-based methods consistently recovers

12 MHNM.KHG.1231 as the sister taxon to *Selmasaurus russelli*, with these taxa forming a

13 clade within the Plioplatecarpinae alongside *S. johnsoni* and *Goronyosaurus nigeriensis* (Fig.

14 10). Due to its unique skull – with unequivocal features such as a highly elongate snout,

15 highly retracted nares, and large supratemporal fenestrae – we propose that

16 MHNM.KHG.1231 represents a new mosasaur genus and species. Features uniting this

17 specimen with *Selmasaurus* include the nature of the parietal constriction and the broadly

18 excavated medial surface of the quadrate suprastapedial process, with general constriction of

19 the parietal also present in *G. nigeriensis*. This new genus is distinguished from *Selmasaurus*

20 by a large, oval pineal foramen that contacts the frontoparietal suture, certain features of the

21 dentary and vertebrae, and a wide postorbitofrontal, among other features such as the

22 aforementioned autapomorphies.

23 Both *Selmasaurus* and *Goronyosaurus* have only rarely been included in mosasaur or

24 squamate phylogenies, and never in the same analysis in the literature. As such, recovery of

25 the aforementioned *Goronyosaurus–Selmasaurus–Gavialimimus* clade provides novel insight

1 into plioplatecarpine evolution. Cranial features present in this clade – including snout
2 elongation and akinetic cranial sutures – suggest morphological specialization into distinct
3 ecological and predatory niches to reduce competition and enable coexistence in diverse
4 ecosystems.

5 The elongate snout of *Gavialimimus almaghribensis* also provides insight into ‘true’
6 external narial retraction in mosasaurs, in contrast to how ‘narial retraction’ is typically but
7 incorrectly interpreted in many studies of mosasaur and varanoid evolution.

8

9 **Acknowledgements**

10

11 We thank: A. Murray for discussions regarding taxonomic guidelines; A. LeBlanc, I.
12 Paparella, and O. Vernygora for helpful discussions regarding phylogenetic analysis and
13 mosasaur anatomy; A. LeBlanc for discussions regarding tooth morphology and histology;
14 and O. Vernygora for assistance in identifying isolated shark teeth used to support the
15 provenance of the holotype. We are especially grateful to L. A. Lindoe for his guidance in the
16 preparation of MHNM.KHG.1231. We also thank Drs. N.-E. Jalil and M. Ghamizi (Museum
17 of Natural History of Marrakech, Cadi Ayadd University, Marrakech) for their assistance
18 with the specimen. Finally, we thank J. Lively and H. Street for their helpful and thorough
19 reviews, both of which greatly improved the quality of this manuscript. Funding was
20 provided via an Alexander Graham Bell Canada Graduate Scholarship awarded by the
21 Natural Sciences and Engineering Research Council of Canada (NSERC) to CRCS, as well as
22 an NSERC Discovery Grant (#23458) and Chair’s Research Allowance to MWC. All authors
23 report no conflicts of interest.

24 Figures 1 and 9 were modified with permission from the respective copyright holders.

25 These include: Figure 1 (Map and stratigraphic column of Oulad Abdoun Basin) of Bardet *et*

1 *al.* (2005), originally published in the Zoological Journal of the Linnean Society vol. 143, pg
2 448, included herein by permission of Oxford University Press; Figure 15 (Tooth
3 morphoguilds of Mesozoic marine predators) of Massare (1987), originally published in the
4 Journal of Vertebrate Paleontology vol. 7 (2), pg 131, adapted herein by permission of the
5 Society of Vertebrate Paleontology, www.vertpaleo.org, and of the publisher, Taylor &
6 Francis; and Figure 7 (Tooth morphoguilds and niche partitioning in Maastrichtian Moroccan
7 mosasaurs) of Bardet *et al.* (2015), originally published in Gondwana Research vol. 27, pg
8 1077, adapted herein with permission from Elsevier.

9

10 **References**

11

12 **Agassiz, L.** 1843. Recherches sur les poisson fossiles. *Imprimerie de Petitpierre, Neuchâtel*,
13 **3**, 390 + 332 pp.

14 **Arambourg, C.** 1952. Les vertébrés fossiles des gisements de phosphates (Maroc–Algérie–
15 Tunisie). *Notes et mémoires du Service géologique du Maroc*, **92**, 1–372.

16 **Azzaroli, A., de Giuli, C., Ficarelli, G. & Torre, D.** 1972. An aberrant mosasaur from the
17 Upper Cretaceous of north-western Nigeria. *Accademia Nazionale dei Lincei, Rendiconti*.
18 *Classe di scienze fisiche matematiche e naturali*, **3**, 398–404.

19 **Azzaroli, A., de Giuli, C., Ficarelli, G. & Torre, D.** 1975. Late Cretaceous mosasaurs
20 from the Sokoto district, Nigeria. *Accademia Nazionale dei Lincei, Memorie. Classe di*
21 *scienze fisiche matematiche e naturali*, **13**, 21–34.

22 **Bardet, N., Cappetta, H., Pereda Superbiola, X., Mouty, M., Al Maleh, A. K., Ahmad,**
23 **A. M., Khrata, O. & Gannoum, N.** 2000. The marine vertebrate faunas from the Late
24 Cretaceous phosphates of Syria. *Geological Magazine*, **137**(3), 269–290.

- 1 **Bardet, N., Gheerbrant, E., Noubhani, A., Cappetta, H., Jouve, S., Bourdon, E., Pereda**
2 **Superbiola, X., Jalil, N.-E., Vincent, P., Houssaye, A., Sole, F., Elhoussaini Darif, K.,**
3 **Adnet, S., Rage, J.-C., de Lapparent de Broin, F., Sudre, J., Bouya, B., Amaghazaz, M. &**
4 **Meslouh, S.** 2018. Les vertébrés fossiles des phosphates crétacés-paléogènes (72,1–47,8 Ma)
5 du Maroc. Pp. 351–452 in S. Zouhri (ed) *Paléontologie des Vertébrés du Maroc: état des*
6 *connaissances*. Mémoires de la Société Géologique de France, Paris.
- 7 **Bardet, N., Houssaye, A., Vincent, P., Pereda Superbiola, X., Amaghazaz, M., Jourani, E.**
8 **& Meslouh, S.** 2015. Mosasaurids (Squamata) from the Maastrichtian Phosphates of
9 Morocco: Biodiversity, palaeobiogeography and palaeoecology based on tooth morphoguilds.
10 *Gondwana Research*, **27**, 1068–1078. doi:10.1016/j.gr.2014.08.014
- 11 **Bardet, N., Pereda Superbiola, X., Jouve, S., Bourdon, E., Vincent, P., Houssaye, A.,**
12 **Rage, J.-C., Jalil, N.-E., Bouya, B. & Amaghazaz, M.** 2010. Reptilian assemblages from the
13 latest Cretaceous – Palaeogene phosphates of Morocco: from Arambourg to present time.
14 *Historical Biology*, **22**, 186–199. doi:10.1080/08912961003754945
- 15 **Bardet, N., Pereda Superbiola, X., Iarochène, M., Bouya, B. & Amaghazaz, M.** 2005. A
16 new species of *Halisaurus* from the Late Cretaceous phosphates of Morocco, and the
17 phylogenetical relationships of the Halisaurinae (Squamata: Mosasauridae). *Zoological*
18 *Journal of the Linnean Society*, **143**, 447–472.
- 19 **Bell, G. L.** 1997. A phylogenetic revision of North American and Adriatic Mosasauroida.
20 Pp. 293–332 in J.M. Callaway and E.L. Nicholls (eds) *Ancient Marine Reptiles*. Academic
21 Press.
- 22 **Caldwell, M. W.** 2007. Ontogeny, anatomy and attachment of the dentition in mosasaurs
23 (Mosasauridae: Squamata). *Zoological Journal of the Linnean Society*, **149**, 687–700.
- 24 **Caldwell, M. W.** 2012. A challenge to categories: “What, if anything, is a mosasaur?”.
25 *Bulletin de la Société Géologique de France*, **183**(1), 7–34.

- 1 **Caldwell, M. W., Carroll, R. L. & Kaiser, H.** 1995. The pectoral girdle and forelimb of
2 *Carsosaurus marchesetti* (Aigialosauridae), with a preliminary phylogenetic analysis of
3 mosasauroids and varanoids. *Journal of Vertebrate Paleontology*, **15**(3), 516–531.
4 doi:10.1080/02724634.1995.10011245
- 5 **Caldwell, M. W., Konishi, T., Obata, I. & Muramoto, K.** 2008. A new species of
6 *Taniwhasaurus* (Mosasauridae, Tylosaurinae) from the upper Santonian-lower Campanian
7 (Upper Cretaceous) of Hokkaido, Japan. *Journal of Vertebrate Paleontology*, **28**(2), 339–348.
8 doi:10.1671/0272-4634(2008)28[339:ANSOTM]2.0.CO;2
- 9 **Callison, G.** 1967. Intracranial mobility in Kansas mosasaurs. *University of Kansas*
10 *Paleontological Contributions*, **26**, 1–15.
- 11 **Camp, C. L.** 1942. California mosasaurs. *Memoirs of the University of California*, **13**, 1–68.
- 12 **Conrad, J. L.** 2008. Phylogeny and systematics of Squamata (Reptilia) based on
13 morphology. *Bulletin of the American Museum of Natural History, New York*, **310**, 1–182.
14 doi:10.1206/310.1
- 15 **Conrad, J. L., Ast, J. C., Montanari, S. & Norell, M. A.** 2011. A combined evidence
16 phylogenetic analysis of Anguimorpha (Reptilia: Squamata). *Cladistics*, **27**, 230–277.
17 doi:10.1111/j.1096-0031.2010.00330.x
- 18 **Conrad, J. L., Rieppel, O. & Grande, L.** 2008. Re-assessment of varanid evolution based
19 on new data from *Saniwa ensidens* Leidy, 1870 (Squamata, Reptilia). *American Museum*
20 *Novitates*, **3630**, 1–15. doi:10.1206/596.1
- 21 **Coombs, W. P.** 1990. Teeth and taxonomy in ankylosaurs. Pp. 269–279 in K. Carpenter and
22 P.J. Currie (eds) *Dinosaur systematics: approaches and perspectives*. Cambridge University
23 Press, New York.
- 24 **Cope, E. D.** 1869. On the reptilian orders, Pythonomorpha and Streptosauria. *Boston Society*
25 *of Natural History Proceedings*, **12**, 250–266.

- 1 **Cope, E. D.** 1874. Review of the Vertebrata of the Cretaceous Period found west of the
2 Mississippi River. *United States Geological Survey of the Territories Bulletin*, **1**, 3–48.
- 3 **Cuff, A. R. & Rayfield, E. J.** 2013. Feeding mechanics in spinosaurid theropods and extant
4 crocodylians. *PLoS ONE*, **8**(5), e65295. doi:10.1371/journal.pone.0065295
- 5 **Dollo, L.** 1884. Le mosasaure. *Revue des questions scientifiques 1e ser.*, **16**, 648–653.
- 6 **Dollo, L.** 1885. Le hainosaure. *Révue des Questions Scientifiques*, **18**, 285–289.
- 7 **Dollo, L.** 1889a. Note sur les vertébrés fossiles récemment offerts au Musée de Bruxelles par
8 M. Alfred Lemonnier. *Bulletin de la Société belge de Géologie, de Paléontologie et*
9 *d'Hydrologie*, **3**, 181–182.
- 10 **Dollo, L.** 1889b. Première note sur les mosasauriens de Mesvin. *Bulletin de la Société Belge*
11 *de Géologie, de Paléontologie, et d'Hydrologie*, **3**, 271–304.
- 12 **Everhart, M. J.** 2005. Rapid evolution, diversification and distribution of mosasaurs
13 (Reptilia; Squamata) prior to the K-T Boundary. Pp. 16–27. *Tate Museum 2005 11th Annual*
14 *Symposium in Paleontology and Geology*. Casper, WY.
- 15 **Fernandez, M. & Martin, J. E.** 2009. Description and phylogenetic relationships of
16 *Taniwhasaurus antarcticus* (Mosasauridae, Tylosaurinae) from the upper Campanian
17 (Cretaceous) of Antarctica. *Cretaceous Research*, **30**, 717–726.
18 doi:10.1016/j.cretres.2008.12.012
- 19 **Garberoglio, F. F., Apesteguía, S., Simões, T. R., Palci, A., Gómez, R. O., Nydam, R. L.,**
20 **Larsson, H. C. E., Lee, M. S. Y. & Caldwell, M. W.** 2019. New skulls and skeletons of the
21 Cretaceous legged snake *Najash*, and the evolution of the modern snake body plan. *Science*
22 *Advances*, **5**(11), eaax5833. doi:10.1126/sciadv.aax5833
- 23 **Gervais, P.** 1852. *Zoologie et Paléontologie Françaises (Animaux Vertébrés). First Edition.*
24 Librairie de la Société de Géographie, Paris, 271 pp.
- 25 **Goloboff, P. A.** 1993. Estimating character weights during tree search. *Cladistics*, **9**, 83–91.

- 1 **Goloboff, P. A., Carpenter, J. M., Arias, J. S. & Esquivel, D. R. M.** 2008a. Weighting
2 against homoplasy improves phylogenetic analysis of morphological data sets. *Cladistics*, **24**,
3 758–773. doi:10.1111/j.1096-0031.2008.00209.x
- 4 **Goloboff, P. A. & Catalano, S. A.** 2016. TNT version 1.5, including a full implementation
5 of phylogenetic morphometrics. *Cladistics*, **32**, 221–238. doi:10.1111/cla.12160
- 6 **Goloboff, P. A., Farris, J. S. & Nixon, K. C.** 2008b. TNT, a free program for phylogenetic
7 analysis. *Cladistics*, **24**, 774–786. doi:10.1111/j.1096-0031.2008.00217.x
- 8 **Holmes, R.** 1996. *Plioplatecarpus primaevus* (Mosasauridae) from the Bearpaw Formation
9 (Campanian, Upper Cretaceous) of the North American Western Interior Seaway. *Journal of*
10 *Vertebrate Paleontology*, **16**(4), 673–687. doi:10.1080/02724634.1996.10011357
- 11 **International Commission on Zoological Nomenclature** 1999. *International Code of*
12 *Zoological Nomenclature*. The International Trust for Zoological Nomenclature, London.
- 13 **Jiménez-Huidobro, P. & Caldwell, M. W.** 2016. Reassessment and reassignment of the
14 early Maastrichtian mosasaur *Hainosaurus bernardi* Dollo, 1885, to *Tylosaurus* Marsh, 1872.
15 *Journal of Vertebrate Paleontology*, **36**(3), e1096275. doi:10.1080/02724634.2016.1096275
- 16 **Jiménez-Huidobro, P. & Caldwell, M. W.** 2019. A new hypothesis of the phylogenetic
17 relationships of the Tylosaurinae (Squamata: Mosasauroidae). *Frontiers in Earth Science*, **7**,
18 47. doi:10.3389/feart.2019.00047
- 19 **Jiménez-Huidobro, P., Simões, T. R. & Caldwell, M. W.** 2016. Re-characterization of
20 *Tylosaurus nepaeolicus* (Cope, 1874) and *Tylosaurus kansasensis* Everhart, 2005: Ontogeny
21 or sympatry? *Cretaceous Research*, **65**, 68–81. doi:10.1016/j.cretres.2016.04.008
- 22 **Kiernan, C. R.** 2002. Stratigraphic distribution and habitat segregation of mosasaurs in the
23 Upper Cretaceous of western and central Alabama, with an historical review of Alabama
24 mosasaur discoveries. *Journal of Vertebrate Paleontology*, **22**(1), 91–103. doi:10.1671/0272-
25 4634(2002)022[0091:SDAHSO]2.0.CO;2

- 1 **Konishi, T.** 2008. A new specimen of *Selmasaurus* sp., cf. *S. russelli* (Mosasauridae:
2 Plioplatecarpini) from Greene County, western Alabama, USA. Pp. 95–105. *Proceedings of*
3 *the Second Mosasaur Meeting*. Hays, Kansas.
- 4 **Konishi, T., Brinkman, D., Massare, J. A. & Caldwell, M. W.** 2011. New exceptional
5 specimens of *Prognathodon overtoni* (Squamata, Mosasauridae) from the upper Campanian
6 of Alberta, Canada, and the systematics and ecology of the genus. *Journal of Vertebrate*
7 *Paleontology*, **31**(5), 1026–1046. doi:10.1080/02724634.2011.601714
- 8 **Konishi, T. & Caldwell, M. W.** 2007. New specimens of *Platecarpus planifrons* (Cope,
9 1874) (Squamata: Mosasauridae) and a revised taxonomy of the genus. *Journal of Vertebrate*
10 *Paleontology*, **27**(1), 59–72. doi:10.1671/0272-4634(2007)27[59:NSOPPC]2.0.CO;2
- 11 **Konishi, T. & Caldwell, M. W.** 2009. New material of the mosasaur *Plioplatecarpus*
12 *nichollsae* Cuthbertson et al., 2007, clarifies problematic features of the holotype specimen.
13 *Journal of Vertebrate Paleontology*, **29**(2), 417–436. doi:10.1671/039.029.0225
- 14 **Konishi, T. & Caldwell, M. W.** 2011. Two new plioplatecarpine (Squamata, Mosasauridae)
15 genera from the Upper Cretaceous of North America, and a global phylogenetic analysis of
16 plioplatecarpines. *Journal of Vertebrate Paleontology*, **31**(4), 754–783.
17 doi:10.1080/02724634.2011.579023
- 18 **Konishi, T., Caldwell, M. W., Nishimura, T., Sakurai, K. & Tanoue, K.** 2016. A new
19 halisaurine mosasaur (Squamata: Halisaurinae) from Japan: the first record in the western
20 Pacific realm and the first documented insights into binocular vision in mosasaurs. *Journal of*
21 *Systematic Palaeontology*, **14**(10), 809–839. doi:10.1080/14772019.2015.1113447
- 22 **Konishi, T., Lindgren, J., Caldwell, M. W. & Chiappe, L.** 2012. *Platecarpus tympaniticus*
23 (Squamata, Mosasauridae): osteology of an exceptionally preserved specimen and its insights
24 into the acquisition of a streamlined body shape in mosasaurs. *Journal of Vertebrate*
25 *Paleontology*, **32**(6), 1313–1327. doi:10.1080/02724634.2012.699811

- 1 **Konishi, T., Newbrey, M. G. & Caldwell, M. W.** 2014. A small, exquisitely preserved
2 specimen of *Mosasaurus missouriensis* (Squamata, Mosasauridae) from the upper Campanian
3 of the Bearpaw Formation, western Canada, and the first stomach contents for the genus.
4 *Journal of Vertebrate Paleontology*, **34**(4), 802–819. doi:10.1080/02724634.2014.838573
- 5 **LeBlanc, A. R. H., Caldwell, M. W. & Bardet, N.** 2012. A new mosasaurine from the
6 Maastrichtian (Upper Cretaceous) phosphates of Morocco and its implications for
7 mosasaurine systematics. *Journal of Vertebrate Paleontology*, **32**(1), 82–104.
8 doi:10.1080/02724634.2012.624145
- 9 **LeBlanc, A. R. H., Caldwell, M. W. & Lindgren, J.** 2013. Aquatic adaptation, cranial
10 kinesis, and the skull of the mosasaurine mosasaur *Plotosaurus bennisoni*. *Journal of*
11 *Vertebrate Paleontology*, **33**(2), 349–362. doi:10.1080/02724634.2013.726675
- 12 **LeBlanc, A. R. H., Mohr, S. R. & Caldwell, M. W.** 2019. Insights into the anatomy and
13 functional morphology of durophagous mosasaurines (Squamata: Mosasauridae) from a new
14 species of *Globidens* from Morocco. *Zoological Journal of the Linnean Society*, **10**, 1–27.
15 doi:10.1093/zoolinnea/zlz008/540165
- 16 **Lindgren, J., Caldwell, M. W., Konishi, T. & Chiappe, L. M.** 2010. Convergent evolution
17 in aquatic tetrapods: Insights from an exceptional fossil mosasaur. *PLoS ONE*, **5**(8), e11998.
18 doi:10.1371/journal.pone.0011998
- 19 **Lindgren, J. & Siverson, M.** 2002. *Tylosaurus ivoensis*: a giant mosasaur from the early
20 Campanian of Sweden. *Transactions of the Royal Society of Edinburgh: Earth Sciences*, **93**,
21 73–93. doi:10.1017/S026359330000033X
- 22 **Lingham-Soliar, T.** 1991. Mosasaurs from the Upper Cretaceous of Niger. *Palaeontology*,
23 **34**, 653–670.

- 1 **Lingham-Soliar, T.** 1998. A new mosasaur *Pluridens walkeri* from the Upper Cretaceous,
2 Maastrichtian of the Iullemeden Basin, southwest Niger. *Journal of Vertebrate*
3 *Paleontology*, **18**(4), 709–717.
- 4 **Lingham-Soliar, T.** 1999. A functional analysis of the skull of *Goronyosaurus nigeriensis*
5 (Squamata: Mosasauridae) and its bearing on the predatory behaviour and evolution of this
6 enigmatic taxon. *Neues Jahrbuch für Geologie und Paläontologie. Abhandlungen*, **213**(3),
7 355–374.
- 8 **Lingham-Soliar, T.** 2002. First occurrence of premaxillary caniniform teeth in the
9 Varanoidea: Presence in the extinct mosasaur *Goronyosaurus* (Squamata: Mosasauridae) and
10 its functional and paleoecological implications. *Lethaia*, **35**, 187–190.
- 11 **Linnaeus, C.** 1758. *Systema Naturae, edition X, vol. 1 (Systema naturae per regna tria*
12 *naturae, secundum classes, ordines, genera, species, cum characteribus, differentiis,*
13 *synonymis, locis. Tomus I. Editio decima, reformata)*. Laurentii Salvii, Holmiae, 824 pp.
- 14 **Liu, K.** 2007. Sequence stratigraphy and orbital cyclostratigraphy of the Mooreville Chalk
15 (Santonian-Campanian), northeastern Gulf of Mexico area, USA. *Cretaceous Research*, **28**,
16 405–418. doi:10.1016/j.cretres.2006.06.005
- 17 **Lucas, J. & Prévôt-Lucas, L.** 1996. Tethyan phosphates and bioproductites. Pp. 367–391 in
18 A.E.M. Nairn, L.-E. Ricou, B. Vrielynck and J. Dercourt (eds) *The Ocean Basins and*
19 *Margins: The Tethys Ocean*.
- 20 **Maddison, W. & Maddison, D.** 2018. Mesquite: a modular system for evolutionary
21 analysis.
- 22 **Massare, J. A.** 1987. Tooth morphology and prey preference of Mesozoic marine reptiles.
23 *Journal of Vertebrate Paleontology*, **7**(2), 121–137. doi:10.1080/02724634.1987.10011647
- 24 **Massare, J. A.** 1988. Swimming capabilities of Mesozoic marine reptiles: implications for
25 method of predation. *Paleobiology*, **14**(2), 187–205.

- 1 **McCurry, M. R., Evans, A. R., Fitzgerald, E. M. G., Adams, J. W., Clausen, P. D. &**
2 **McHenry, C. R.** 2017. The remarkable convergence of skull shape in crocodylians and
3 toothed whales. *Proceedings of the Royal Society of London, Series B: Biological Sciences*,
4 **284**, 20162348. doi:10.1098/rspb.2016.2348
- 5 **McHenry, C. R., Clausen, P. D., Daniel, W. J. T., Meers, M. B. & Pendharkar, A.** 2006.
6 Biomechanics of the rostrum in crocodylians: A comparative analysis using finite-element
7 modeling. *The Anatomical Record*, **288**, 827–849. doi:10.1002/ar.a.20360
- 8 **Merriam, J. C.** 1894. Ueber die Pythonomorphen der Kansas Kreide. *Palaeontographica*,
9 **41**, 1–39.
- 10 **Modesto, S. P.** 1996. *Noteosaurus africanus* Broom is a nomen dubium. *Journal of*
11 *Vertebrate Paleontology*, **16**(1), 172–174. doi:10.1080/02724634.1996.10011296
- 12 **Novas, F. E., Fernández, M., de Gasparini, Z., Lirio, J. M., Nuñez, H. J. & Puerta, P.**
13 2002. *Lakumasaurus antarcticus*, n. gen. et sp., a new mosasaur (Reptilia, Squamata) from
14 the Upper Cretaceous of Antarctica. *Ameghiniana*, **39**, 245–249.
- 15 **Ogg, J. G., Hinnov, L. A. & Huang, C.** 2012. Cretaceous. Pp. 793–853 in F.M. Gradstein,
16 J.G. Ogg, M.B. Schmitz and G.M. Ogg (eds) *The Geologic Time Scale 2012*. Elsevier.
- 17 **Oppel, M.** 1811. *Die Ordnungen Familien, und Gattungen der Reptilien als Prodrum einer*
18 *Naturgeschichte derselben*. J. Lindauer, München, 86 pp.
- 19 **Palci, A., Caldwell, M. W. & Papazzoni, C. A.** 2013. A new genus and subfamily of
20 mosasaurs from the Upper Cretaceous of northern Italy. *Journal of Vertebrate Paleontology*,
21 **33**(3), 599–612. doi:10.1080/02724634.2013.731024
- 22 **Persson, P. O.** 1963. Studies on Mesozoic marine reptile faunas with particular regard to the
23 Plesiosauria. *Publications from the Institutes of Mineralogy, Paleontology, and Quaternary*
24 *Geology, University of Lund, Sweden*, **118**, 1–15.

- 1 **Pierce, S. E., Angielczyk, K. D. & Rayfield, E. J.** 2008. Patterns of morphospace
2 occupation and mechanical performance in extant crocodylian skulls: A combined geometric
3 morphometric and finite element modeling approach. *Journal of Morphology*, **269**, 840–864.
4 doi:10.1002/jmor.10627
- 5 **Polcyn, M. J. & Everhart, M. J.** 2008. Description and phylogenetic analysis of a new
6 species of *Selmasaurus* (Mosasauridae: Plioplatecarpinae) from the Niobrara Chalk of
7 western Kansas. Pp. 13–28. *Proceedings of the Second Mosasaur Meeting*. Hays, Kansas.
- 8 **Rieppel, O., Conrad, J. L. & Maisano, J. A.** 2007. New morphological data for *Eosaniwa*
9 *koehni* Haubold, 1977 and a revised phylogenetic analysis. *Journal of Paleontology*, **81**(4),
10 760–769.
- 11 **Rieppel, O. & Kearney, M.** 2002. Similarity. *Biological Journal of the Linnean Society*, **75**,
12 59–82.
- 13 **Russell, D. A.** 1967. Systematics and morphology of American mosasaurs. *Bulletin of the*
14 *Peabody Museum of Natural History*, **23**, 1–241.
- 15 **Schaeffer, B.** 1969. Adaptive radiation of the fishes and the fish-amphibian transition. *Annals*
16 *of the New York Academy of Sciences*, **167**, 5–17.
- 17 **Seeley, H. G.** 1881. On remains of a small lizard from Neocomian rocks of Comen, near
18 Trieste, preserved in the Geological Museum of the University of Vienna. *Quarterly Journal*
19 *of the Geological Society of London*, **37**, 52–56.
- 20 **Simões, T. R., Caldwell, M. W., Palci, A. & Nydam, R. L.** 2017a. Giant taxon-character
21 matrices: Quality of character constructions remains critical regardless of size. *Cladistics*, **33**,
22 198–219. doi:10.1111/cla.12163
- 23 **Simões, T. R., Caldwell, M. W., Talanda, M., Bernardi, M., Palci, A., Vernygora, O.,**
24 **Bernardini, F., Mancini, L. & Nydam, R. L.** 2018. The origin of squamates revealed by a

- 1 Middle Triassic lizard from the Italian Alps. *Nature*, **557**, 706–709. doi:10.1038/s41586-018-
2 0093-3
- 3 **Simões, T. R., Vernygora, O., Paparella, I., Jimenez-Huidobro, P. & Caldwell, M. W.**
4 2017b. Mosasauroid phylogeny under multiple phylogenetic methods provides new insights
5 on the evolution of aquatic adaptations in the group. *PLoS ONE*, **12**(5), e0176773.
6 doi:10.1371/journal.pone.0176773
- 7 **Soliar, T.** 1988. The mosasaur *Goronyosaurus* from the Upper Cretaceous of Sokoto state,
8 Nigeria. *Palaeontology*, **31**, 747–762.
- 9 **Swinton, W. E.** 1930. On fossil Reptilia from Sokoto Province. *Bulletin of the Geological*
10 *Survey of Nigeria*, **13**, 1–56.
- 11 **Thévenin, A.** 1896. Mosasauriens de la craie grise de Vaux-Éclusier près Péronne (Somme).
12 *Bulletin de la Société Géologique de France*, **24**, 900–916.
- 13 **Vaeth, R. H., Rossman, D. A. & Shoop, W.** 1985. Observations of tooth surface
14 morphology in snakes. *Journal of Herpetology*, **19**(1), 20–26.
- 15 **Williston, S. W.** 1897a. *Brachysaurus*, a new genus of mosasaurs. *Kansas University*
16 *Quarterly*, **6**, 95–98.
- 17 **Williston, S. W.** 1897b. Range and distribution of the mosasaurs. *Kansas University*
18 *Quarterly*, **6**, 177–189.
- 19 **Wright, K. R. & Shannon, S. W.** 1988. *Selmasaurus russelli*, a new plioplatecarpine
20 mosasaur (Squamata, Mosasauridae) from Alabama. *Journal of Vertebrate Paleontology*,
21 **8**(1), 102–107. doi:10.1080/02724634.1988.10011686

22

23 **Figure Captions**

24

1 **Figure 1.** Map and stratigraphic column of relevant geological features of Morocco. (A) Map
2 of northwestern Morocco, showing the Atlantic Ocean (light grey), Atlas Mountains (grey
3 lines), Oulad Abdoun Basin (black), and other major phosphatic basins (dark grey). Each
4 section of the scale bar represents 30 km. (B) Stratigraphy of the Oulad Abdoun basin. Beds
5 associated with the provenance of MHNM.KHG.1231 are italicized. Abbreviations: **BB**,
6 basal limestone bonebed; **LCIII**, Lower Couche III; **UCIII**, Upper Couche III; **Ma**, marls;
7 **Ph**, phosphates; **Li**, limestone. Modified from Arambourg (1952), and from Bardet *et al.*
8 (2005) by permission of Oxford University Press.

9 **Figure 2.** MHNM.KHG.1231 (articulated skull) in dorsal view. (A) Diagram; (B)
10 photograph. Light grey shading indicates the external nares and other openings in the skull.
11 Dark grey shading indicates openings in the skull resulting from taphonomic breakage.
12 Double-dashed lines indicate major breaks in or taphonomic distortion to the corresponding
13 elements. Bracketed numbers indicate tooth positions. Abbreviations: **f**, frontal; **h**, humerus;
14 **mx**, maxilla; **oen**, opening for the external naris; **p**, parietal; **pf**, pineal foramen; **pmx**,
15 premaxilla; **pof**, postorbitofrontal; **prf**, prefrontal; **sq**, squamosal; **stf**, supratemporal fenestra;
16 **v**, vomer. Paired bones are preceded by **r** (right) or **l** (left). Scale bar represents 5 cm.

17 **Figure 3.** MHNM.KHG.1231 (articulated skull) in ventral view. (A) Diagram; (B)
18 photograph. Black shading represents matrix. Light grey shading indicates the internal nares
19 and other openings in the skull. Dark grey shading indicates openings in the skull resulting
20 from taphonomic breakage. Solid arrowheads indicate interdental pits; fletched arrowheads
21 indicate replacement teeth. Double-dashed lines indicate major breaks in the corresponding
22 elements. Bracketed numbers indicate tooth positions. Abbreviations: **f**, frontal; **fpf**, frontal
23 posteromedian flange; **h**, humerus; **mx**, maxilla; **p**, parietal; **pal**, palatine; **pf**, pineal foramen;
24 **pmx**, premaxilla; **pof**, postorbitofrontal; **prf**, prefrontal; **smx**, septomaxilla; **sq**, squamosal;

1 **stf**, supratemporal fenestra; **v**, vomer; **vp**, vomerine process of the premaxilla. Paired bones
2 are preceded by **r** (right) or **l** (left). Scale bar represents 5 cm.

3 **Figure 4.** Select palatal views of MHNM.KHG.1231. **(A)** Anterior palate; **(B)** mid-palatal
4 view; **(C)** posterior palate and ventral skull roof. Major anatomical features are labelled on
5 the diagram or photographs, with sutures indicated on the diagram. Insets on line drawing
6 correspond to panels denoted by the same letter. Arrows indicate interdental pits. Shading of
7 line drawing as in Figures 2 and 3. Abbreviations: **ch/os**, location of cerebral hemisphere or
8 of articulation of the orbitosphenoid; **ls**, lingual shelf of maxilla; **mx**, maxilla; **oc**, olfactory
9 canal; **p**, parietal; **pal**, palatine; **pmx**, premaxilla; **pmx-v**, premaxilla-vomer articulation; **pof**,
10 postorbitofrontal; **prf**, prefrontal; **sq**, squamosal; **tb**, tabular boss; **v**, vomer; **vp**, vomerine
11 process of the premaxilla. Paired bones are preceded by **r** (right) or **l** (left). Scale bars each
12 represent 2 cm.

13 **Figure 5.** Orbital region and skull roof of MHNM.KHG.1231. **(A)** Ventral view of skull roof;
14 **(B)** dorsal view of skull roof; **(C)** lateral view of left orbit. Major anatomical features are
15 labelled on the diagrams or photographs, with sutures indicated on the diagrams. Line
16 drawings correspond to panels denoted by the same letter. Shading of line drawings as in
17 Figures 2 and 3. In **(c)**, dashed line indicates approximate dorsal midline and double-dashed
18 line indicates estimated location of suture given taxonomic distortion to specimen.
19 Abbreviations: **ch/os**, location of cerebral hemisphere or of articulation of the orbitosphenoid;
20 **f**, frontal; **fa**, frontal ala; **fpf**, frontal posteromedian flange; **jp**, jugal process of
21 postorbitofrontal; **mx**, maxilla; **oc**, olfactory canal; **p**, parietal; **pal**, palatine; **pof**,
22 postorbitofrontal; **prf**, prefrontal; **sq**, squamosal; **tb**, tabular boss. Paired bones are preceded
23 by **r** (right) or **l** (left) where relevant. Scale bars each represent 5 cm. Line drawings not to
24 scale.

1 **Figure 6.** Select views of the dentition of MHNM.KHG.1231, highlighting key aspects of
2 dental anatomy and tooth development. (A) Anterior premaxillary teeth; (B) right maxillary
3 tooth 3; (C) left maxillary tooth 11; (D) left dentary tooth 3; (E) left dentary tooth 5; (F) left
4 dentary tooth 6 and tooth position 7. Insets on overview photographs correspond to panels
5 denoted by the same letter. Solid arrowheads point to interdental pits; fletched arrowheads
6 point to replacement teeth. Replacement teeth in early (C), intermediate (B), and late (F)
7 stages of development are preserved in this specimen. Several stages of post-eruption tooth
8 development are also visible, from early stages in which the marginal teeth are unfused to
9 their respective alveolus (A & F), to intermediate stages of partial fusion to the tooth-bearing
10 element (B & D), to the final stage of being fully fused to the alveolus (E). Abbreviations:
11 **mp**, medial parapet of the dentary. Scale bars each represent 1 cm. Overview photographs not
12 to scale.

13 **Figure 7.** Mandibular elements of MHNM.KHG.1231. (A) Left dentary in lateral view; (B)
14 right dentary in medial view; (C–D) right posterior mandibular unit in lateral view; (E–F)
15 right posterior mandibular unit in medial view. Solid arrowheads indicate interdental pits;
16 fletched arrowheads indicate replacement teeth. Bracketed numbers indicate tooth positions.
17 Abbreviations: **a**, angular; **art**, articular; **gf**, glenoid fossa; **mg**, Meckelian groove; **mp**,
18 medial parapet of the dentary; **part**, prearticular; **sa**, surangular. Each scale bar represents 5
19 cm. Upper scale bar applies to panels A & B; lower scale bar applies to panels D & F. Panels
20 C & E show the location of sutures and are not to scale.

21 **Figure 8.** Partial right quadrate of MHNM.KHG.1231 in (A) lateral, (B) medial, (C) dorsal,
22 and (D) ventral views. Abbreviations: **mex**, medial excavation; **qs**, quadrate shaft (top
23 portion); **sn**, stapedial notch; **sp**, stapedial pit; **ssp**, suprastapedial process. Scale bar
24 represents 2 cm.

1 **Figure 9.** Disarticulated cranial and postcranial material of MHNM.KHG.1231. (A) Left
 2 pterygoid in ventral view; (B) left pterygoid in dorsal view; (C) right pterygoid (ventral view)
 3 and two vertebrae, the left one cervical and the right one caudal; (D) opposite view of C (i.e.,
 4 right pterygoid in dorsal view); (E) complete cervical vertebra in left lateral view and crushed
 5 vertebral centrum; (F) opposite view of E (i.e., the more complete vertebra is in right lateral
 6 view); (G) right humerus in extensor view (proximal is to the top). Abbreviations: **bp**,
 7 basisphenoid process; **ecpp**, ectopterygoid process of pterygoid; **ect**, ectepicondyle; **ent**,
 8 entepicondyle; **fl**, flange; **hae**, haemapophysis; **hyp**, hypapophysis; **ns**, neural spine; **pozyg**,
 9 postzygapophysis; **pt**, pterygoid; **pzyg**, prezygapophysis; **qr**, quadrate ramus; **syn**,
 10 synapophysis; **vc**, vertebral centrum; **zg**, zygantum. Scale bar represents 5 cm; all bones to
 11 scale.

12 **Figure 10.** Phylogenetic trees generated via implied weighting maximum parsimony analysis
 13 of the dataset utilizing multistate character coding (Mu-IWMP). (A) Single most
 14 parsimonious tree (MPT) (468 steps) generated when $k = 3.0$; (B) single MPT (465 steps)
 15 generated when $k = 7.0$; (C) single MPT (465 steps) generated when $k = 11.0$; (D) enlarged
 16 phylogeny of the subfamily Plioplatecarpinae. Abbreviations for mosasaur subfamilies: **Ha**,
 17 Halisaurinae; **Mo**, Mosasaurinae; **Pl**, Plioplatecarpinae; **Te**, Tethysaurinae; **Ty**,
 18 Tylosaurinae; **Ya**, Yaguarasaurinae.

19 **Figure 11.** Comparison of various marginal teeth of (A–C) *Platecarpus* *ptychodon*, (D–F)
 20 *Gavialimimus almaghribensis*, (G–I) *Platecarpus somenensis*, (J–L) *Prognathodon solvayi*,
 21 and (M–O) *Mosasaurus lemonnieri*. Note how all of the teeth match the diagnosis of '*P.*'
 22 *ptychodon*, rendering this diagnosis – and thus this species – invalid. (A–C) Isolated teeth as
 23 photographed by Arambourg (1952) in Plate 39, Fig. 2 (holotype of '*P.*' *ptychodon*), Fig. 4,
 24 and Fig. 6, respectively; (D–E) MHNM.KHG.1231 (holotype), maxillary; (F)
 25 MHNM.KHG.1231 (holotype), premaxillary; (G–I) MNHN 1895-7 (holotype), maxillary; (J)

1 IRSNB R33-4672 (holotype), maxillary; (**K–L**) IRSNB R33-4565, dentary; (**M–N**) IRSNB
2 3109, maxillary and dentary; (**O**) IRSNB 3119, maxillary. Scale bar represents 1 cm; all teeth
3 to scale.

4 **Figure 12.** Predatory guilds of Mesozoic marine reptiles based on tooth morphology
5 [modified from Massare (1987) and Bardet *et al.* (2015) with permission from Taylor &
6 Francis and Elsevier, respectively]. These marine predators – including Moroccan mosasaurs,
7 indicated in italicized text – can be classified into eight gradational feeding guilds based on
8 tooth size, shape, carinae, and pattern of wear. These tooth morphoguilds reflect similar prey
9 preference, regardless of phylogenetic position. Ideal ‘end member’ tooth morphologies are
10 depicted at each apex of the diagram. Teeth assigned to *‘Platecarpus’ ptychodon*
11 (morphologically indistinguishable from those of *Gavialimimus almaghribensis*, pictured in
12 the diagram) were originally used to classify this organism as a member of the ‘Pierce II’–
13 ‘Cut’ guilds (Bardet *et al.* 2015). However, cranial adaptations of *G. almaghribensis* suggest
14 ecological specialization as a highly adapted piscivore, thus supporting placement as a
15 ‘Pierce I’–‘Pierce II’ predator.

16 **Figure 13.** Life reconstruction of *Gavialimimus almaghribensis*, gen. et sp. nov., hunting a
17 school of teleosts. Image credit: Tatsuya Shinmura.

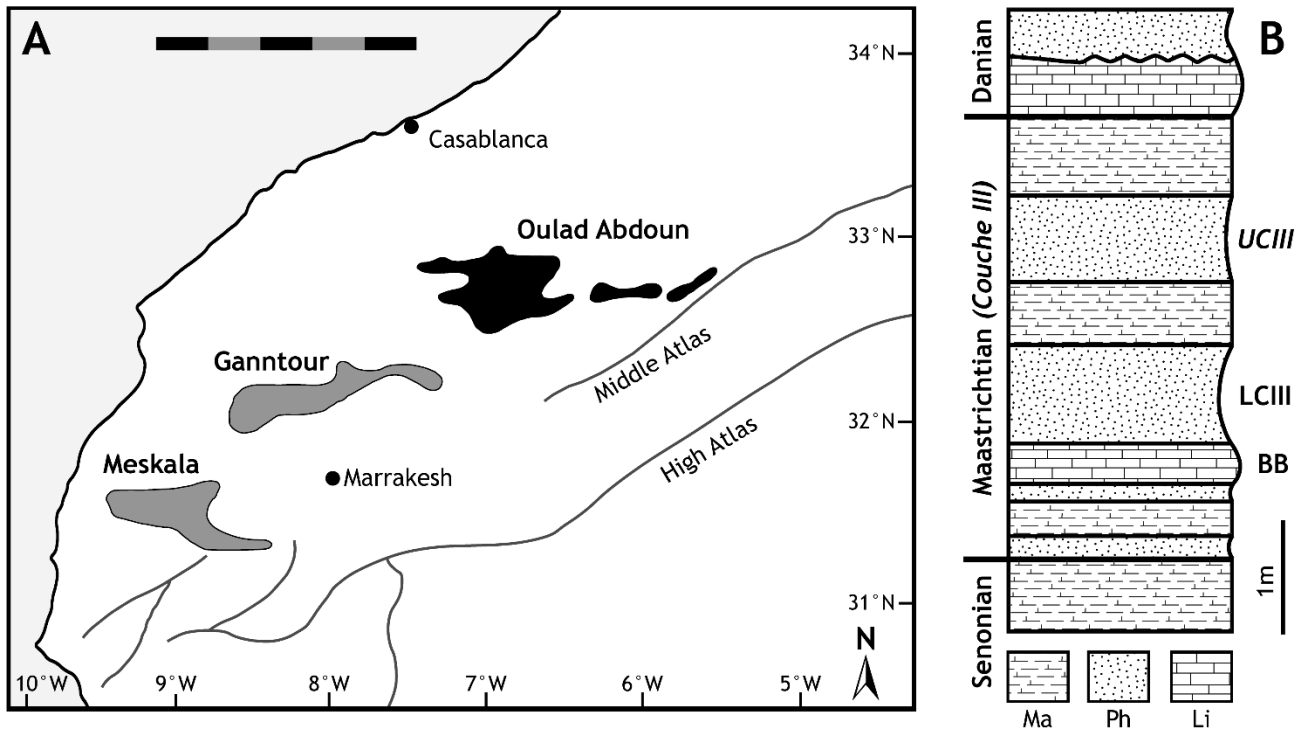


Figure 1. Map and stratigraphic column of relevant geological features of Morocco. **(A)** Map of northwestern Morocco, showing the Atlantic Ocean (light grey), Atlas Mountains (grey lines), Oulad Abdoun Basin (black), and other major phosphatic basins (dark grey). Each section of the scale bar represents 30 km. **(B)** Stratigraphy of the Oulad Abdoun basin. Beds associated with the provenance of MHNM.KHG.1231 are italicized. Abbreviations: **BB**, basal limestone bonebed; **LCIII**, Lower Couche III; **UCIII**, Upper Couche III; **Ma**, marls; **Ph**, phosphates; **Li**, limestone. Modified from Arambourg (1952), and from Bardet *et al.* (2005) by permission of Oxford University Press.

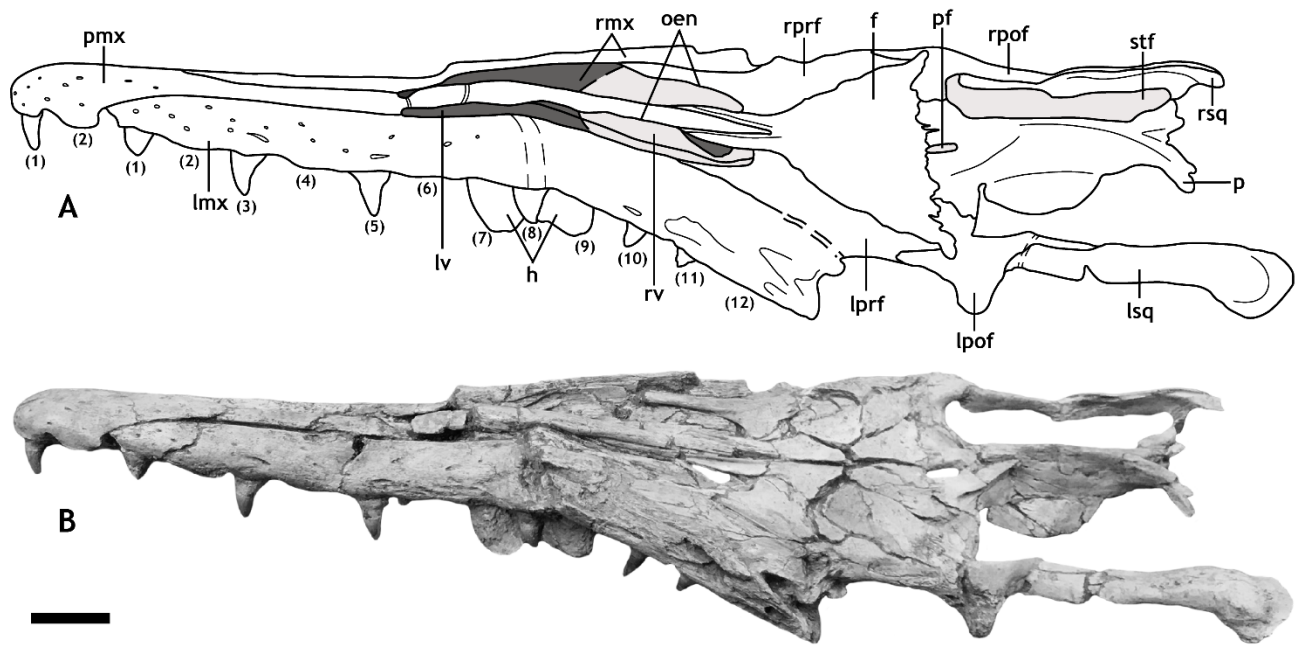


Figure 2. MHNK.KHG.1231 (articulated skull) in dorsal view. **(A)** Diagram; **(B)** photograph. Light grey shading indicates the external nares and other openings in the skull. Dark grey shading indicates openings in the skull resulting from taphonomic breakage. Double-dashed lines indicate major breaks in or taphonomic distortion to the corresponding elements. Bracketed numbers indicate tooth positions. Abbreviations: **f**, frontal; **h**, humerus; **mx**, maxilla; **oen**, opening for the external naris; **p**, parietal; **pf**, pineal foramen; **pmx**, premaxilla; **pof**, postorbitofrontal; **prf**, prefrontal; **sq**, squamosal; **stf**, supratemporal fenestra; **v**, vomer. Paired bones are preceded by **r** (right) or **l** (left). Scale bar represents 5 cm.

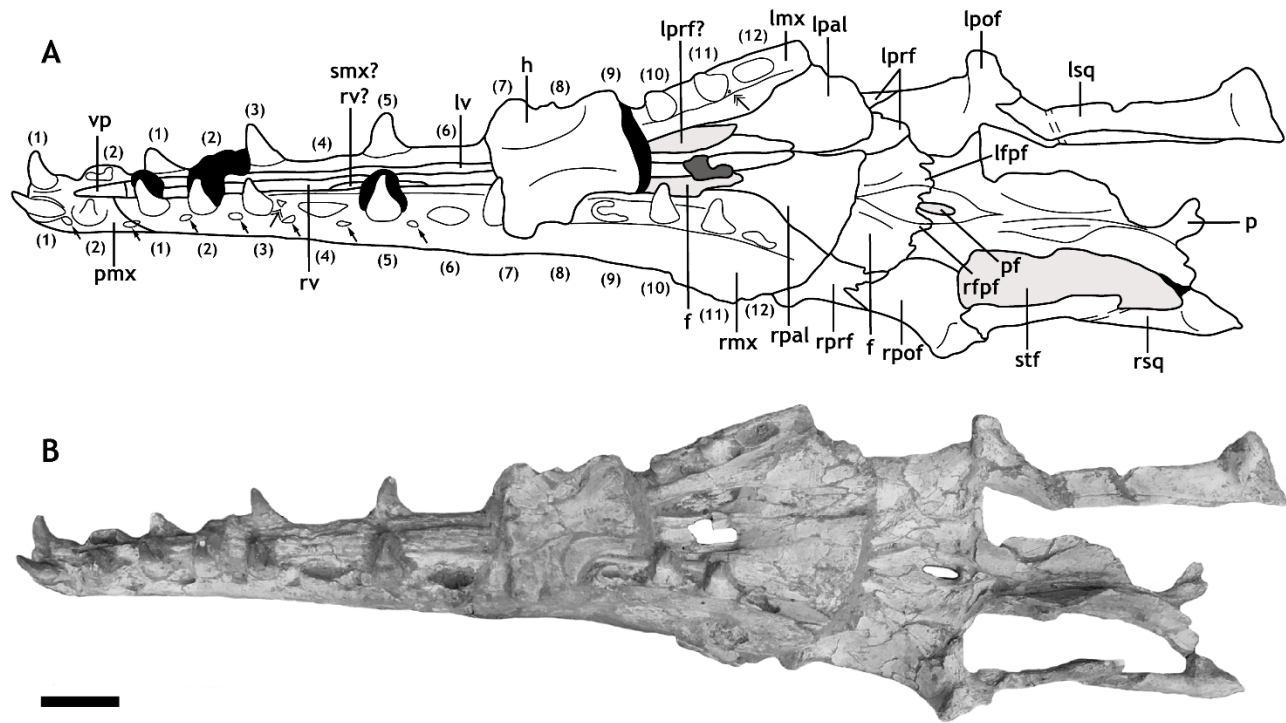


Figure 3. MHN.M.KHG.1231 (articulated skull) in ventral view. (A) Diagram; (B) photograph. Black shading represents matrix. Light grey shading indicates the internal nares and other openings in the skull. Dark grey shading indicates openings in the skull resulting from taphonomic breakage. Solid arrowheads indicate interdental pits; fletched arrowheads indicate replacement teeth. Double-dashed lines indicate major breaks in the corresponding elements. Bracketed numbers indicate tooth positions. Abbreviations: **f**, frontal; **fpf**, frontal posteromedian flange; **h**, humerus; **mx**, maxilla; **p**, parietal; **pal**, palatine; **pf**, pineal foramen; **pmx**, premaxilla; **pof**, postorbitofrontal; **prf**, prefrontal; **smx**, septomaxilla; **sq**, squamosal; **stf**, supratemporal fenestra; **v**, vomer; **vp**, vomerine process of the premaxilla. Paired bones are preceded by **r** (right) or **l** (left). Scale bar represents 5 cm.

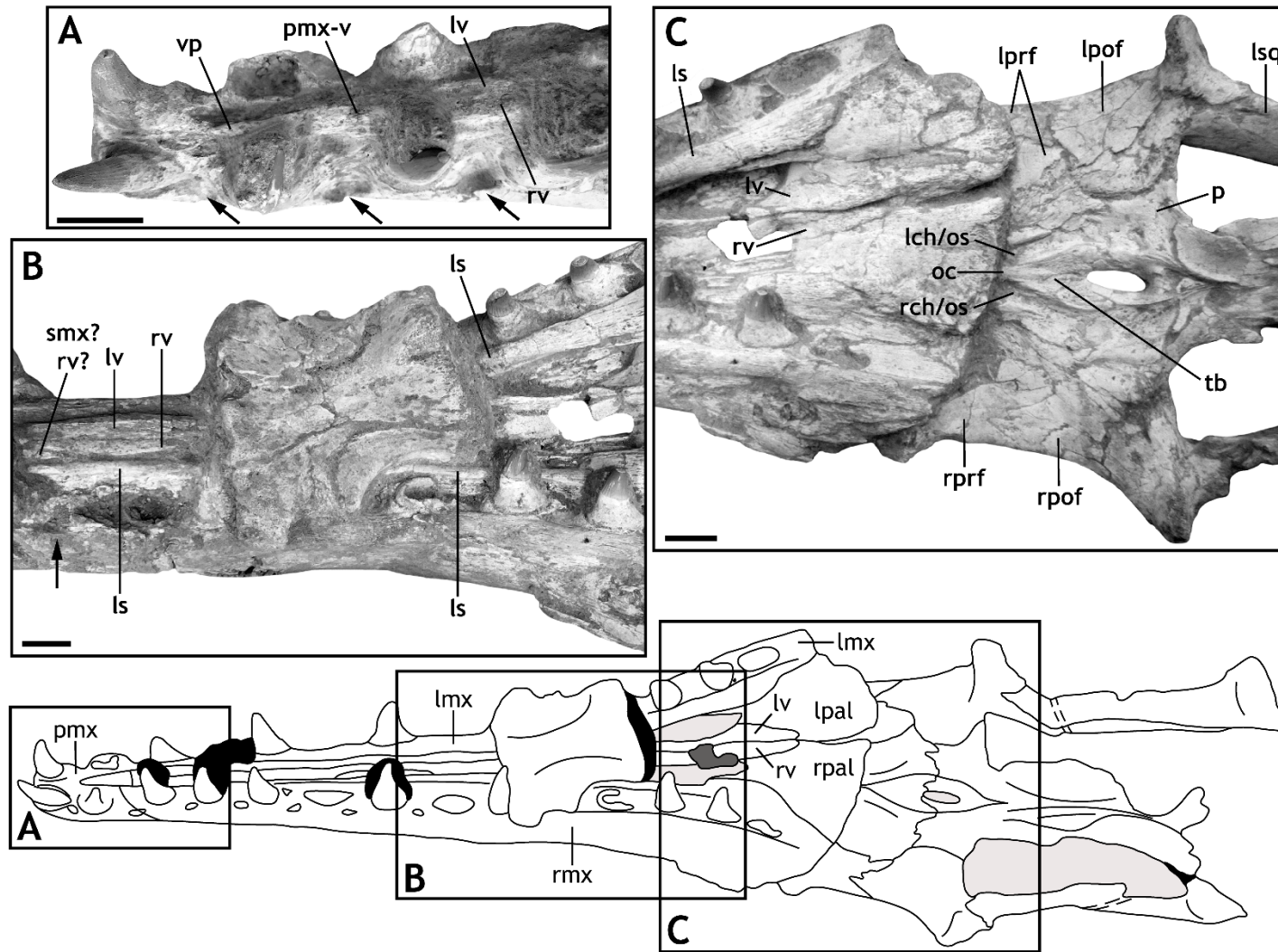


Figure 4. Select palatal views of MHNM.KHG.1231. (A) Anterior palate; (B) mid-palatal view; (C) posterior palate and ventral skull roof. Major anatomical features are labelled on the diagram or photographs, with sutures indicated on the diagram. Insets on line drawing correspond to panels denoted by the same letter. Arrows indicate interdental pits. Shading of line drawing as in Figures 2 and 3. Abbreviations: **ch/os**, location of cerebral hemisphere or of articulation of the orbitosphenoid; **ls**, lingual shelf of maxilla; **mx**, maxilla; **oc**, olfactory canal; **p**, parietal; **pal**, palatine; **pmx**, premaxilla; **pmx-v**, premaxilla-vomer articulation; **pof**, postorbitofrontal; **prf**, prefrontal; **sq**, squamosal; **tb**, tabular boss; **v**, vomer; **vp**, vomerine process of the premaxilla. Paired bones are preceded by **r** (right) or **l** (left). Scale bars each represent 2 cm.

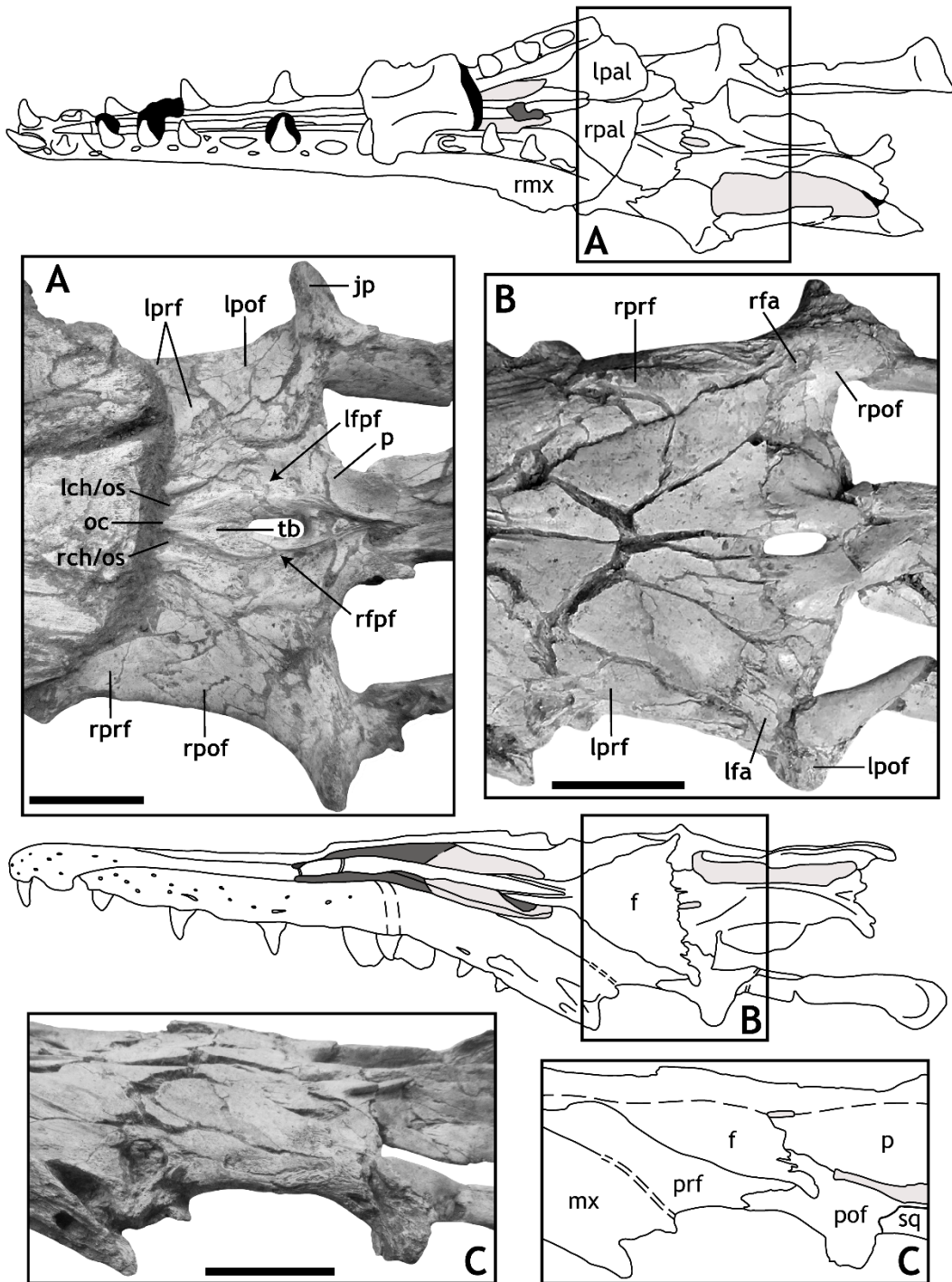


Figure 5. Orbital region and skull roof of MHNM.KHG.1231. (A) Ventral view of skull roof; (B) dorsal view of skull roof; (C) lateral view of left orbit. Major anatomical features are labelled on the diagrams or photographs, with sutures indicated on the diagrams. Line drawings correspond to panels denoted by the same letter. Shading of line drawings as in Figures 2 and 3. In (c), dashed line indicates approximate dorsal midline and double-dashed line indicates estimated location of suture given taphonomic distortion to specimen. Abbreviations: **ch/os**, location of cerebral hemisphere or of articulation of the orbitosphenoid; **f**, frontal; **fa**, frontal ala; **fpf**, frontal posteromedian flange; **jp**, jugal process of postorbitofrontal; **mx**, maxilla; **oc**, olfactory canal; **p**, parietal; **pal**, palatine; **pof**, postorbitofrontal; **prf**, prefrontal; **sq**, squamosal; **tb**, tabular boss. Paired bones are preceded by **r** (right) or **l** (left) where relevant. Scale bars each represent 5 cm. Line drawings not to scale.

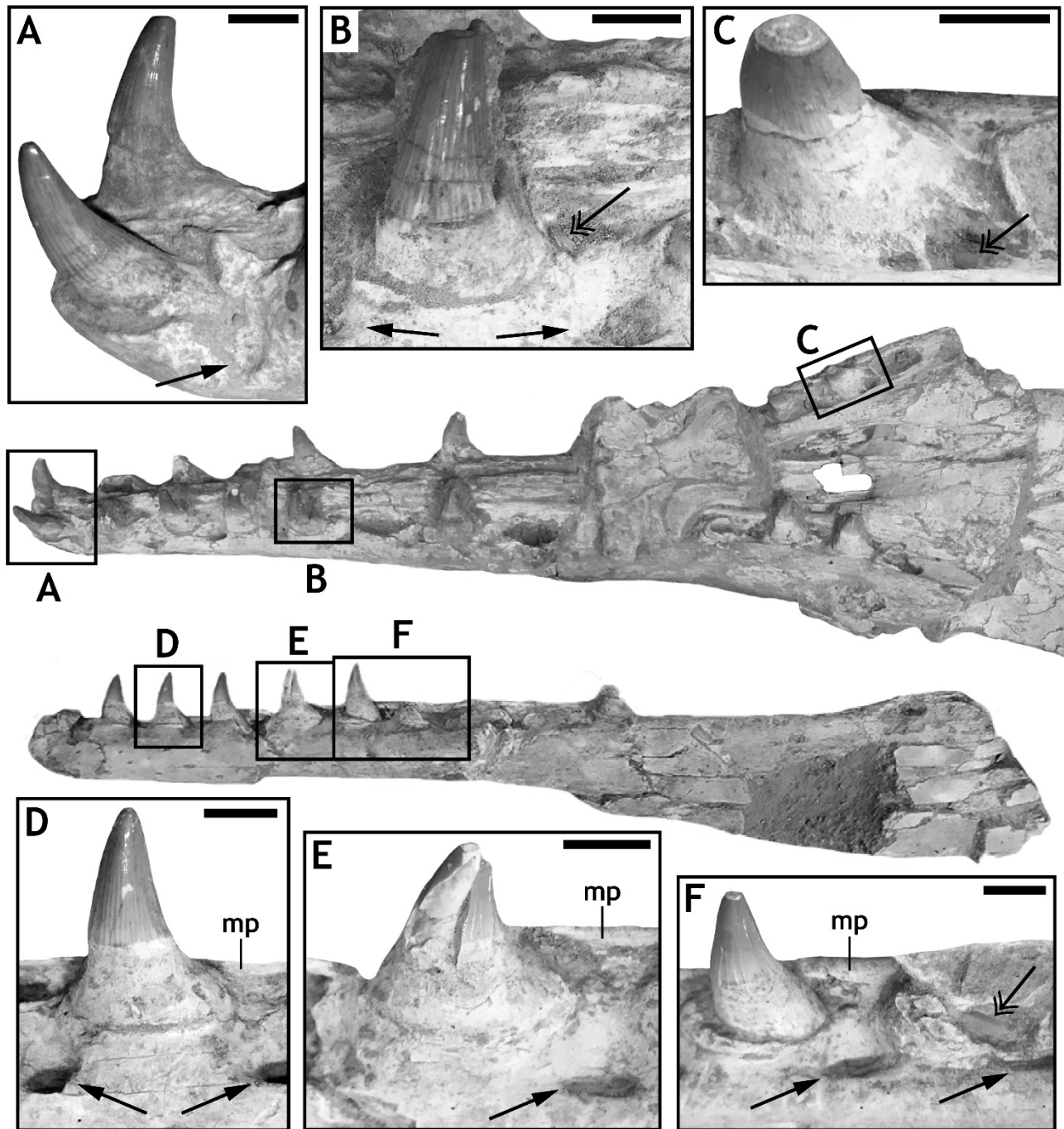


Figure 6. Select views of the dentition of MHNM.KHG.1231, highlighting key aspects of dental anatomy and tooth development. (A) Anterior premaxillary teeth; (B) right maxillary tooth 3; (C) left maxillary tooth 11; (D) left dentary tooth 3; (E) left dentary tooth 5; (F) left dentary tooth 6 and tooth position 7. Insets on overview photographs correspond to panels denoted by the same letter. Solid arrowheads point to interdental pits; fletched arrowheads point to replacement teeth. Replacement teeth in early (C), intermediate (B), and late (F) stages of development are preserved in this specimen. Several stages of post-eruption tooth development are also visible, from early stages in which the marginal teeth are unfused to their respective alveolus (A & F), to intermediate stages of partial fusion to the tooth-bearing element (B & D), to the final stage of being fully fused to the alveolus (E). Abbreviations: **mp**, medial parapet of the dentary. Scale bars each represent 1 cm. Overview photographs not to scale.

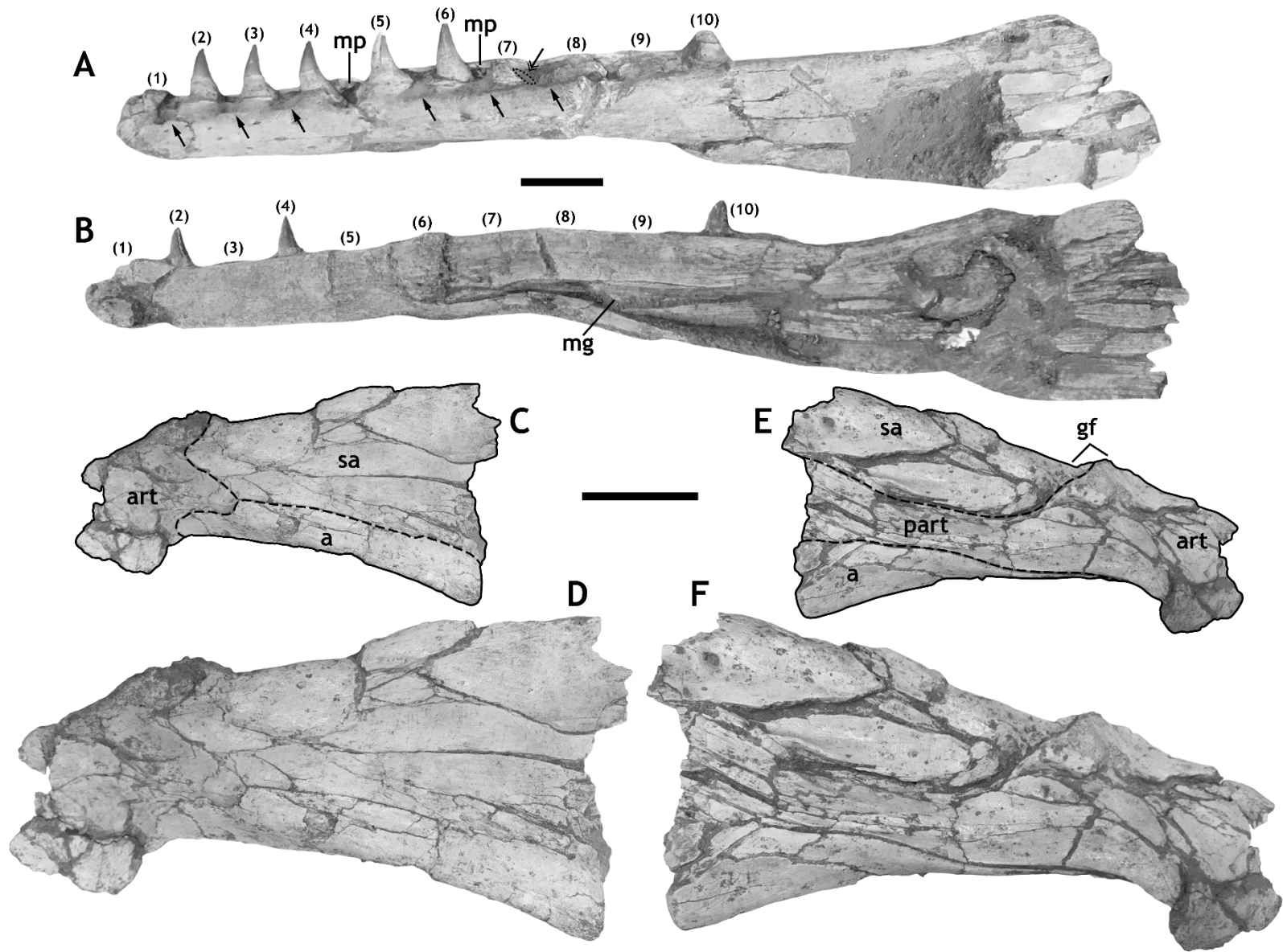


Figure 7. Mandibular elements of MHNM.KHG.1231. (A) Left dentary in lateral view; (B) right dentary in medial view; (C–D) right posterior mandibular unit in lateral view; (E–F) right posterior mandibular unit in medial view. Solid arrowheads indicate interdental pits; fletched arrowheads indicate replacement teeth. Bracketed numbers indicate tooth positions. Abbreviations: **a**, angular; **art**, articular; **gf**, glenoid fossa; **mg**, Meckelian groove; **mp**, medial parapet of the dentary; **part**, prearticular; **sa**, surangular. Each scale bar represents 5 cm. Upper scale bar applies to panels A & B; lower scale bar applies to panels D & F. Panels C & E show the location of sutures and are not to scale.

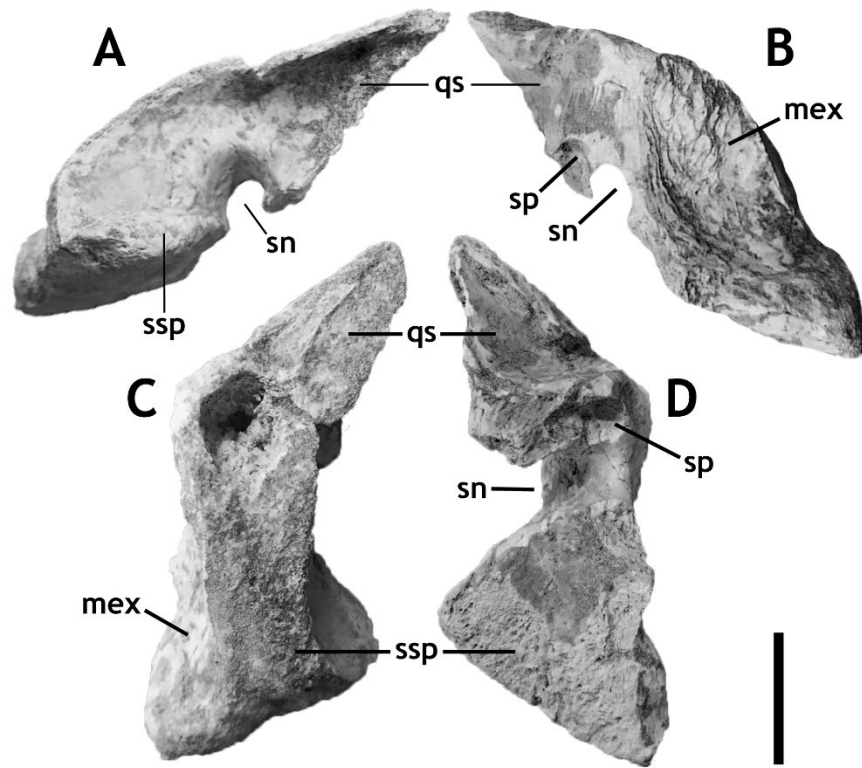


Figure 8. Partial right quadrate of MHNM.KHG.1231 in (A) lateral, (B) medial, (C) dorsal, and (D) ventral views. Abbreviations: **mex**, medial excavation; **qs**, quadrate shaft (top portion); **sn**, stapedial notch; **sp**, stapedial pit; **ssp**, suprastapedial process. Scale bar represents 2 cm.

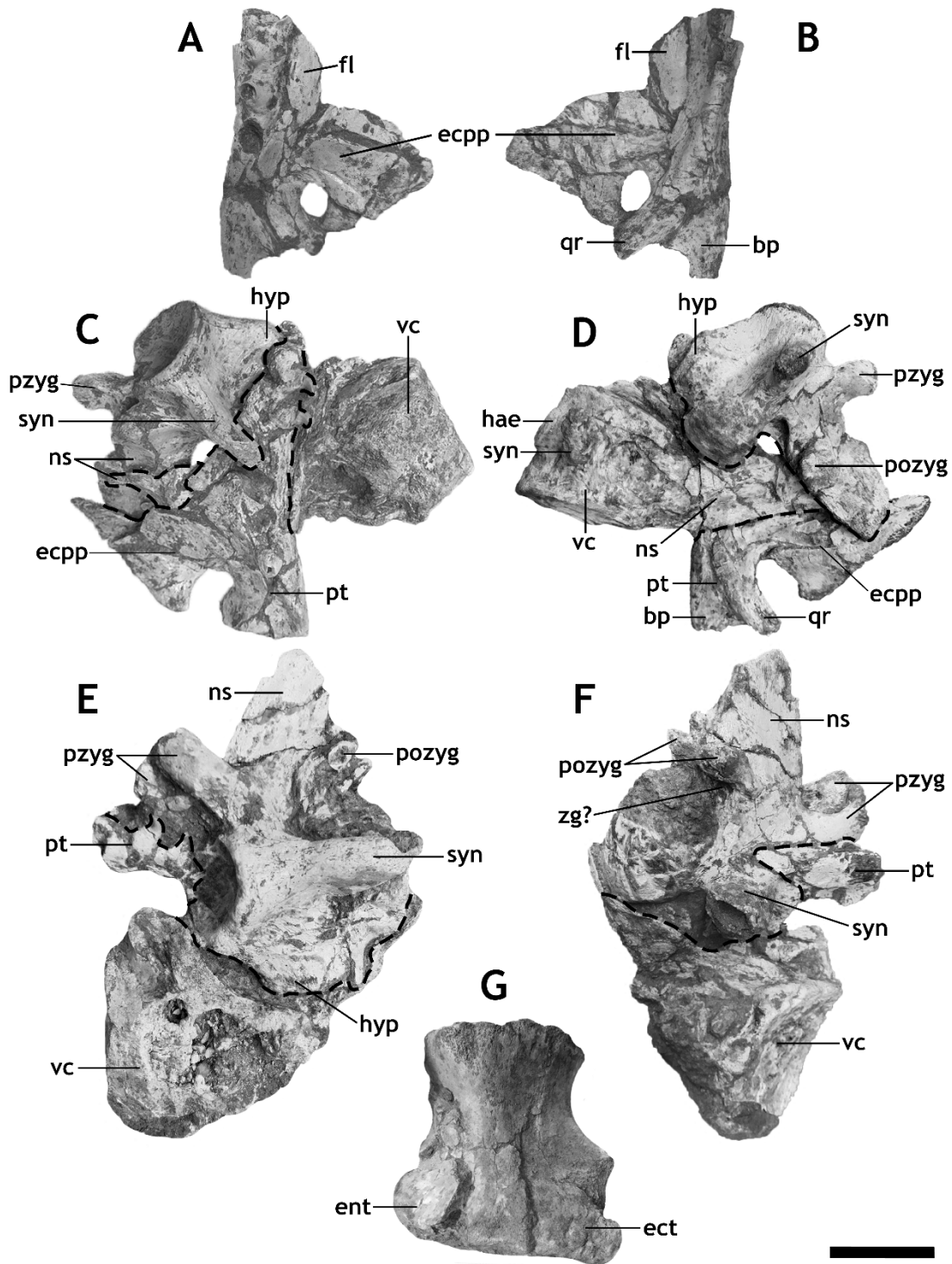


Figure 9. Disarticulated cranial and postcranial material of MHNM.KHG.1231. (A) Left pterygoid in ventral view; (B) left pterygoid in dorsal view; (C) right pterygoid (ventral view) and two vertebrae, the left one cervical and the right one caudal; (D) opposite view of C (i.e., right pterygoid in dorsal view); (E) complete cervical vertebra in left lateral view and crushed vertebral centrum; (F) opposite view of E (i.e., the more complete vertebra is in right lateral view); (G) right humerus in extensor view (proximal is to the top). Abbreviations: **bp**, basisphenoid process; **ecpp**, ectopterygoid process of pterygoid; **ect**, ectepicondyle; **ent**, entepicondyle; **fl**, flange; **hae**, haemapophysis; **hyp**, hypapophysis; **ns**, neural spine; **pozyg**, postzygapophysis; **pt**, pterygoid; **pzyg**, prezygapophysis; **qr**, quadrate ramus; **syn**, synapophysis; **vc**, vertebral centrum; **zg**, zygantum. Scale bar represents 5 cm; all bones to scale.

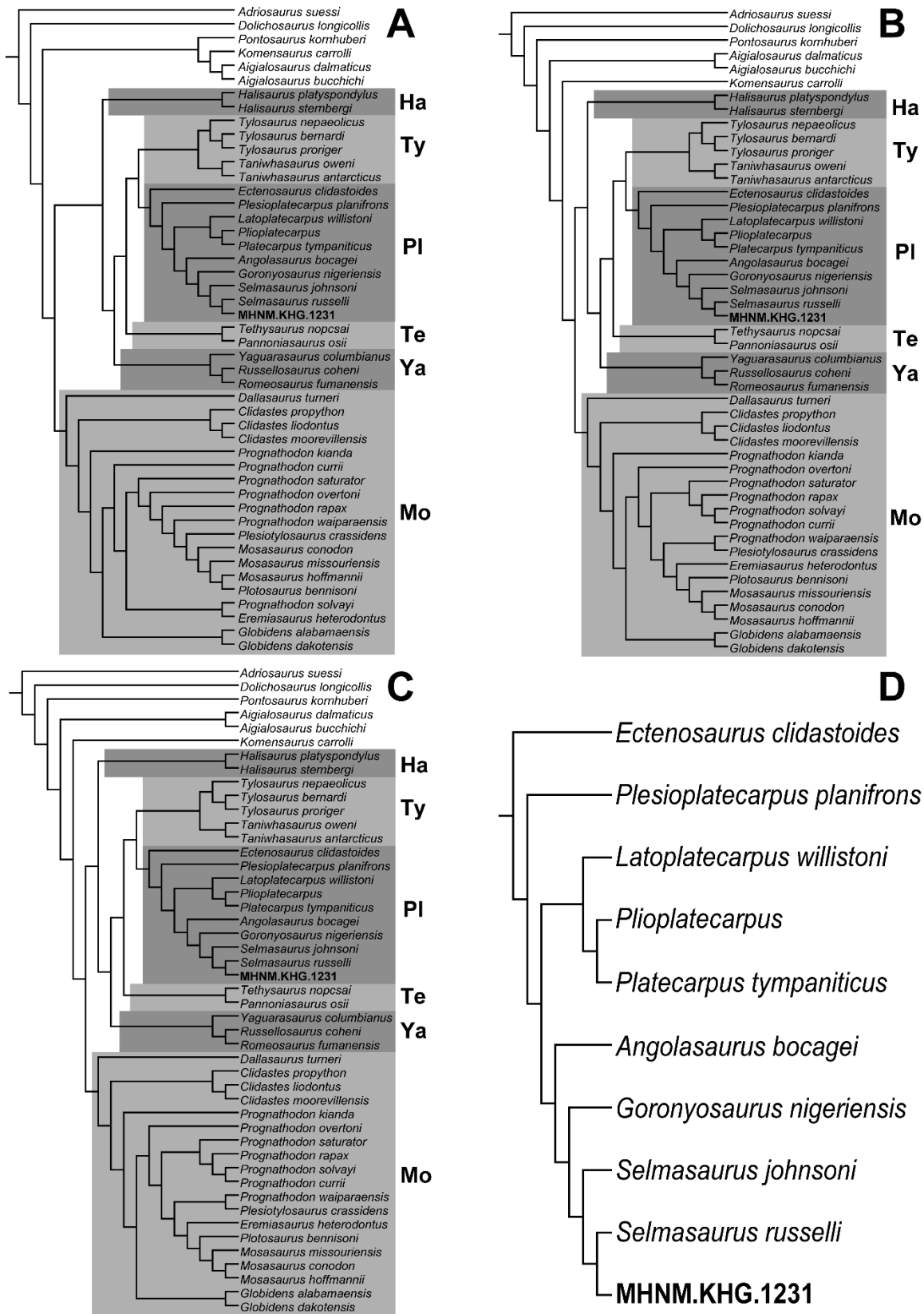


Figure 10. Phylogenetic trees generated via implied weighting maximum parsimony analysis of the dataset utilizing multistate character coding (Mu-IWMP). (A) Single most parsimonious tree (MPT) (468 steps) generated when $k = 3.0$; (B) single MPT (465 steps) generated when $k = 7.0$; (C) single MPT (465 steps) generated when $k = 11.0$; (D) enlarged phylogeny of the subfamily Plioplatecarpinae. Abbreviations for mosasaur subfamilies: **Ha**, Halisaurinae; **Mo**, Mosasaurinae; **PI**, Plioplatecarpinae; **Te**, Tethysaurinae; **Ty**, Tylosaurinae; **Ya**, Yaguarasaurinae.

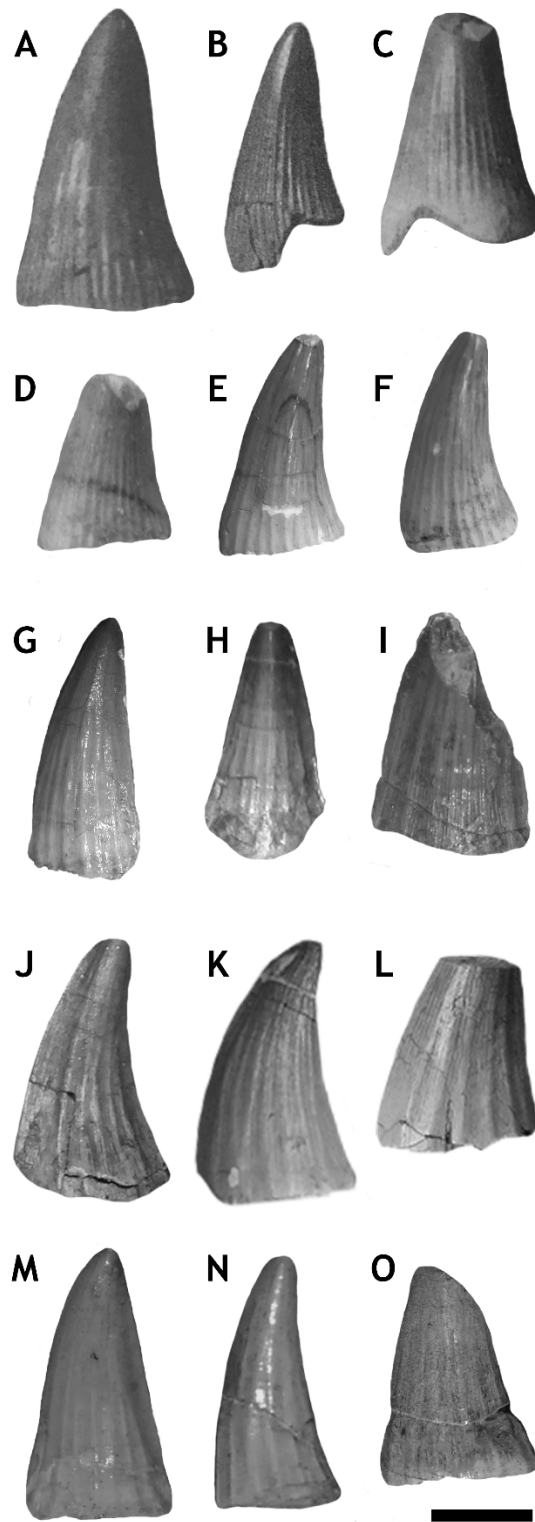


Figure 11. Comparison of various marginal teeth of (A–C) *Platecarpus* *ptychodon*, (D–F) *Gavialimimus* *almaghribensis*, (G–I) *Platecarpus* *somenensis*, (J–L) *Prognathodon* *solwayi*, and (M–O) *Mosasaurus* *lemonnieri*. Note how all of the teeth match the diagnosis of '*P.* *ptychodon*', rendering this diagnosis – and thus this species – invalid. (A–C) Isolated teeth as photographed by Arambourg (1952) in Plate 39, Fig. 2 (holotype of '*P.* *ptychodon*'), Fig. 4, and Fig. 6, respectively; (D–E) MHN.M.KHG.1231 (holotype), maxillary; (F) MHN.M.KHG.1231 (holotype), premaxillary; (G–I) MNHN 1895-7 (holotype), maxillary; (J) IRSNB R33-4672 (holotype), maxillary; (K–L) IRSNB R33-4565, dentary; (M–N) IRSNB 3109, maxillary and dentary; (O) IRSNB 3119, maxillary. Scale bar represents 1 cm; all teeth to scale.

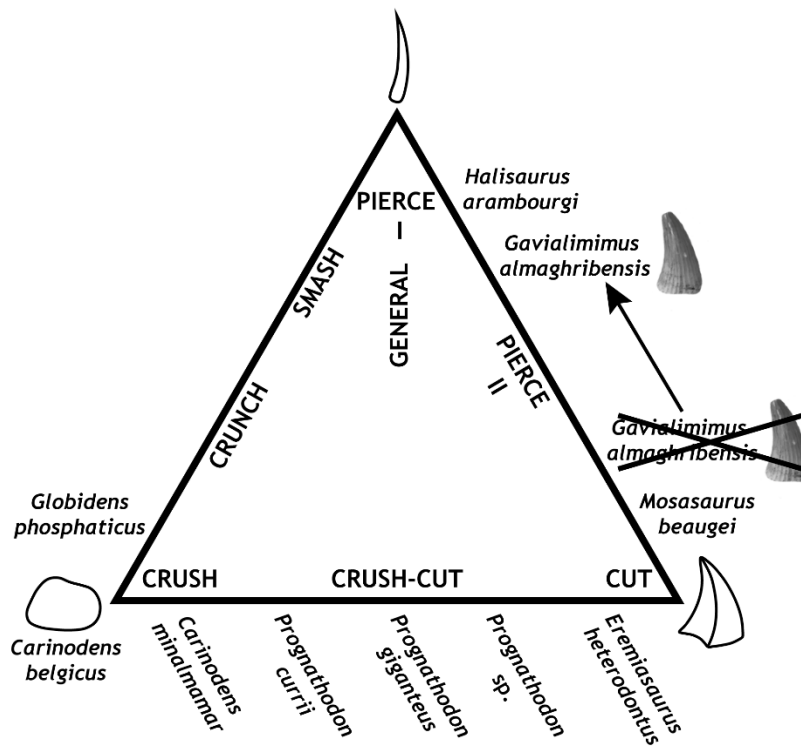


Figure 12. Predatory guilds of Mesozoic marine reptiles based on tooth morphology [modified from Massare (1987) and Bardet *et al.* (2015) with permission from Taylor & Francis and Elsevier, respectively]. These marine predators – including Moroccan mosasaurs, indicated in italicized text – can be classified into eight gradational feeding guilds based on tooth size, shape, carinae, and pattern of wear. These tooth morphoguilds reflect similar prey preference, regardless of phylogenetic position. Ideal ‘end member’ tooth morphologies are depicted at each apex of the diagram. Teeth assigned to ‘*Platecarpus*’ *ptychodon* (morphologically indistinguishable from those of *Gaviolimimus almaghribensis*, pictured in the diagram) were originally used to classify this organism as a member of the ‘Pierce II’–‘Cut’ guilds (Bardet *et al.* 2015). However, cranial adaptations of *G. almaghribensis* suggest ecological specialization as a highly adapted piscivore, thus supporting placement as a ‘Pierce I’–‘Pierce II’ predator.



Figure 13. Life reconstruction of *Gavialimimus almaghribensis*, gen. et sp. nov., hunting a school of teleosts. Image credit: Tatsuya Shinmura.

REFERENCES

- Arambourg, C.** 1952. Les vertébrés fossiles des gisements de phosphates (Maroc–Algérie–Tunisie). *Notes et mémoires du Service géologique du Maroc*, **92**, 1–372.
- Bardet, N., Houssaye, A., Vincent, P., Pereda Superbiola, X., Amaghaz, M., Jourani, E. & Meslouh, S.** 2015. Mosasaurids (Squamata) from the Maastrichtian Phosphates of Morocco: Biodiversity, palaeobiogeography and palaeoecology based on tooth morphoguilds. *Gondwana Research*, **27**, 1068–1078. doi:10.1016/j.gr.2014.08.014
- Bardet, N., Pereda Superbiola, X., Iarochène, M., Bouya, B. & Amaghaz, M.** 2005. A new species of *Halisaurus* from the Late Cretaceous phosphates of Morocco, and the phylogenetical relationships of the Halosaurinae (Squamata: Mosasauridae). *Zoological Journal of the Linnean Society*, **143**, 447–472.
- Massare, J. A.** 1987. Tooth morphology and prey preference of Mesozoic marine reptiles. *Journal of Vertebrate Paleontology*, **7**(2), 121–137. doi:10.1080/02724634.1987.10011647

SUPPLEMENTARY MATERIAL

**A new species of longirostrine plioplatecarpine mosasaur (Squamata: Mosasauridae) from
the Late Cretaceous of Morocco, with a re-evaluation of the problematic taxon
*'Platecarpus' ptychodon***

Catherine R. C. Strong^{a*}, Michael W. Caldwell^{a,b}, Takuya Konishi^c, and Alessandro Palci^{d,e}

^a*Department of Biological Sciences, University of Alberta, Edmonton, Canada, T6G 2E9;*

^b*Department of Earth and Atmospheric Sciences, University of Alberta, Edmonton, Canada, T6G*

2E9; ^c*Department of Biological Sciences, University of Cincinnati, Cincinnati, U.S.A., 45221-*

0006; ^d*Earth Sciences Section, South Australian Museum, Adelaide, Australia, 5000;* ^e*College of*

Science and Engineering, Flinders University, Adelaide, Australia, 5042

* Corresponding author. Email: crstrong@ualberta.ca

TABLE OF CONTENTS**S1. Character List (Multistate)****S2. Character List (Contingent)****S3. Multistate Matrix (see separate Nexus file)****S4. Contingent Matrix (see separate Nexus file)****S5–7. Supplementary Figures**

Figure S5. Consensus trees produced via unweighted maximum parsimony analysis of the dataset utilizing multistate character coding (Mu-UMP).

Figure S6. Consensus trees produced via unweighted maximum parsimony analysis of the dataset utilizing contingent character coding (Co-UMP).

Figure S7. Trees produced via implied weighting maximum parsimony analysis of a dataset utilizing contingent character coding (Co-IWMP).

S8. Topology (Extended)

S1. CHARACTER LIST (MULTISTATE)

Description of the characters used in the phylogenetic analysis applying multistate character coding, modified from Simões *et al.* (2017b) and Konishi & Caldwell (2011).

Part 1. Modifications to original character matrix in Simões *et al.* (2017)

- Three taxa were added to the source matrices: MHNM.KHG.1231 as a new species (*Gavialimimus almaghribensis*), *Goronyosaurus nigeriensis*, and *Selmasaurus russelli*. These latter two taxa were included because they each exhibit certain morphological similarities to MHNM.KHG.1231 (e.g., snout elongation and deep interdental pits for *G. nigeriensis*; similar medial excavation of the suprastapedial process of the quadrate for *S. russelli*), suggesting the potential for a close evolutionary relationship worth being tested phylogenetically.
- Characters 51 and 74 in the original matrix were removed from the analysis, though are listed here for reference. Character 51 (basioccipital tubera shape) was deleted from this analysis on the basis of poor character construction. This character's states (tubera not anteroposteriorly elongate [0], or anteroposteriorly elongate with rugose ventrolateral surfaces [1]) conflate different features – elongation and rugosity – thus exemplifying problematic character type I A.6 as outlined by Simões *et al.* (2017a). Character 74 (tooth replacement mode) was also deleted on the basis of poor character construction, as its character states (replacement teeth form in shallow excavations [0], or in subdental crypts [1]) simply refer to different stages of tooth replacement [e.g., see Caldwell (2007)] and therefore carry no phylogenetic signal.
- The state for character 12 (frontal olfactory canal embrasure) was changed from '1' (canal almost or completely enclosed ventrally by descending processes) to '0' (canal not embraced ventrally) for *Selmasaurus johnsoni* in light of re-interpretation of this character and its condition in *S. johnsoni* and *S. russelli*.
- The character states for multistate character 26 (prefrontal-postorbitofrontal contact) were originally mis-labelled as '0', '0', and '1' in the source character list; this typographic error was corrected to '0', '1', '2' in the modified dataset.
- For character 54 (dentary medial parapet), a new character state (state 3: medial parapet taller than lateral wall of bone) was added to the original states (parapet positioned at base of tooth roots [0], or parapet elevated and strap-like, enclosing about half of height of tooth attachment in shallow channel [1], or parapet equal in height to lateral wall of bone [2]). This new state accounts for additional variation present in

MHNM.KHG.1231/*Gavialimimus* and some individuals of *Plioplatecarpus*.

- A new character (Character 124): quadrate mid-shaft lateral deflection; absent [0], or present [1]) was added to both the multistate and contingent datasets. This is a modified version of character 95 in Konishi & Caldwell (2011) and was included because the quadrate shaft deflection to which it refers is a synapomorphy of *Selmasaurus*.

Part 2. Character list applying multistate coding

- (1) Premaxilla premental rostrum II: rostrum absent (0); rostrum very short and obtuse (1); or distinctly protruding (2); or very large and inflated (3). In *Clidastes* a short, acute, protruding rostrum (state 1) produces a ‘V’-shaped dorsal profile and, as far as is known, is peculiar to that genus. An alternative condition, described as ‘U’- shaped, includes those taxa whose rostral conditions span the whole range of states of characters 1 and 2. Hence, the descriptive character is abandoned in favor of a more informative structure-based series.
- (2) Premaxilla shape: bone broadly arcuate anteriorly (0); or relatively narrowly arcuate or acute anteriorly (1). In virtually all lizards the premaxilla is a very widely arcuate and lightly constructed element, and the base of the internarial process is quite narrow as in *Aigialosaurus bucchichi*. All other mosasaurids have a very narrowed premaxilla with the teeth forming a tight curve and the internarial process being proportionally wider (state 1). *Tethysaurus* was recoded as having state 0.
- (3) Premaxilla internarial bar width: narrow, distinctly less than half of the maximum width of the rostrum in dorsal view (0); or wide, being barely narrower than the rostrum (1). *Aigialosaurus* was recoded as having state 0.
- (4) Premaxilla internarial bar base shape: triangular (0); or rectangular (1). A vertical cross-section through the junction of the internarial bar and the dentigerous rostrum produces an inverted triangle in most taxa. But in state 1, this cross-section is transversely rectangular because the broad ventral surface of the bar is planar.
- (5) Premaxilla internarial bar dorsal keel: absent (0); or present (1). In state 1 a ridge rises above the level of a normally smoothly continuous transverse arch formed by the bones of the anterior muzzle.
- (6) Premaxilla internarial bar venter: with entrance for the fifth cranial nerve close to rostrum (0); or far removed from rostrum (1). The conduit that marks the path of the fifth cranial nerve from the maxilla into the premaxilla is expressed as a ventrolateral foramen within the premaxillo-maxillary sutural surface at the junction of the internarial bar and the dentigerous rostrum. State 1 includes a long shallow groove on the ventral surface of the bar. Anteriorly,

this groove becomes a tunnel entering the bone at an extremely shallow angle, but disappearing below the surface at least 1 cm behind the rostrum.

- (7) Frontal shape in front of the orbits: sides sinusoidal (0); or bone nearly triangular and sides relatively straight (1). In state 1, the area above the orbits is expanded and an isosceles triangle is formed by the rectilinear sides. In certain taxa, a slight concavity is seen above the orbits, but anterior and posterior to this, there is no indication of a sinusoidal or recurved edge.
- (8) Frontal width: element broad and short (0); intermediate dimensions (1); or long and narrow (2). Mosasauroid frontals can be separated into a group that generally has a maximum length to maximum width ratio greater than 2:1 (state 2), between 1.5:1 and 2:1 (state 1), or equal to or less than 1.5:1 (state 0).
- (9) Frontal narial emargination: frontal not invaded by posterior end of nares (0); or distinct embayment present (1). In some mosasauroids, the posterior ends of the nares are concomitant with the anterior terminus of the frontal-prefrontal suture and, therefore, there is no marginal invasion of the frontal by the opening. However, in other mosasauroids this suture begins anterior and lateral to the posterior ends of the nares, causing a short emargination into the frontal.
- (10) Frontal midline dorsal keel: absent (0); or low, fairly inconspicuous (1); or high, thin, and well-developed (2).
- (11) Frontal ala shape: sharply acuminate (0); or more broadly pointed or rounded (1). In state 0, the anterolateral edge of the ala is smoothly concave, thus helping to form the sharply pointed or rounded and laterally oriented posterior corners. In some forms the anterolateral edge of the ala may be concave, but the tip is not sharp and directed laterally.
- (12) Frontal olfactory canal embrasure: canal not embraced ventrally by descending processes (0); or canal almost or completely enclosed below (1). In state 1, very short descending processes from the sides of the olfactory canal surround and almost, or totally, enclose the olfactory nerve.
- (13) Frontal posteroventral midline: tabular boss immediately anterior to the frontal-parietal suture absent (0); or present (1). A triangular boss with a flattened ventral surface at the posterior end of the olfactory canal is represented by state 1.
- (14) Frontal-parietal suture overlap orientation: apposing surfaces with no overlap (0); suture with oblique median frontal and parietal ridges contributing to overlap (1); or with all three ridges

almost horizontal (2). In state 0, the median ridge from the frontal and the single parietal ridge are oriented at a distinct angle to the upper skull surface while the outer, or lateral, frontal ridge appears to be nearly horizontal. In *Tylosaurus nepaeolicus* and *T. proriger* (state 1), the obliquity of the intercalating ridges is reclined almost to the horizontal, greatly extending the amount of lateral overlap.

- (15) Frontal invasion of parietal I: lateral sutural flange of frontal posteriorly extended (0); or median frontal sutural flange posteriorly extended (1); or both extended (2); or suture straight (3). In all mosasaurines the oblique median frontal sutural ridge extends onto the dorsal surface of the parietal table and embraces a portion of the anterior table within a tightly crescentic midline embayment. In *Plioplatecarpus* and *Platecarpus*, the lateral oblique sutural ridge from the frontal is greatly protracted posteriorly to cause a large, anteriorly convex embayment in the dorsal frontal-parietal suture. In this case the entire posterolateral corner of the frontal is extended backwards to embrace the anterolateral portion of the parietal table on both sides. Consequently, the pineal foramen is very widely embraced laterally and the oblique anterior sutural ridge of the parietal occupies a position inside the embayment within the frontal. *Dallasaurus* was recorded as ?.
- (16) Frontal medial invasion of parietal II: if present, posteriorly extended median sutural flange short (0); or long (1). The median oblique sutural flange is either short, not reaching back to the pineal foramen (state 0), or tightly embraces the foramen while extending backwards to a position even with or beyond its posterior edge (state 1).
- (17) Parietal length: dorsal surface relatively short with epaxial musculature insertion posterior, between suspensorial rami only (0); or dorsal surface elongate, with epaxial musculature insertion dorsal as well as posterior (1).
- (18) Parietal table shape: generally rectangular to trapezoidal, with sides converging, but not meeting (0); or triangular, with sides contacting in front of suspensorial rami (1); or parietal table elongate, triangular to subrectangular, and highly medially constricted, with a distinct mid- or parasagittal crest anterior to the divergence of the suspensorial rami (2)
- (19) Pineal foramen size: relatively small (0); or large (1). If the foramen is smaller than or equal to the area of the stapedia pit, it is considered small. If the foramen is significantly larger or if the distance across the foramen is more than half the distance between it and the nearest edge of the parietal table, the derived state is achieved.
- (20) Pineal foramen position I: foramen generally nearer to center of parietal table, well away from frontal-parietal suture (0); or close to or barely touching suture (1); or huge foramen straddling suture and deeply invading frontal (2). Generally in state 1, the distance from the

foramen to the suture is about equal to or less than one foramen's length.

- (21) Pineal foramen ventral opening: opening is level with main ventral surface (0); or opening surrounded by a rounded, elongate ridge (1).
- (22) Parietal posterior shelf: presence of a distinct horizontal shelf projecting posteriorly from between the suspensorial rami (0); or shelf absent (1). In some mosasauroids, a somewhat crescent-shaped shelf (in dorsal view) lies at the posterior end of the bone medial to, and below, the origination of the suspensorial rami.
- (23) Parietal suspensorial ramus compression: greatest width vertical or oblique (0); or greatest width horizontal (1). In *Tylosaurus*, the anterior edge of the ramus begins very low on the lateral wall of the descending process, leading to formation of a proximoventral sulcus, but the straps are horizontal distally.
- (24) Parietal union with supratemporal: suspensorial ramus from parietal overlaps supratemporal without interdigitation (0); or forked distal ramus sandwiches proximal end of supratemporal (1).
- (25) Prefrontal supraorbital process: process absent, or present as a very small rounded knob (0); or a distinct, to large, triangular, or rounded overhanging wing (1).
- (26) Prefrontal-postorbitofrontal contact: absent (0); prefrontal overlapped ventrally by postorbitofrontal (1); or prefrontal overlapped laterally by postorbitofrontal (2). Postorbitofrontal ventral overlap of the prefrontal is extreme in *Platecarpus tympaniticus* and *Plioplatecarpus*, such that there is even a thin flange of the frontal interjected between the prefrontal above and the postorbitofrontal below. In *T. proriger*, the postorbitofrontal sends a long narrow process forward to fit into a lateral groove on the prefrontal. In *Plesiotylosaurus*, the overlap is relatively short and more oblique, and there is no groove on the prefrontal.
- (27) Postorbitofrontal shape: narrow (0); or wide (1). In *Clidastes* and the *Globidensini*, the lateral extent of the element is almost equal to half of the width of the frontal and the outline of the bone is basically squared.
- (28) Postorbitofrontal transverse dorsal ridge: absent (0); or present (1). In state 1, an inconspicuous, low, and narrowly rounded ridge traces from the anterolateral corner of the parietal suture across the top of the element to disappear behind the origin of the jugal process.
- (29) Maxilla tooth number: 20–24 (0); or 17–19 (1); or 15–16 (2); 12–14 (3).

- (30) Maxillo-premaxillary suture posterior terminus: suture ends above a point that is anterior to or level with the midline of the fourth maxillary tooth (0); or between the fourth and ninth teeth (1); or level with or posterior to the ninth tooth (2). These somewhat arbitrary divisions of the character states are meant to describe in more concrete terms those sutures that terminate far anteriorly, those that terminate less anteriorly, and those that terminate near the midlength of the maxilla, respectively.
- (31) Maxilla posterodorsal extent: process absent (0); recurved wing of maxilla prevents emargination of prefrontal on dorsolateral edge of external naris (1); or does not (2).
- (32) Jugal posteroventral angle: angle very obtuse or curvilinear (0); or slightly obtuse, near 120° (1); or 90° (2). *Aigialosaurus* was recoded as having state 1, *Russellosaurus* and *Tethysaurus* were recoded as having state 2.
- (33) Jugal posteroventral process: absent (0); or present (1).
- (34) Ectopterygoid contact with maxilla: present (0); or absent (1).
- (35) Pterygoid tooth row elevation: teeth arise from robust, transversely flattened, main shaft of pterygoid (0); or teeth arise from thin pronounced vertical ridge (1). In state 0, the teeth emanate from the relatively planar surface of the thick, slightly dorsoventrally compressed main shaft of the pterygoid. In state 1, a tall, thin dentigerous ridge emanates ventrally from a horizontal flange that forms the base of the quadratic ramus and the ectopterygoid process, thus causing the main shaft to be trough-shaped. Although the outgroup we selected (*Varanus*) does not possess pterygoid teeth we decided to code the primitive condition as state 0 because that is the condition observed in fossil varanoids like *Ovoo gurval* and basal anguimorphs like *Ophisaurus apodus*.
- (36) Pterygoid tooth size: anterior teeth significantly smaller than marginal teeth (0); or anterior teeth large, approaching size of marginal teeth (1). As per the argument discussed for character 40 we coded the outgroup as having state 0.
- (37) Quadrate suprastapedial process length: process short, ends at a level well above midheight (0); or of moderate length, ending very near midheight (1); or long, distinctly below midheight (2); suprastapedial process absent (3). *Russellosaurus* was recoded as having state 2.
- (38) Quadrate suprastapedial process constriction: distinct dorsal constriction (0); or virtually no dorsal constriction (1). Lack of constriction results in an essentially parallel-sided process in posterodorsal view, but can also include the tapering form characteristic of some *Tylosaurus*.

Remarks: This character refers to whether the sides of the suprastapedial process are parallel or not in posterodorsal view. State 0 occurs when there is a localized narrowing or 'pinching' of the suprastapedial process near its attachment with the quadrate shaft, causing the sides of the process to be non-parallel. This is generally typical of mosasaurines (see *Clidastes* as an exemplar). In some other taxa (e.g., *Selmasaurus*, *Gavialimimus*), the suprastapedial process is 'dorsally constricted' in terms of being broadly medially excavated; however, this is different from the morphology to which the present character is referring. Rather than being 'pinched in' at the junction of the suprastapedial process and quadrate shaft, the sides of the suprastapedial process remain continuous/parallel throughout its length in these taxa (see holotypes of *Gavialimimus* or *Selmasaurus* as exemplars). Based on the above criterion that a parallel-sided process reflects lack of constriction, these taxa would fall under state 1 (dorsal constriction – i.e., the narrowed base of the suprastapedial process – not present).

- (39) Quadrate suprastapedial ridge: if present, ridge on ventromedial edge of suprastapedial process indistinct, straight and/or narrow (0); or ridge wide, broadly rounded, and curving downward, especially above stapedial pit (1).
- (40) Quadrate suprastapedial process fusion: no fusion present (0); or process fused to, or in extensive contact with, elaborated process from below (1). A posterior rugose area may be inflated and broadened mediolaterally to partially enclose the ventral end of a broad and elongate suprastapedial process as in *Halisaurus*. In *Globidens*, *Prognathodon*, and *Plesiotylosaurus*, the process is fused ventrally to a narrow pedunculate medial extension of the tympanic rim. A similar condition is present in *Ectenosaurus*, except that the tympanic rim is not medially extended and has a short projection that overlaps a portion of the suprastapedial process posteriorly.
- (41) Quadrate stapedial pit shape: pit broadly oval to almost circular (0); or relatively narrowly oval (1); or extremely elongate with a constricted middle (2). In state 0, the length to width ratio is less than 1.8:1; in state 1 it ranges from 1.8:1 to 2.4:1; and in state 2, it is greater than 2.4:1.
- (42) Quadrate posteroventral ascending tympanic rim condition: ascending ridge small or absent (0); or a high, elongate triangular crest (1); or a crest extremely produced laterally (2). In state 1, this extended rim causes a fairly deep sulcus in the ventral portion of the intratympanic cavity. In *Plioplatecarpus*, the entire lower tympanic rim and ala are expanded into a large conch (state 2), which tremendously increases the depth of the intratympanic cavity.
- (43) Quadrate ala thickness: ala thin (0); or thick (1). In state 0, the bone in the central area of the ala is only about 1 mm thick in medium-sized specimens and that area is usually badly crushed or completely destroyed. Alternatively, the ala extends from the main shaft with only

minor thinning, providing a great deal of strength to the entire bone. *Tethysaurus* was recoded as having state 0.

- (44) Quadrate conch: ala and main shaft encompassing a deeply bowled area (0); or alar concavity shallow (1). A relatively deeper sulcus in the anterior part of the intratympanic cavity and more definition to the ala and the main shaft are features of state 0. *Tethysaurus* was recoded as having state 0.
- (45) Basisphenoid pterygoid process shape: process relatively narrow with articular surface facing mostly anterolaterally (0); or somewhat thinner, more fan-shaped with a posterior extension of the articular surface causing a more lateral orientation (1).
- (46) Quadrate ala groove: absent (0); or long, distinct, and deep groove present in anterolateral edge of ala (1); or groove along dorsal margin of quadrate ala (2).
- (47) Quadrate median ridge: single thin, high ridge, dorsal to ventral (0); or ridge low and rounded with divergent ventral ridges (1).
- (48) Quadrate anterior ventral condyle modification: no upward deflection of anterior edge of condyle (0); or distinct deflection present (1). A relatively narrow bump in the otherwise horizontal trace of the anterior articular edge is also subtended by a sulcus on the anteroventral face of the bone.
- (49) Quadrate ventral condyle: condyle saddle-shaped, concave in anteroposterior view (0); or gently domed, convex in any view (1).
- (50) Basioccipital tubera size: short (0); or long (1). Long tubera are typically parallel-sided in posterior profile and protrude ventrolaterally at exactly 45° from horizontal. Short tubera have relatively large bases that taper distally, and emanate more horizontally.
- (former character 51) Basioccipital tubera shape: tubera not anteroposteriorly elongate (0); or anteroposteriorly elongate with rugose ventrolateral surfaces (1).**
- (51) Basioccipital canal: absent (0); or present as a pair separated by a median septum (1); or present as a single bilobate canal (2).
- (52) Dentary tooth number: 20–24 (0); 17–19 (1); 15–16 (2); 14 (3); 13 (4); 12 (5). It is easy to assume this character is correlated with the number of maxillary teeth, except that is not the case in *Ectenosaurus clidastoides*, which has 16 or 17 maxillary teeth and only 13 dentary teeth.

- (53) Dentary anterior projection: absent (0); short (1); or long (2). In state 1, the projection of bone anterior to the first tooth is at least the length of a complete tooth space. *Russellosaurus* was recoded as not applicable.
- (54) Dentary medial parapet: parapet positioned at base of tooth roots (0); or elevated and strap-like, enclosing about half of height of tooth attachment in shallow channel (1); or strap equal in height to lateral wall of bone (2); or medial parapet taller than lateral wall of bone (3). States 1, 2, and 3 are possible sequential stages of modification from a classically pleurodont dentition to the typical mosasaur ‘sub-theodont’ dentition. *Tethysaurus* was recoded as ?.
- (55) Splenial-angular articulation shape: splenial articulation in posterior view almost circular (0); or laterally compressed (1).
- (56) Splenial-angular articular surface: essentially smooth concavoconvex surfaces (0); or distinct horizontal tongues and grooves present (1).
- (57) Coronoid shape: coronoid with slight dorsal curvature, posterior wing not widely fan-shaped (0); or very concave above, posterior wing greatly expanded (1). *Ectenosaurus* was recoded as having state 0.
- (58) Coronoid posteromedial process: small but present (0); or absent (1). *Russellosaurus* was recoded as having state 0, *Ectenosaurus* was recoded as having state 1.
- (59) Coronoid medial wing: does not reach angular (0); or contacts angular (1). *Aigialosaurus* was recoded as ?.
- (60) Coronoid posterior wing: without medial crescentic pit (0); or with distinct excavation (1). In state 1, there is a posteriorly open, ‘C’-shaped excavation in the medial side of the posterior wing of this element. *Dallasaurus* was recoded as ?.
- (61) Surangular coronoid buttress: low, thick, about parallel to lower edge of mandible (0); or high, thin, rapidly rising anteriorly (1). A rounded dorsal edge of the surangular remains almost parallel to the ventral edge as it approaches the posterior end of the coronoid, meeting the latter element near its posteroventral edge in state 0. In state 1, the dorsal edge rises and thins anteriorly until meeting the posterior edge of the coronoid near its apex, producing a triangular posterior mandible in lateral aspect.
- (62) Surangular-articular suture position: behind the condyle in lateral view (0); or at middle of glenoid on lateral edge (1); anterior to condyle (2). In state 1, there is usually an

interdigitation in the dorsal part of the suture. *Aigialosaurus dalmaticus* was rescored as 2.

- (63) Surangular-articular lateral suture trace: suture descends and angles or curves anteriorly (0); or is virtually straight throughout its length (1). In state 1, the suture trails from the glenoid posteriorly about halfway along the dorsolateral margin of the retroarticular process, then abruptly turns anteriorly off the edge and strikes in a straight line for the posterior end of the angular.
- (64) Articular retroarticular process inflection: moderate inflection, less than 60° (0); or extreme inflection, almost 90° (1).
- (65) Articular retroarticular process innervation foramina: no large foramina on lateral face of retroarticular process (0); or one to three large foramina present (1).
- (66) Tooth surface I: teeth finely striate medially (0); or not medially striate (1). In “Russellosaurinae,” medial tooth striations are very fine and groups of tightly spaced striae are usually set apart by facets, leading to a fasciculate appearance. *Angolasaurus* was recoded as ?, *Aigialosaurus* was recoded as having state 1.
- (67) Tooth surface II: teeth not coarsely textured (0); or very coarsely ornamented with bumps and ridges (1). In both species of *Globidens* and in *Prognathodon overtoni*, the coarse surface texture is extreme, consisting of thick pustules, and vermiform or anastomosing ridges. Teeth in *P. rapax* are smooth over the majority of their surface, but usually a few widely scattered, large, very long, sharp-crested vermiform ridges are present.
- (68) Tooth facets: absent (0); or present (1). *Halisaurus* teeth are smoothly rounded except for the inconspicuous carinae. *Clidastes* is described in numerous places as having smooth unfaceted teeth, but many immature individuals and some larger specimens have teeth with three distinct facets on the medial faces. Adult *Tylosaurus proriger* has indistinct facets. *Mosasaurus* has taken this characteristic to the extreme. *Russellosaurus*, *Tethysaurus*, *Angolasaurus*, *Ectenosaurus*, *Platecarpus* (*P. planifrons* and *P. tympaniticus*), and *Plioplatecarpus* have been recoded as having state 0.
- (69) Tooth fluting: absent (0); or present (1). In *Ectenosaurus*, and some *Platecarpus planifrons*, several broadly rounded vertical ridges alternate with shallow, round-bottomed grooves completely around the teeth. *Tethysaurus* was recoded as having both states 0 and 1, because grooves can be observed in larger specimens. *Angolasaurus* was recoded as having state 1.
- (70) Tooth inflation: crowns of posterior marginal teeth conical, tapering throughout (0); or crowns of posterior marginal teeth swollen near the tip or above the base (1). The rear teeth of *Globidens* and *Prognathodon overtoni* are distinctly fatter than other mosasauroid teeth, but

those of *P. rapax* are also swollen immediately distal to the base.

- (71) Tooth carinae I: absent (0); or present but extremely weak (1); or strong and elevated (2). *Halisaurus* exhibits the minimal expression of this character (state 1) in that its marginal teeth are almost perfectly round in cross-section; the carinae are extremely thin and barely stand above the surface of the teeth.
- (72) Tooth carinae serration: absent (0); or present (1).
- (73) Atlas neural arch: notch in anterior border (0); or no notch in anterior border (1). *Dallasaurus* was recoded as ?.

(former character 74) Tooth replacement mode: replacement teeth form in shallow excavations (0); or in subdental crypts (1). All mosasauroids that can be evaluated have an ‘anguimorph’ type of tooth replacement, which is to have interdental positioning of replacement teeth and resorption pits associated with each. *Angolasaurus* was recoded as ?.

- (74) Atlas synapophysis: extremely reduced (0); or large and elongate (1). In state 1, a robust synapophysis extends well posteroventral to the medial articular surface for the atlas centrum, and it may be pedunculate (*Clidastes*) or with a ventral ‘skirt’ that gives it a triangular shape (*Mosasaurus*). A very small triangular synapophysis barely, if at all, extends posterior to the medial articular edge in state 0.
- (75) Zygosphenes and zygantra: absent (0); or present (1). This character assesses only the presence of zygosphenes and zygantra, not their relative development. ^[SEP]Nonfunctional and functional are considered as present. Although the outgroup we selected (*Varanus*) does not possess zygosphenes and zygantra we decided to code the primitive condition as present because these structures can be observed in primitive varanoids like *Saniwa*.
- (76) Zygosphenes and zygantra number: present on many vertebrae (0); or present on only a few (1). As per the argument discussed for character 84 we coded the outgroup as having state 0.
- (77) Hypapophyses: last hypapophysis occurs on or anterior to seventh vertebra (0); or on eight or posteriorly (1).
- (78) Synapophysis height: facets for rib articulations tall and narrow on posterior cervicals and anterior trunk vertebrae (0); or facets ovoid, shorter than the centrum height on those vertebrae (1).

- (79) Synapophysis length: synapophyses of middle trunk vertebrae not laterally elongate (0); or distinctly laterally elongate (1). The lateral extension of the synapophyses from the middle of the trunk is as much as 70–80% of the length of the same vertebra is represented by state 1.
- (80) Synapophysis ventral extension: synapophyses extend barely or not at all below ventral margin of cervical centra (0); or some extend far below ventral margin of centrum (1). In state 1, two or more anterior cervical vertebrae have rib articulations that dip well below the centrum, causing a very deeply concave ventral margin in anterior profile.
- (81) Vertebral condyle inclination: condyles of trunk vertebrae inclined (0); or condyles vertical (1).
- (82) Vertebral condyle shape I: condyles of anterior-most trunk vertebrae extremely dorsoventrally depressed (0); or essentially equidimensional (1). In state 0, posterior height: width ratios of anterior trunk vertebrae are close to 2:1. In state 1, they are between to 4:3 and 1:1.
- (83) Vertebral condyle shape II: condyles of posterior trunk vertebrae not higher than wide (0); or slightly compressed (1). In state 1, the posterior condylar aspect reveals outlines that appear to be higher than wide and even perhaps slightly subrectangular, due to the slight emargination for the dorsal nerve cord.
- (84) Vertebral synapophysis dorsal ridge: sharp ridge absent on posterior trunk synapophyses (0); or with a sharp-edged and anteriorly precipitous ridge connecting distal synapophysis with prezygapophysis (1). In state 0, the ridge in question, if present, may be incomplete or it may be rounded across the crest with the anterior and posterior sides about equally sloping.
- (85) Vertebral length proportions: cervical vertebrae distinctly shorter than longest vertebrae (0); or almost equal or are the longest (1).
- (86) Presacral vertebrae number II: if few, then 28 or 29 (0); 30 or 31 (1); 39 or more (2). Here, presacral vertebrae are considered to be all those anterior to the first bearing an elongate transverse process.
- (87) Sacral vertebrae number: two (0); or less than two (1). Numerous well preserved specimens of derived mosasauroids have failed to show any direct contact of the pelvic girdle with vertebrae in the sacral area. Certainly, no transverse processes bear any type of concave facet for the ilium, and so it is generally assumed that a ligamentous contact was established with only one transverse process. Depending on one's perspective, it could be said that derived mosasauroids have either no or one sacral vertebra.

- (88) Caudal dorsal expansion: neural spines of tail all uniformly shortened posteriorly (0); or several spines dorsally elongated behind middle of tail (1). *Dallasaurus* was recoded as ?.
- (89) Haemal arch length: haemal arches about equal in length to neural arch of same vertebra (0); or length about 1.5 times greater than neural arch length (1). This ratio may be as great as 1.2:1 in state 0. Comparison is most accurate in the middle of the tail and is consistent even on those vertebrae in which the neural spines are also elongated.
- (90) Haemal arch articulation: arches articulating (0); or arches fused to centra (1).
- (91) Tail curvature: no structural downturn of tail (0); or tail with curved posterior portion (1).
- (92) Body proportions: head and trunk shorter than or about equal to tail length (0); or head and trunk longer than tail (1).
- (93) Scapula/coracoid size: both bones about equal (0); or scapula about half the size of coracoid (1). *Dallasaurus* was recoded as ?.
- (94) Scapula width: no anteroposterior widening (0); or distinct fan-shaped widening (1); or extreme widening (2). In state 0, the anterior and posterior edges of the scapula encompass less than one quarter of the arc of a circle, but in state 1, the arc is increased to approximately one third. In state 2, the distal margin encompasses almost a half-circle and the anterior and posterior borders are of almost equal length.
- (95) Scapula dorsal convexity: if scapula widened, dorsal margin very convex (0); or broadly convex (1). In state 0, the anteroposterior dimension is almost the same as the proximodistal dimension. In state 1, the anteroposterior dimension is much larger.
- (96) Scapula posterior emargination: posterior border of bone gently concave (0); or deeply concave (1). In state 1, there is a deeply arcuate emargination on the posterior scapular border, just dorsal to the glenoid. It is immediately bounded dorsally by a corner, which begins a straight-edged segment that continues to the dorsal margin.
- (97) Scapula-coracoid suture: unfused scapula-coracoid contact has interdigitate suture anteriorly (0); or apposing surfaces without interdigitation (1). *Dallasaurus* was recoded as ?.
- (98) Coracoid neck elongation: neck rapidly tapering from medial corners to a relatively broad base (0); or neck gradually tapering to a relatively narrow base (1); coracoid neck absent (2). In state 1, this character describes an outline of the bone, which is nearly symmetrical and gracefully fan-shaped, with gently concave, nearly equidistant sides.

- (99) Coracoid anterior emargination: present (0); or absent (1).
- (100) Humerus length: humerus distinctly elongate, about three or more times longer than distal width (0); or greatly shortened, about 1.5 to 2 times longer than distal width (1); or length and distal width virtually equal (2); or distal width slightly greater than length (3).
- (101) Humerus postglenoid process: absent or very small (0); or distinctly enlarged (1).
- (102) Humerus glenoid condyle: if present, condyle gently domed and elongate, ovoid in proximal view (0); or condyle saddle-shaped, subtriangular in proximal view and depressed (1); or condyle highly domed or protuberant and short ovoid to almost round in proximal view (2). In some taxa, the condylar surfaces of the limbs were finished in thick cartilage and there was no bony surface of the condyle to be preserved. This condition is scored as not represented. In some taxa, the glenoid condyle extends more proximally than does the postglenoid process (state 2), and it is not ovoid as state 0. *Dallasaurus* was recoded as having state 0.
- (103) Humerus deltopectoral crest: crest undivided (0); or split into two separate insertional areas (1). In state 1, the deltoid crest occupies an anterolateral or anterior position confluent with the glenoid condyle, while the pectoral crest occupies a medial or anteromedial area that may or may not be confluent with the glenoid condyle. The deltoid crest is often quite short, broad, and indistinct, being easily erased by degradational taphonomic processes.
- (104) Humerus pectoral crest: located anteriorly (0); or medially (1). In state 1, the pectoral crest is located near the middle of the flexor (or medial) side on the proximal end of the bone.
- (105) Humerus ectepicondylar groove: groove or foramen present on distolateral edge (0); or absent (1).
- (106) Humerus ectepicondyle: absent (0); or present as a prominence (1). A radial tuberosity is reduced in size in *Prognathodon*, but very elongated in *Plesiotylosaurus*. *Tethysaurus* was recoded as having state 0.
- (107) Humerus entepicondyle: absent (0); or present as a prominence (1). The ulnar tuberosity protrudes posteriorly and medially from the posterodistal corner of the bone immediately proximal to the ulnar facet, causing a substantial dilation of the posterodistal corner of the humerus. *Tethysaurus* was recoded as having state 0.
- (108) Radius shape: radius not expanded anterodistally (0); or slightly expanded (1); or broadly expanded (2).

- (109) Ulna contact with centrale: broad ulnare prevents contact (0); or ulna contacts centrale (1). In state 1, the ulnare is omitted from the border of the antebrachial foramen. There is usually a well-developed faceted articulation between the ulna and the centrale (or intermedium, as used by Russell, 1967).
- (110) Radiale size: large and broad (0); or small to absent (1).
- (111) Carpal reduction: carpals number six or more (0); or five or less (1).
- (112) Pisiform: present (0); or absent (1).
- (113) Metacarpal I expansion: spindle-shaped, elongate (0); or broadly expanded (1). The broad expansion is also associated with an anteroproximal overhanging crest in every case observed.
- (114) Phalanx shape: phalanges elongate, spindle-shaped (0); or blocky, hourglass-shaped (1). *Mosasaurus* and *Plotosaurus* have phalanges that are slightly compressed and anteroposteriorly expanded on both ends. *Dallasaurus* was recoded as ?.
- (115) Ilium crest: crest blade-like, articulates with sacral ribs (0); or elongate, cylindrical, does not articulate with sacral ribs (1).
- (116) Ilium acetabular area: arcuate ridge supertending acetabulum (0); or acetabulum set into broad, short 'V'-shaped notch (1). The primitive ilium has the acetabulum impressed on the lateral wall of the bone, with a long narrow crest anterodorsally as the only surrounding topographic feature. In state 1, the acetabular area is set into a short, broadly 'V'-shaped depression that tapers dorsally. The lateral walls of the ilium are therefore distinctly higher than the rim of the acetabulum.
- (117) Pubic tubercle condition: tubercle an elongate protuberance located closer to the midlength of the shaft (0); or a thin semicircular crest-like blade located close to the acetabulum (1).
- (118) Ischiadic tubercle size: elongate (0); or short (1). In state 0, the tubercle is as long as the shaft of the ischium is wide, but it is only a short narrow spur in state 1.
- (119) Astragalus: notched emargination for the crural foramen, without pedunculate fibular articulation (0); or without notch, pedunculate fibular articulation present (1). For state 0, the tibia and fibula are of equal length about the crural foramen and the astragalus contacts both to about the same degree. The form of the latter element is symmetrical and subcircular with a sharp proximal notch. In state 1, the outline of the element is basically reniform and the tibial

articulation is on the same line as the crural emargination. The fibula is also shortened and its contact with the astragalus is narrow.

- (120) Appendicular epiphyses: formed from ossified cartilage (0); or from thick unossified cartilage (1); or epiphyses missing or extremely thin (2). Ends of the limb bones show distinct vascularization and rugose surfaces indicating an apparently thick non-vascularized, unossified cartilage cap. Extremely smooth articular surfaces suggest the epiphyses were excessively thin or perhaps even lost.
- (121) Hyperphalangy: absent (0); or present (1). Hyperphalangy is defined as presence of one or more extra phalanges as compared to the primitive amniote formula of 2-3-4-5-3.
- (122) Posterior thoracic vertebra: not markedly longer than anterior thoracic vertebrae (0); or are markedly longer (1).
- (123) Ectopterygoid process of pterygoid: distal portion of process not offset anterolaterally and/or lacking longitudinal grooves and ridges (0); distal portion of process is offset anterolaterally and bears longitudinal grooves and ridges (1).
- (124) Quadrate mid-shaft lateral deflection: absent (0); present (1). In state 1, the quadrate shaft is bent laterally such that the suprastapedial process is deflected dorsolaterally relative to the main shaft of the quadrate.
 NB: the wording of this character has been modified from Konishi and Caldwell (2011). The original character was phrased as “Quadrate mid-shaft medial bending,” referring to the bend itself projecting medially, resulting in the ventromedial/dorsolateral deflection of the quadrate. The wording was changed to avoid confusion, as the original phrasing gave the impression of the dorsal quadrate shaft and suprastapedial process being deflected medially, when in reality they are deflected laterally [e.g., see amended diagnosis of quadrate in Konishi (2008); see also specimens GSATC 221 (*S. russelli* holotype) and ALMNH PV 995.4.1 (*Selmasaurus* quadrate, cf. *S. russelli*)].

S2. CHARACTER LIST (CONTINGENT)

Description of the characters used in the phylogenetic analysis applying contingent character coding, modified from Simões *et al.* (2017b) and Konishi & Caldwell (2011).

Part 1. Modifications to original character matrix in Simões *et al.* (2017)

- Three taxa were added to the source matrices: MHNM.KHG.1231 as a new species (*Gavialimimus almaghribensis*), *Goronyosaurus nigeriensis*, and *Selmasaurus russelli* Wright and Shannon, 1988. These latter two taxa were included because they each exhibit certain morphological similarities to MHNM.KHG.1231 (e.g., snout elongation and deep interdental pits for *G. nigeriensis*; similar medial excavation of the suprastapedial process of the quadrate for *S. russelli*), suggesting the potential for a close evolutionary relationship worth being tested phylogenetically.
- Characters 55 and 79 in the original matrix were removed from the analysis, though are listed here for reference. Character 55 (basioccipital tubera shape) was deleted from this analysis on the basis of poor character construction. This character's states (tubera not anteroposteriorly elongate [0], or anteroposteriorly elongate with rugose ventrolateral surfaces [1]) conflate different features – elongation and rugosity – thus exemplifying problematic character type I A.6 as outlined by Simões *et al.* (2017a). Character 79 (tooth replacement mode) was also deleted on the basis of poor character construction, as its character states (replacement teeth form in shallow excavations [0], or in subdental crypts [1]) simply refer to different stages of tooth replacement [e.g., see Caldwell (2007)] and therefore carry no phylogenetic signal.
- The state for character 13 (frontal olfactory canal embrasure) was changed from '1' (canal almost or completely enclosed ventrally by descending processes) to '0' (canal not embraced ventrally) for *Selmasaurus johnsoni* Polcyn and Everhart, 2008 in light of re-interpretation of this character and its condition in *S. johnsoni* and *S. russelli*.
- For character 59 (dentary medial parapet), a new character state (state 3: medial parapet taller than lateral wall of bone) was added to the original states (parapet positioned at base of tooth roots [0], or parapet elevated and strap-like, enclosing about half of height of tooth attachment in shallow channel [1], or parapet equal in height to lateral wall of bone [2]). This new state accounts for additional variation present in MHNM.KHG.1231/*Gavialimimus* and some individuals of *Plioplatecarpus*.
- A new character (Character 130): quadrate mid-shaft lateral deflection; absent [0], or present [1] was added to both the multistate and contingent datasets. This is a modified

version of character 95 in Konishi & Caldwell (2011) and was included because the quadrate shaft deflection to which it refers is a synapomorphy of *Selmasaurus*.

Part 2. Character list applying contingent coding

- (1) Premaxilla predental rostrum I: total lack of a bony rostrum (0); or presence of any predental rostrum (1). In lateral profile, the anterior end of the premaxilla either exhibits some bony anterior projection above the dental margin, or the bone recedes posterodorsally from the dental margin. State 1 produces a relatively taller lateral profile with an obvious ‘bow’ or ‘prow.’
- (2) Premaxilla predental rostrum II: rostrum very short and obtuse (0); or distinctly protruding (1); or very large and inflated (2). In *Clidastes* a short, acute, protruding rostrum (state 1) produces a ‘V’-shaped dorsal profile and, as far as is known, is peculiar to that genus. An alternative condition, described as ‘U’- shaped, includes those taxa whose rostral conditions span the whole range of states of characters 1 and 2. Hence, the descriptive character is abandoned in favor of a more informative structure-based series.
- (3) Premaxilla shape: bone broadly arcuate anteriorly (0); or relatively narrowly arcuate or acute anteriorly (1). In virtually all lizards the premaxilla is a very widely arcuate and lightly constructed element, and the base of the internarial process is quite narrow as in *Aigialosaurus bucchichi*. All other mosasaurids have a very narrowed premaxilla with the teeth forming a tight curve and the internarial process being proportionally wider (state 1). *Tethysaurus* was recoded as having state 0.
- (4) Premaxilla internarial bar width: narrow, distinctly less than half of the maximum width of the rostrum in dorsal view (0); or wide, being barely narrower than the rostrum (1). *Aigialosaurus* was recoded as having state 0.
- (5) Premaxilla internarial bar base shape: triangular (0); or rectangular (1). A vertical cross-section through the junction of the internarial bar and the dentigerous rostrum produces an inverted triangle in most taxa. But in state 1, this cross-section is transversely rectangular because the broad ventral surface of the bar is planar.
- (6) Premaxilla internarial bar dorsal keel: absent (0); or present (1). In state 1 a ridge rises above the level of a normally smoothly continuous transverse arch formed by the bones of the anterior muzzle.
- (7) Premaxilla internarial bar venter: with entrance for the fifth cranial nerve close to rostrum (0); or far removed from rostrum (1). The conduit that marks the path of the fifth cranial nerve from the maxilla into the premaxilla is expressed as a ventrolateral foramen within the

premaxillo-maxillary sutural surface at the junction of the internarial bar and the dentigerous rostrum. State 1 includes a long shallow groove on the ventral surface of the bar. Anteriorly, this groove becomes a tunnel entering the bone at an extremely shallow angle, but disappearing below the surface at least 1 cm behind the rostrum.

- (8) Frontal shape in front of the orbits: sides sinusoidal (0); or bone nearly triangular and sides relatively straight (1). In state 1, the area above the orbits is expanded and an isosceles triangle is formed by the rectilinear sides. In certain taxa, a slight concavity is seen above the orbits, but anterior and posterior to this, there is no indication of a sinusoidal or recurved edge.
- (9) Frontal width: element broad and short (0); intermediate dimensions (1); or long and narrow (2). Mosasauroid frontals can be separated into a group that generally has a maximum length to maximum width ratio greater than 2:1 (state 2), between 1.5:1 and 2:1 (state 1), or equal to or less than 1.5:1 (state 0).
- (10) Frontal narial emargination: frontal not invaded by posterior end of nares (0); or distinct embayment present (1). In some mosasauroids, the posterior ends of the nares are concomitant with the anterior terminus of the frontal-prefrontal suture and, therefore, there is no marginal invasion of the frontal by the opening. However, in other mosasauroids this suture begins anterior and lateral to the posterior ends of the nares, causing a short emargination into the frontal.
- (11) Frontal midline dorsal keel: absent (0); or low, fairly inconspicuous (1); or high, thin, and well-developed (2).
- (12) Frontal ala shape: sharply acuminate (0); or more broadly pointed or rounded (1). In state 0, the anterolateral edge of the ala is smoothly concave, thus helping to form the sharply pointed or rounded and laterally oriented posterior corners. In some forms the anterolateral edge of the ala may be concave, but the tip is not sharp and directed laterally.
- (13) Frontal olfactory canal embrasure: canal not embraced ventrally by descending processes (0); or canal almost or completely enclosed below (1). In state 1, very short descending processes from the sides of the olfactory canal surround and almost, or totally, enclose the olfactory nerve.
- (14) Frontal posteroventral midline: tabular boss immediately anterior to the frontal-parietal suture absent (0); or present (1). A triangular boss with a flattened ventral surface at the posterior end of the olfactory canal is represented by state 1.

- (15) Frontal-parietal suture: apposing surfaces with low interlocking ridges (0); or with overlapping flanges (1). In state 0, an oblique ridge on the anterior sutural surface of the parietal intercalates between a single median posterior and a single lateral posterior ridge from the frontal. In state 1, these ridges are protracted into strongly overlapping flanges. The dorsal trace of the suture can be quite complex with a portion of the parietal embraced by the posterior extension of these frontal flanges.
- (16) Frontal-parietal suture overlap orientation: suture with oblique median frontal and parietal ridges contributing to overlap (0); or with all three ridges almost horizontal (1). In state 0, the median ridge from the frontal and the single parietal ridge are oriented at a distinct angle to the upper skull surface while the outer, or lateral, frontal ridge appears to be nearly horizontal. In *Tylosaurus nepaeolicus* and *T. proriger* (state 1), the obliquity of the intercalating ridges is reclined almost to the horizontal, greatly extending the amount of lateral overlap.
- (17) Frontal invasion of parietal I: lateral sutural flange of frontal posteriorly extended (0); or median frontal sutural flange posteriorly extended (1); or both extended (2); or suture straight (3). In all mosasaurines the oblique median frontal sutural ridge extends onto the dorsal surface of the parietal table and embraces a portion of the anterior table within a tightly crescentic midline embayment. In *Plioplatecarpus* and *Platecarpus*, the lateral oblique sutural ridge from the frontal is greatly protracted posteriorly to cause a large, anteriorly convex embayment in the dorsal frontal-parietal suture. In this case the entire posterolateral corner of the frontal is extended backwards to embrace the anterolateral portion of the parietal table on both sides. Consequently, the pineal foramen is very widely embraced laterally and the oblique anterior sutural ridge of the parietal occupies a position inside the embayment within the frontal. *Dallasaurus* was recoded as ?.
- (18) Frontal medial invasion of parietal II: if present, posteriorly extended median sutural flange short (0); or long (1). The median oblique sutural flange is either short, not reaching back to the pineal foramen (state 0), or tightly embraces the foramen while extending backwards to a position even with or beyond its posterior edge (state 1).
- (19) Parietal length: dorsal surface relatively short with epaxial musculature insertion posterior, between suspensorial rami only (0); or dorsal surface elongate, with epaxial musculature insertion dorsal as well as posterior (1).
- (20) Parietal table shape: generally rectangular to trapezoidal, with sides converging, but not meeting (0); or triangular, with sides contacting in front of suspensorial rami (1); or parietal table elongate, triangular to subrectangular, and highly medially constricted, with a distinct mid- or parasagittal crest anterior to the divergence of the suspensorial rami (2).

- (21) Pineal foramen size: relatively small (0); or large (1). If the foramen is smaller than or equal to the area of the stapedia pit, it is considered small. If the foramen is significantly larger or if the distance across the foramen is more than half the distance between it and the nearest edge of the parietal table, the derived state is achieved.
- (22) Pineal foramen position I: foramen generally nearer to center of parietal table, well away from frontal-parietal suture (0); or close to or barely touching suture (1); or huge foramen straddling suture and deeply invading frontal (2). Generally in state 1, the distance from the foramen to the suture is about equal to or less than one foramen's length.
- (23) Pineal foramen ventral opening: opening is level with main ventral surface (0); or opening surrounded by a rounded, elongate ridge (1).
- (24) Parietal posterior shelf: presence of a distinct horizontal shelf projecting posteriorly from between the suspensorial rami (0); or shelf absent (1). In some mosasauroids, a somewhat crescent-shaped shelf (in dorsal view) lies at the posterior end of the bone medial to, and below, the origination of the suspensorial rami.
- (25) Parietal suspensorial ramus compression: greatest width vertical or oblique (0); or greatest width horizontal (1). In *Tylosaurus*, the anterior edge of the ramus begins very low on the lateral wall of the descending process, leading to formation of a proximoventral sulcus, but the straps are horizontal distally.
- (26) Parietal union with supratemporal: suspensorial ramus from parietal overlaps supratemporal without interdigitation (0); or forked distal ramus sandwiches proximal end of supratemporal (1).
- (27) Prefrontal supraorbital process: process absent, or present as a very small rounded knob (0); or a distinct, to large, triangular, or rounded overhanging wing (1).
- (28) Prefrontal contact with postorbitofrontal: no contact at edge of frontal (0); or elements in contact there (1). State 1 is usually described as the frontal being emarginated above the orbits. Often this character can be evaluated by examining the ventral surface of the frontal where depressions outline the limits of the sutures for the two ventral elements.
- (29) Prefrontal-postorbitofrontal overlap: prefrontal overlapped ventrally by postorbitofrontal (0); or prefrontal overlapped laterally (1). Postorbitofrontal ventral overlap of the prefrontal is extreme in *Platecarpus tympaniticus* and *Plioplatecarpus*, such that there is even a thin flange of the frontal interjected between the prefrontal above and the postorbitofrontal

below. In *T. proriger*, the postorbitofrontal sends a long narrow process forward to fit into a lateral groove on the prefrontal. In *Plesiotylosaurus*, the overlap is relatively short and more oblique, and there is no groove on the prefrontal.

- (30) Postorbitofrontal shape: narrow (0); or wide (1). In *Clidastes* and the *Globidensini*, the lateral extent of the element is almost equal to half of the width of the frontal and the outline of the bone is basically squared.
- (31) Postorbitofrontal transverse dorsal ridge: absent (0); or present (1). In state 1, an inconspicuous, low, and narrowly rounded ridge traces from the anterolateral corner of the parietal suture across the top of the element to disappear behind the origin of the jugal process.
- (32) Maxilla tooth number: 20–24 (0); or 17–19 (1); or 15–16 (2); 12–14 (3).
- (33) Maxillo-premaxillary suture posterior terminus: suture ends above a point that is anterior to or level with the midline of the fourth maxillary tooth (0); or between the fourth and ninth teeth (1); or level with or posterior to the ninth tooth (2). These somewhat arbitrary divisions of the character states are meant to describe in more concrete terms those sutures that terminate far anteriorly, those that terminate less anteriorly, and those that terminate near the midlength of the maxilla, respectively.
- (34) Maxilla posterodorsal process: recurved wing of maxilla dorsolaterally overlaps a portion of the anterior end of the prefrontal (0); or process absent (1).
- (35) Maxilla posterodorsal extent: recurved wing of maxilla prevents emargination of prefrontal on dorsolateral edge of external naris (0); or does not (1).
- (36) Jugal posteroventral angle: angle very obtuse or curvilinear (0); or slightly obtuse, near 120° (1); or 90° (2). *Aigialosaurus* was recoded as having state 1, *Russellosaurus* and *Tethysaurus* were recoded as having state 2.
- (37) Jugal posteroventral process: absent (0); or present (1).
- (38) Ectopterygoid contact with maxilla: present (0); or absent (1).
- (39) Pterygoid tooth row elevation: teeth arise from robust, transversely flattened, main shaft of pterygoid (0); or teeth arise from thin pronounced vertical ridge (1). In state 0, the teeth emanate from the relatively planar surface of the thick, slightly dorsoventrally compressed main shaft of the pterygoid. In state 1, a tall, thin dentigerous ridge emanates ventrally from

a horizontal flange that forms the base of the quadratic ramus and the ectopterygoid process, thus causing the main shaft to be trough-shaped. Although the outgroup we selected (*Varanus*) does not possess pterygoid teeth we decided to code the primitive condition as state 0 because that is the condition observed in fossil varanoids like *Ovoo gurval* and basal anguimorphs like *Ophisaurus apodus*.

- (40) Pterygoid tooth size: anterior teeth significantly smaller than marginal teeth (0); or anterior teeth large, approaching size of marginal teeth (1). As per the argument discussed for character 40 we coded the outgroup as having state 0.
- (41) Quadrate suprastapedial process length: process short, ends at a level well above midheight (0); or of moderate length, ending very near midheight (1); or long, distinctly below midheight (2); suprastapedial process absent (3). *Russellosaurus* was recoded as having state 2.
- (42) Quadrate suprastapedial process constriction: distinct dorsal constriction (0); or virtually no dorsal constriction (1). Lack of constriction results in an essentially parallel-sided process in posterodorsal view, but can also include the tapering form characteristic of some *Tylosaurus*.
 Remarks: This character refers to whether the sides of the suprastapedial process are parallel or not in posterodorsal view. State 0 occurs when there is a localized narrowing or 'pinching' of the suprastapedial process near its attachment with the quadrate shaft, causing the sides of the process to be non-parallel. This is generally typical of mosasaurines (see *Clidastes* as an exemplar). In some other taxa (e.g., *Selmasaurus*, *Gavialimimus*), the suprastapedial process is 'dorsally constricted' in terms of being broadly medially excavated; however, this is different from the morphology to which the present character is referring. Rather than being 'pinched in' at the junction of the suprastapedial process and quadrate shaft, the sides of the suprastapedial process remain continuous/parallel throughout its length in these taxa (see holotypes of *Gavialimimus* or *Selmasaurus* as exemplars). Based on the above criterion that a parallel-sided process reflects lack of constriction, these taxa would fall under state 1 (dorsal constriction – i.e., the narrowed base of the suprastapedial process – not present).
- (43) Quadrate suprastapedial ridge: if present, ridge on ventromedial edge of suprastapedial process indistinct, straight and/or narrow (0); or ridge wide, broadly rounded, and curving downward, especially above stapedial pit (1).
- (44) Quadrate suprastapedial process fusion: no fusion present (0); or process fused to, or in extensive contact with, elaborated process from below (1). A posterior rugose area may be inflated and broadened mediolaterally to partially enclose the ventral end of a broad and elongate suprastapedial process as in *Halisaurus*. In *Globidens*, *Prognathodon*, and

Plesiotylosaurus, the process is fused ventrally to a narrow pedunculate medial extension of the tympanic rim. A similar condition is present in *Ectenosaurus*, except that the tympanic rim is not medially extended and has a short projection that overlaps a portion of the suprastapedial process posteriorly.

- (45) Quadrate stapedial pit shape: pit broadly oval to almost circular (0); or relatively narrowly oval (1); or extremely elongate with a constricted middle (2). In state 0, the length to width ratio is less than 1.8:1; in state 1 it ranges from 1.8:1 to 2.4:1; and in state 2, it is greater than 2.4:1.
- (46) Quadrate posteroventral ascending tympanic rim condition: ascending ridge small or absent (0); or a high, elongate triangular crest (1); or a crest extremely produced laterally (2). In state 1, this extended rim causes a fairly deep sulcus in the ventral portion of the intratympanic cavity. In *Plioplatecarpus*, the entire lower tympanic rim and ala are expanded into a large conch (state 2), which tremendously increases the depth of the intratympanic cavity.
- (47) Quadrate ala thickness: ala thin (0); or thick (1). In state 0, the bone in the central area of the ala is only about 1 mm thick in medium-sized specimens and that area is usually badly crushed or completely destroyed. Alternatively, the ala extends from the main shaft with only minor thinning, providing a great deal of strength to the entire bone. *Tethysaurus* was recoded as having state 0.
- (48) Quadrate conch: ala and main shaft encompassing a deeply bowled area (0); or alar concavity shallow (1). A relatively deeper sulcus in the anterior part of the intratympanic cavity and more definition to the ala and the main shaft are features of state 0. *Tethysaurus* was recoded as having state 0.
- (49) Basisphenoid pterygoid process shape: process relatively narrow with articular surface facing mostly anterolaterally (0); or somewhat thinner, more fan-shaped with a posterior extension of the articular surface causing a more lateral orientation (1).
- (50) Quadrate ala groove: absent (0); or long, distinct, and deep groove present in anterolateral edge of ala (1); or groove along dorsal margin of quadrate ala (2).
- (51) Quadrate median ridge: single thin, high ridge, dorsal to ventral (0); or ridge low and rounded with divergent ventral ridges (1).
- (52) Quadrate anterior ventral condyle modification: no upward deflection of anterior edge of condyle (0); or distinct deflection present (1). A relatively narrow bump in the otherwise

horizontal trace of the anterior articular edge is also supertended by a sulcus on the anteroventral face of the bone.

- (53) Quadrate ventral condyle: condyle saddle-shaped, concave in anteroposterior view (0); or gently domed, convex in any view (1).
- (54) Basioccipital tubera size: short (0); or long (1). Long tubera are typically parallel-sided in posterior profile and protrude ventrolaterally at exactly 45° from horizontal. Short tubera have relatively large bases that taper distally, and emanate more horizontally.
- (former character 55) Basioccipital tubera shape: tubera not anteroposteriorly elongate (0); or anteroposteriorly elongate with rugose ventrolateral surfaces (1).**
- (55) Basioccipital canal: absent (0); or present as a pair separated by a median septum (1); or present as a single bilobate canal (2).
- (56) Dentary tooth number: 20–24 (0); 17–19 (1); 15–16 (2); 14 (3); 13 (4); 12 (5). It is easy to assume this character is correlated with the number of maxillary teeth, except that is not the case in *Ectenosaurus clidastoides*, which has 16 or 17 maxillary teeth and only 13 dentary teeth.
- (57) Dentary anterior projection: projection of bone anterior to first tooth present (0); or absent (1).
- (58) Dentary anterior projection length: short (0); or long (1). In state 1, the projection of bone anterior to the first tooth is at least the length of a complete tooth space. *Russellosaurus* was recoded as not applicable.
- (59) Dentary medial parapet: parapet positioned at base of tooth roots (0); or elevated and strap-like, enclosing about half of height of tooth attachment in shallow channel (1); or strap equal in height to lateral wall of bone (2); or medial parapet taller than lateral wall of bone (3). States 1,2, and 3 are possible sequential stages of modification from a classically pleurodont dentition to the typical mosasaur ‘sub-theodont’ dentition. *Tethysaurus* was recoded as ?.
- (60) Splenial-angular articulation shape: splenial articulation in posterior view almost circular (0); or laterally compressed (1).
- (61) Splenial-angular articular surface: essentially smooth concavoconvex surfaces (0); or distinct horizontal tongues and grooves present (1).

- (62) Coronoid shape: coronoid with slight dorsal curvature, posterior wing not widely fan-shaped (0); or very concave above, posterior wing greatly expanded (1). *Ectenosaurus* was recoded as having state 0.
- (63) Coronoid posteromedial process: small but present (0); or absent (1). *Russellosaurus* was recoded as having state 0, *Ectenosaurus* was recoded as having state 1.
- (64) Coronoid medial wing: does not reach angular (0); or contacts angular (1). *Aigialosaurus* was recoded as ?.
- (65) Coronoid posterior wing: without medial crescentic pit (0); or with distinct excavation (1). In state 1, there is a posteriorly open, 'C'-shaped excavation in the medial side of the posterior wing of this element. *Dallasaurus* was recoded as ?.
- (66) Surangular coronoid buttress: low, thick, about parallel to lower edge of mandible (0); or high, thin, rapidly rising anteriorly (1). A rounded dorsal edge of the surangular remains almost parallel to the ventral edge as it approaches the posterior end of the coronoid, meeting the latter element near its posteroventral edge in state 0. In state 1, the dorsal edge rises and thins anteriorly until meeting the posterior edge of the coronoid near its apex, producing a triangular posterior mandible in lateral aspect.
- (67) Surangular-articular suture position: behind the condyle in lateral view (0); or at middle of glenoid on lateral edge (1); anterior to condyle (2). In state 1, there is usually an interdigitation in the dorsal part of the suture. *Aigialosaurus dalmaticus* was rescored as 2.
- (68) Surangular-articular lateral suture trace: suture descends and angles or curves anteriorly (0); or is virtually straight throughout its length (1). In state 1, the suture trails from the glenoid posteriorly about halfway along the dorsolateral margin of the retroarticular process, then abruptly turns anteriorly off the edge and strikes in a straight line for the posterior end of the angular.
- (69) Articular retroarticular process inflection: moderate inflection, less than 60° (0); or extreme inflection, almost 90° (1).
- (70) Articular retroarticular process innervation foramina: no large foramina on lateral face of retroarticular process (0); or one to three large foramina present (1).
- (71) Tooth surface I: teeth finely striate medially (0); or not medially striate (1). In "Russellosaurinae," medial tooth striations are very fine and groups of tightly spaced striae

are usually set apart by facets, leading to a fasciculate appearance. *Angolasaurus* was recoded as ?, *Aigialosaurus* was recoded as having state 1.

- (72) Tooth surface II: teeth not coarsely textured (0); or very coarsely ornamented with bumps and ridges (1). In both species of *Globidens* and in *Prognathodon overtoni*, the coarse surface texture is extreme, consisting of thick pustules, and vermiform or anastomosing ridges. Teeth in *P. rapax* are smooth over the majority of their surface, but usually a few widely scattered, large, very long, sharp-crested vermiform ridges are present.
- (73) Tooth facets: absent (0); or present (1). *Halisaurus* teeth are smoothly rounded except for the inconspicuous carinae. *Clidastes* is described in numerous places as having smooth unfaceted teeth, but many immature individuals and some larger specimens have teeth with three distinct facets on the medial faces. Adult *Tylosaurus proriger* has indistinct facets. *Mosasaurus* has taken this characteristic to the extreme. *Russellosaurus*, *Tethysaurus*, *Angolasaurus*, *Ectenosaurus*, *Platecarpus* (*P. planifrons* and *P. tympaniticus*), and *Plioplatecarpus* have been recoded as having state 0.
- (74) Tooth fluting: absent (0); or present (1). In *Ectenosaurus*, and some *Platecarpus planifrons*, several broadly rounded vertical ridges alternate with shallow, round-bottomed grooves completely around the teeth. *Tethysaurus* was recoded as having both states 0 and 1, because grooves can be observed in larger specimens. *Angolasaurus* was recoded as having state 1.
- (75) Tooth inflation: crowns of posterior marginal teeth conical, tapering throughout (0); or crowns of posterior marginal teeth swollen near the tip or above the base (1). The rear teeth of *Globidens* and *Prognathodon overtoni* are distinctly fatter than other mosasauroid teeth, but those of *P. rapax* are also swollen immediately distal to the base.
- (76) Tooth carinae I: absent (0); or present but extremely weak (1); or strong and elevated (2). *Halisaurus* exhibits the minimal expression of this character (state 1) in that its marginal teeth are almost perfectly round in cross-section; the carinae are extremely thin and barely stand above the surface of the teeth.
- (77) Tooth carinae serration: absent (0); or present (1).
- (78) Atlas neural arch: notch in anterior border (0); or no notch in anterior border (1). *Dallasaurus* was recoded as ?.

(former character 79) Tooth replacement mode: replacement teeth form in shallow excavations (0); or in subdental crypts (1). All mosasauroids that can be evaluated have an ‘anguimorph’ type of tooth replacement, which is to have interdental positioning of

replacement teeth and resorption pits associated with each. *Angolasaurus* was recoded as ?.

- (79) Atlas synapophysis: extremely reduced (0); or large and elongate (1). In state 1, a robust synapophysis extends well posteroventral to the medial articular surface for the atlas centrum, and it may be pedunculate (*Clidastes*) or with a ventral ‘skirt’ that gives it a triangular shape (*Mosasaurus*). A very small triangular synapophysis barely, if at all, extends posterior to the medial articular edge in state 0.
- (80) Zygosphenes and zygantra: absent (0); or present (1). This character assesses only the presence of zygosphenes and zygantra, not their relative development. [L_{SEP}] Nonfunctional and functional are considered as present. Although the outgroup we selected (*Varanus*) does not possess zygosphenes and zygantra we decided to code the primitive condition as present because these structures can be observed in primitive varanoids like *Saniwa*.
- (81) Zygosphenes and zygantra number: present on many vertebrae (0); or present on only a few (1). As per the argument discussed for character 84 we coded the outgroup as having state 0.
- (82) Hypapophyses: last hypapophysis occurs on or anterior to seventh vertebra (0); or on eight or posteriorly (1).
- (83) Synapophysis height: facets for rib articulations tall and narrow on posterior cervicals and anterior trunk vertebrae (0); or facets ovoid, shorter than the centrum height on those vertebrae (1).
- (84) Synapophysis length: synapophyses of middle trunk vertebrae not laterally elongate (0); or distinctly laterally elongate (1). The lateral extension of the synapophyses from the middle of the trunk is as much as 70–80% of the length of the same vertebra is represented by state 1.
- (85) Synapophysis ventral extension: synapophyses extend barely or not at all below ventral margin of cervical centra (0); or some extend far below ventral margin of centrum (1). In state 1, two or more anterior cervical vertebrae have rib articulations that dip well below the centrum, causing a very deeply concave ventral margin in anterior profile.
- (86) Vertebral condyle inclination: condyles of trunk vertebrae inclined (0); or condyles vertical (1).
- (87) Vertebral condyle shape I: condyles of anterior-most trunk vertebrae extremely dorsoventrally depressed (0); or essentially equidimensional (1). In state 0, posterior height:

width ratios of anterior trunk vertebrae are close to 2:1. In state 1, they are between to 4:3 and 1:1.

- (88) Vertebral condyle shape II: condyles of posterior trunk vertebrae not higher than wide (0); or slightly compressed (1). In state 1, the posterior condylar aspect reveals outlines that appear to be higher than wide and even perhaps slightly subrectangular, due to the slight emargination for the dorsal nerve cord.
- (89) Vertebral synapophysis dorsal ridge: sharp ridge absent on posterior trunk synapophyses (0); or with a sharp-edged and anteriorly precipitous ridge connecting distal synapophysis with prezygapophysis (1). In state 0, the ridge in question, if present, may be incomplete or it may be rounded across the crest with the anterior and posterior sides about equally sloping.
- (90) Vertebral length proportions: cervical vertebrae distinctly shorter than longest vertebrae (0); or almost equal or are the longest (1).
- (91) Presacral vertebrae number I: relatively few, 32 or less (0); or numerous, 39 or more (1). Here, presacral vertebrae are considered to be all those anterior to the first bearing an elongate transverse process.
- (92) Presacral vertebrae number II: if few, then 28 or 29 (0); 30 or 31 (1).
- (93) Sacral vertebrae number: two (0); or less than two (1). Numerous well preserved specimens of derived mosasauroids have failed to show any direct contact of the pelvic girdle with vertebrae in the sacral area. Certainly, no transverse processes bear any type of concave facet for the ilium, and so it is generally assumed that a ligamentous contact was established with only one transverse process. Depending on one's perspective, it could be said that derived mosasauroids have either no or one sacral vertebra.
- (94) Caudal dorsal expansion: neural spines of tail all uniformly shortened posteriorly (0); or several spines dorsally elongated behind middle of tail (1). *Dallasaurus* was recoded as ?.
- (95) Haemal arch length: haemal arches about equal in length to neural arch of same vertebra (0); or length about 1.5 times greater than neural arch length (1). This ratio may be as great as 1.2:1 in state 0. Comparison is most accurate in the middle of the tail and is consistent even on those vertebrae in which the neural spines are also elongated.
- (96) Haemal arch articulation: arches articulating (0); or arches fused to centra (1).

- (97) Tail curvature: no structural downturn of tail (0); or tail with curved posterior portion (1).
- (98) Body proportions: head and trunk shorter than or about equal to tail length (0); or head and trunk longer than tail (1).
- (99) Scapula/coracoid size: both bones about equal (0); or scapula about half the size of coracoid (1). *Dallasaurus* was recoded as ?.
- (100) Scapula width: no anteroposterior widening (0); or distinct fan-shaped widening (1); or extreme widening (2). In state 0, the anterior and posterior edges of the scapula encompass less than one quarter of the arc of a circle, but in state 1, the arc is increased to approximately one third. In state 2, the distal margin encompasses almost a half-circle and the anterior and posterior borders are of almost equal length.
- (101) Scapula dorsal convexity: if scapula widened, dorsal margin very convex (0); or broadly convex (1). In state 0, the anteroposterior dimension is almost the same as the proximodistal dimension. In state 1, the anteroposterior dimension is much larger.
- (102) Scapula posterior emargination: posterior border of bone gently concave (0); or deeply concave (1). In state 1, there is a deeply arcuate emargination on the posterior scapular border, just dorsal to the glenoid. It is immediately bounded dorsally by a corner, which begins a straight-edged segment that continues to the dorsal margin.
- (103) Scapula-coracoid suture: unfused scapula-coracoid contact has interdigitate suture anteriorly (0); or apposing surfaces without interdigitation (1). *Dallasaurus* was recoded as ?.
- (104) Coracoid neck elongation: neck rapidly tapering from medial corners to a relatively broad base (0); or neck gradually tapering to a relatively narrow base (1); coracoid neck absent (2). In state 1, this character describes an outline of the bone, which is nearly symmetrical and gracefully fan-shaped, with gently concave, nearly equidistant sides.
- (105) Coracoid anterior emargination: present (0); or absent (1).
- (106) Humerus length: humerus distinctly elongate, about three or more times longer than distal width (0); or greatly shortened, about 1.5 to 2 times longer than distal width (1); or length and distal width virtually equal (2); or distal width slightly greater than length (3).
- (107) Humerus postglenoid process: absent or very small (0); or distinctly enlarged (1).

- (108) Humerus glenoid condyle: if present, condyle gently domed and elongate, ovoid in proximal view (0); or condyle saddle-shaped, subtriangular in proximal view and depressed (1); or condyle highly domed or protuberant and short ovoid to almost round in proximal view (2). In some taxa, the condylar surfaces of the limbs were finished in thick cartilage and there was no bony surface of the condyle to be preserved. This condition is scored as not represented. In some taxa, the glenoid condyle extends more proximally than does the postglenoid process (state 2), and it is not ovoid as state 0. *Dallasaurus* was recoded as having state 0.
- (109) Humerus deltopectoral crest: crest undivided (0); or split into two separate insertional areas (1). In state 1, the deltoid crest occupies an anterolateral or anterior position confluent with the glenoid condyle, while the pectoral crest occupies a medial or anteromedial area that may or may not be confluent with the glenoid condyle. The deltoid crest is often quite short, broad, and indistinct, being easily erased by degradational taphonomic processes.
- (110) Humerus pectoral crest: located anteriorly (0); or medially (1). In state 1, the pectoral crest is located near the middle of the flexor (or medial) side on the proximal end of the bone.
- (111) Humerus ectepicondylar groove: groove or foramen present on distolateral edge (0); or absent (1).
- (112) Humerus ectepicondyle: absent (0); or present as a prominence (1). A radial tuberosity is reduced in size in *Prognathodon*, but very elongated in *Plesiotylosaurus*. *Tethysaurus* was recoded as having state 0.
- (113) Humerus entepicondyle: absent (0); or present as a prominence (1). The ulnar tuberosity protrudes posteriorly and medially from the posterodistal corner of the bone immediately proximal to the ulnar facet, causing a substantial dilation of the posterodistal corner of the humerus. *Tethysaurus* was recoded as having state 0.
- (114) Radius shape: radius not expanded anterodistally (0); or slightly expanded (1); or broadly expanded (2).
- (115) Ulna contact with centrale: broad ulnare prevents contact (0); or ulna contacts centrale (1). In state 1, the ulnare is omitted from the border of the antebrachial foramen. There is usually a well-developed faceted articulation between the ulna and the centrale (or intermedium, as used by Russell, 1967).
- (116) Radiale size: large and broad (0); or small to absent (1).

- (117) Carpal reduction: carpals number six or more (0); or five or less (1).
- (118) Pisiform: present (0); or absent (1).
- (119) Metacarpal I expansion: spindle-shaped, elongate (0); or broadly expanded (1). The broad expansion is also associated with an anteroproximal overhanging crest in every case observed.
- (120) Phalanx shape: phalanges elongate, spindle-shaped (0); or blocky, hourglass-shaped (1). *Mosasaurus* and *Plotosaurus* have phalanges that are slightly compressed and anteroposteriorly expanded on both ends. *Dallasaurus* was recoded as ?.
- (121) Ilium crest: crest blade-like, articulates with sacral ribs (0); or elongate, cylindrical, does not articulate with sacral ribs (1).
- (122) Ilium acetabular area: arcuate ridge supertending acetabulum (0); or acetabulum set into broad, short 'V'-shaped notch (1). The primitive ilium has the acetabulum impressed on the lateral wall of the bone, with a long narrow crest anterodorsally as the only surrounding topographic feature. In state 1, the acetabular area is set into a short, broadly 'V'-shaped depression that tapers dorsally. The lateral walls of the ilium are therefore distinctly higher than the rim of the acetabulum.
- (123) Pubic tubercle condition: tubercle an elongate protuberance located closer to the midlength of the shaft (0); or a thin semicircular crest-like blade located close to the acetabulum (1).
- (124) Ischiadic tubercle size: elongate (0); or short (1). In state 0, the tubercle is as long as the shaft of the ischium is wide, but it is only a short narrow spur in state 1.
- (125) Astragalus: notched emargination for the crural foramen, without pedunculate fibular articulation (0); or without notch, pedunculate fibular articulation present (1). For state 0, the tibia and fibula are of equal length about the crural foramen and the astragalus contacts both to about the same degree. The form of the latter element is symmetrical and subcircular with a sharp proximal notch. In state 1, the outline of the element is basically reniform and the tibial articulation is on the same line as the crural emargination. The fibula is also shortened and its contact with the astragalus is narrow.
- (126) Appendicular epiphyses: formed from ossified cartilage (0); or from thick unossified cartilage (1); or epiphyses missing or extremely thin (2). Ends of the limb bones show

distinct vascularization and rugose surfaces indicating an apparently thick non-vascularized, unossified cartilage cap. Extremely smooth articular surfaces suggest the epiphyses were excessively thin or perhaps even lost.

- (127) Hyperphalangy: absent (0); or present (1). Hyperphalangy is defined as presence of one or more extra phalanges as compared to the primitive amniote formula of 2-3-4-5-3.
- (128) Posterior thoracic vertebra: not markedly longer than anterior thoracic vertebrae (0); or are markedly longer (1).
- (129) Ectopterygoid process of pterygoid: distal portion of process not offset anterolaterally and/or lacking longitudinal grooves and ridges (0); distal portion of process is offset anterolaterally and bears longitudinal grooves and ridges (1).
- (130) Quadrate mid-shaft lateral deflection: absent (0); present (1). In state 1, the quadrate shaft is bent laterally such that the suprastapedial process is deflected dorsolaterally relative to the main shaft of the quadrate.
 NB: the wording of this character has been modified from Konishi and Caldwell (2011). The original character was phrased as “Quadrate mid-shaft medial bending,” referring to the bend itself projecting medially, resulting in the ventromedial/dorsolateral deflection of the quadrate. The wording was changed to avoid confusion, as the original phrasing gave the impression of the dorsal quadrate shaft and suprastapedial process being deflected medially, when in reality they are deflected laterally [e.g., see amended diagnosis of quadrate in Konishi (2008); see also specimens GSATC 221 (*S. russelli* holotype) and ALMNH PV 995.4.1 (*Selmasaurus* quadrate, cf. *S. russelli*)].

S5-7. SUPPLEMENTARY FIGURES

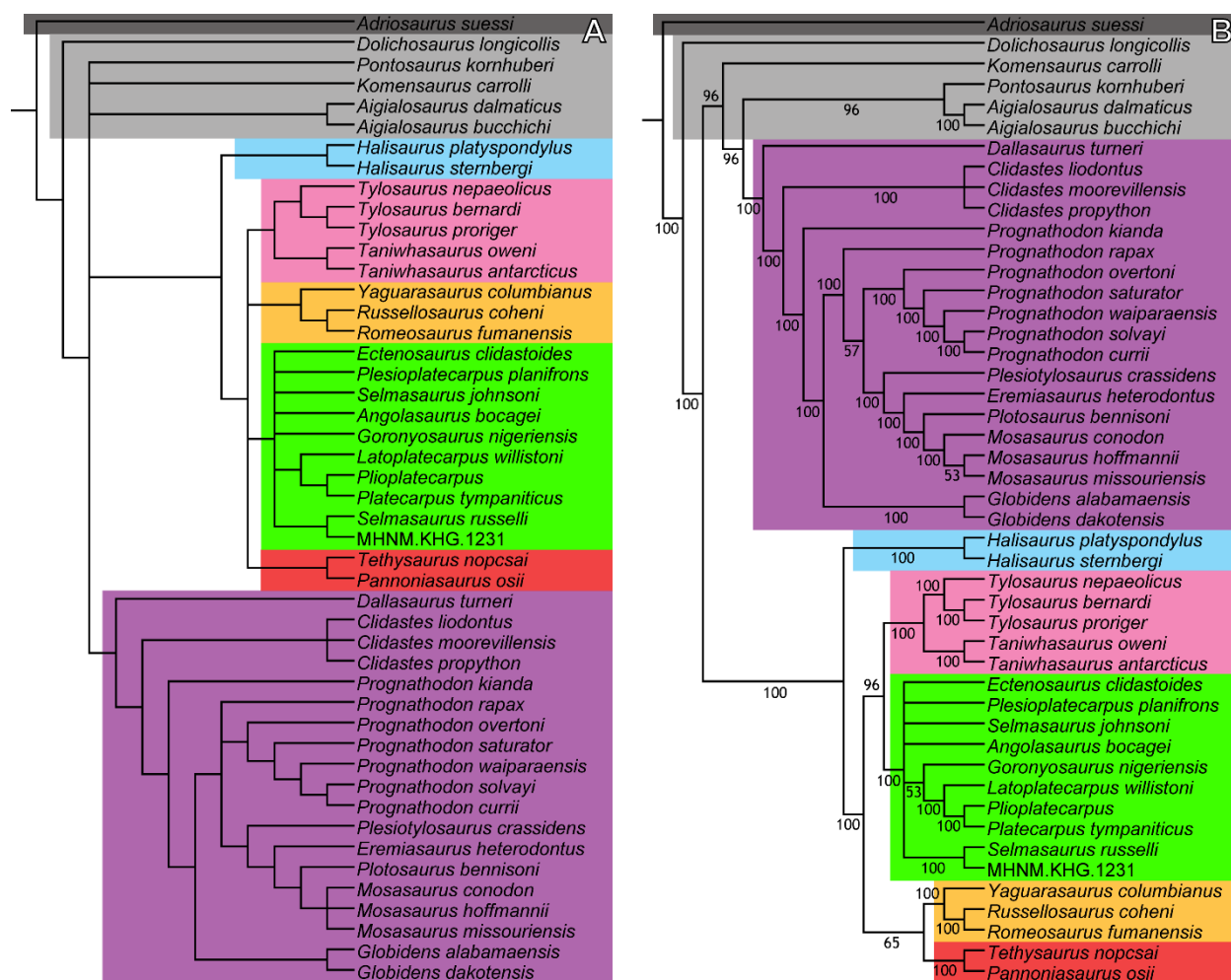


FIGURE S5. Consensus trees produced via unweighted maximum parsimony analysis of the dataset utilizing multistate character coding (Mu-UMP). (A) Strict consensus tree of 26 most parsimonious trees (MPTs) of 464 steps each; (B) 50% majority rule consensus tree of these 26 MPTs, including percentage of MPTs in which each clade was recovered. Each colour represents a mosasaur subfamily: **purple** = Mosasaurinae; **green** = Plioplatecarpinae; **blue** = Halisaurinae; **light pink** = Tylosaurinae; **dark pink** = Tethysaurinae; **yellow** = Yaguarasaurinae; **light grey** = non-mosasaurid Mosasauria; **dark grey** = outgroup.

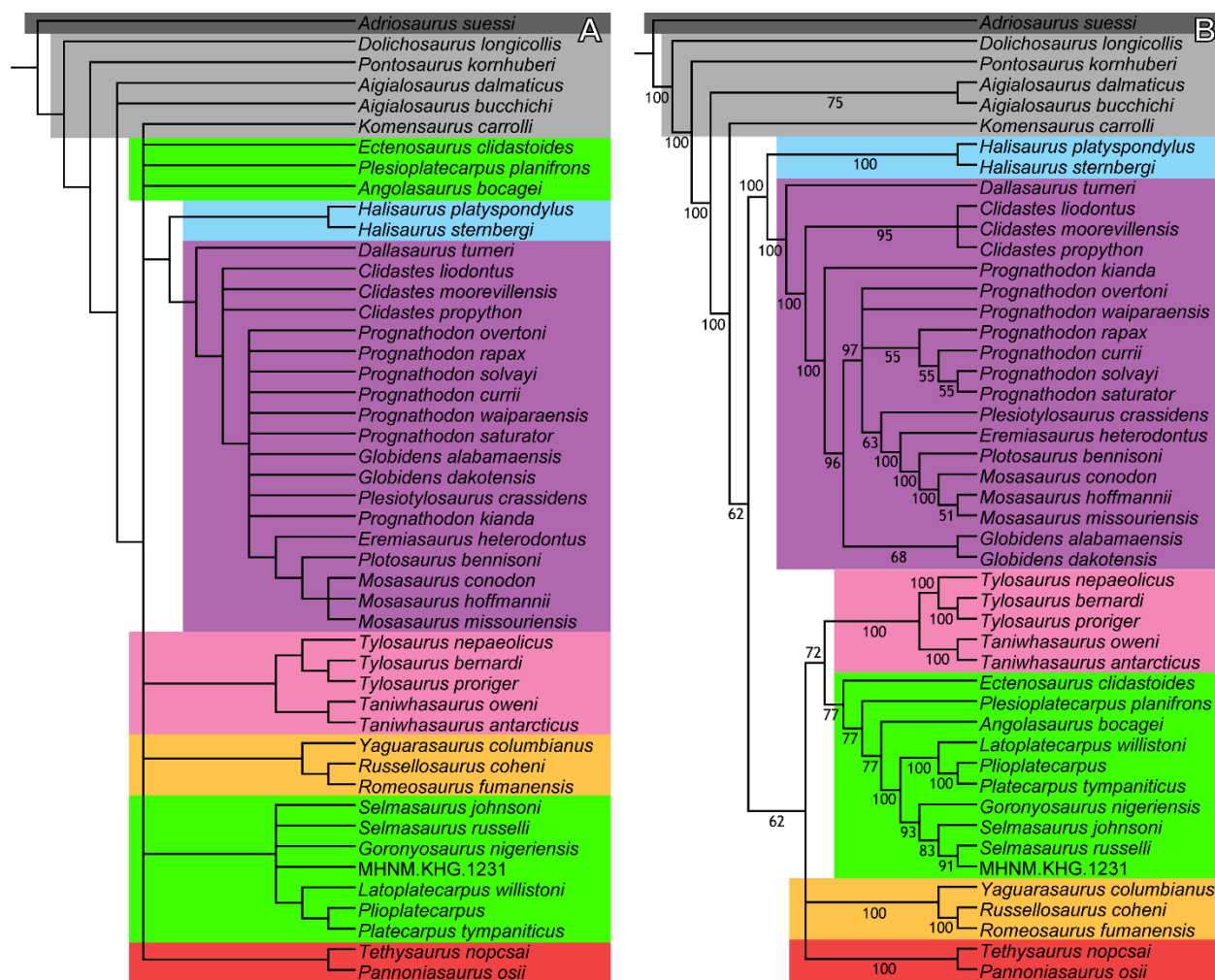


FIGURE S6. Consensus trees produced via unweighted maximum parsimony analysis of the dataset utilizing contingent character coding (Co-UMP). (A) Strict consensus tree of 112 most parsimonious trees (MPTs) of 468 steps each; (B) 50% majority rule consensus tree of these 112 MPTs, including percentage of MPTs (if >50%) in which each clade was recovered. Colouration of boxes as in Fig. S5.

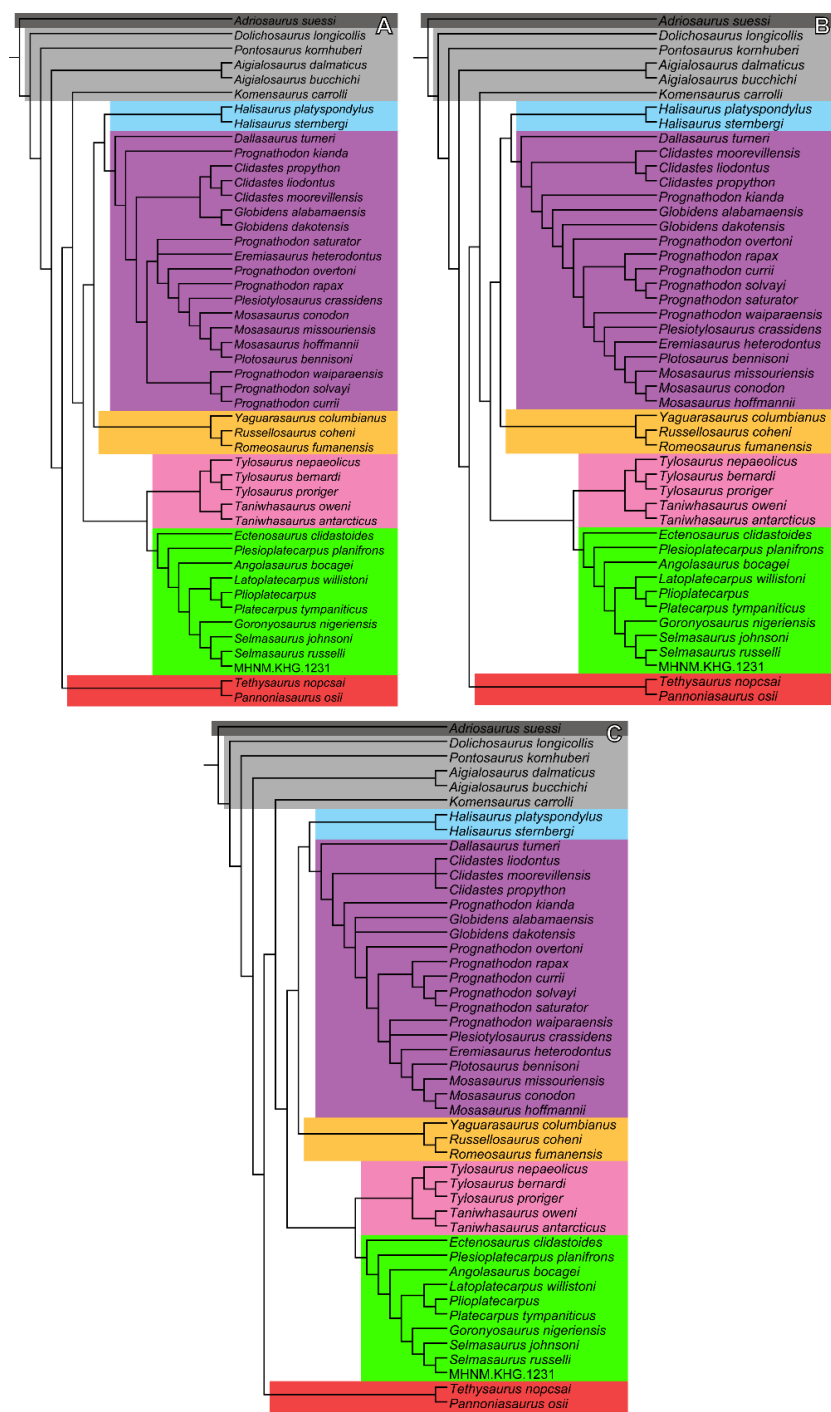


FIGURE S7. Trees produced via implied weighting maximum parsimony analysis of the dataset utilizing contingent character coding (Co-IWMP). (A) Strict consensus tree of the two most parsimonious trees (MPTs) (472 steps) produced when $k = 3.0$; (B) single MPT (468 steps) produced when $k = 7.0$; (C) strict consensus tree of the two MPTs (468 steps) produced when $k = 11.0$. Colouration of boxes as in Fig. S5.

S8. TOPOLOGY (EXTENDED)

As mentioned in the main text, all of the phylogenies recovered similar general topologies, with the major differences among them resulting from variation in resolution. Both of the implied weighting analyses produced the fewest and the best resolved MPTs, as expected due to their down-weighting of homoplastic characters. In contrast, the strict consensus trees in both the Mu-UMP (Fig. S5A) and Co-UMP (Fig. S6A) analyses exhibited extensive polytomies basally within the Mosasauridae. In the Mu-UMP strict consensus tree, this polytomy extended even more broadly into the Mosasauria (Dolichosauridae + Aigialosauridae + Mosasauridae), such that there was no clear distinction between these three constituent groups. In this sense, this analysis supports the findings of Simões *et al.* (2017b), in which the Mu-UMP strict consensus tree produced the least resolved topology of any of the analyses. The strict consensus trees both produced similar degrees of resolution at more internal nodes; for example, the Tylosaurinae, Yaguarasaurinae, Tethysaurinae, and Halisaurinae were fully resolved in both trees, whereas the Mosasaurinae and Plioplatecarpinae had much lower internal resolution.

Despite the aforementioned variation in resolution among the analyses, certain clades were recovered under all analytical conditions. The Tylosaurinae were consistently recovered as a clade in all of the analyses (Figs 7, S5–7), with the topology ((*Tylosaurus nepaeolicus* (*T. bernardi*, *T. proriger*))(*Taniwhasaurus oweni*, *Ta. antarcticus*)). The Tylosaurinae were also recovered as the sister group to the Plioplatecarpinae in all phylogenies, except for the unweighted strict consensus trees (Figs S5A, S6A), where lack of resolution collapsed this relationship.

The Mu-UMP and Co-UMP analyses both recovered a monophyletic Russellosaurina [*sensu* Polcyn & Bell (2005): Tylosaurinae + Plioplatecarpinae + the common ancestor of *Tethysaurus/Russellosaurus/Yaguarasaurus* and all of its descendants] in their respective majority rule consensus trees (Figs S5B, S6B), as did the Mu-UMP strict consensus tree (Fig. S5A) and the Mu-IWMP analyses (Fig. 7). The Co-UMP strict consensus tree (Fig. S6A) failed to recover this topology due to a basal polytomy, whereas the Co-IWMP analyses (Fig. S7) recovered the Yaguarasaurinae as sister to a clade containing the Halisaurinae and Mosasaurinae, and recovered the Tethysaurinae as the sister to all other mosasaurs and *Komensaurus carrolli* Caldwell & Palci, 2007. This recovery of a monophyletic Russellosaurina is consistent with the findings of Simões *et al.* (2017b), who recovered this clade in all of their parsimony-based

analyses.

The Yaguarasaurinae and Tethysaurinae were consistently recovered with the respective topologies (*Yaguarasaurus* (*Russellosaurus*, *Romeosaurus*)) and (*Tethysaurus*, *Pannoniasaurus*) (Figs 7, S5–7). These clades were in turn recovered as sister groups in the Mu-UMP majority rule consensus tree (Fig. S5B) and as successive outgroups to (Tylosaurinae + Plioplatecarpinae) in the Mu-IWMP trees (Fig. 7).

The Halisaurinae were also recovered as consistently monophyletic, though the placement of this clade varied (Figs 7, S5–7). In the multistate analyses (Figs 7, S5), the Halisaurinae formed the sister group to the Russellosaurina. In contrast, all contingent analyses recovered the Halisaurinae as sister to the monophyletic Mosasaurinae (Figs S6, S7). This varied placement of the Halisaurinae is a common occurrence in mosasaur phylogenies. For example, in the phylogenetic analyses of Simões *et al.* (2017b), the Mu-IWMP analysis recovered the Halisaurinae as sister to the Russellosaurina and the Co-UMP analysis recovered the Halisaurinae as sister to the Mosasaurinae, similar to the results reported herein. Several other studies have also reported contrasting placements of the Halisaurinae as associated with either the Russellosaurina (e.g., Bell & Polcyn 2005; LeBlanc *et al.* 2012; Grigoriev 2013; LeBlanc *et al.* 2019) or Mosasaurinae (e.g., Palci *et al.* 2013; Jiménez-Huidobro & Caldwell 2016).

In contrast to these more universal clades, other taxa were recovered less consistently. Though the Mosasaurinae were consistently recovered as monophyletic, the internal topology of this clade was quite variable, with particularly low internal resolution in the Co-UMP strict consensus tree (Fig. S6A). This internal topology was also the only major aspect of the trees to vary with different *k*-values in the implied weighting analyses (Figs 7, S7). The placement of *Prognathodon* spp. was particularly inconsistent, reflecting the likely non-monophyletic nature of this genus (LeBlanc *et al.* 2012; Palci *et al.* 2013; Simões *et al.* 2017b). The Globidensini – containing *Globidens*, *Plesiotylosaurus*, and *Prognathodon* – were universally recovered as paraphyletic, supporting the findings of LeBlanc *et al.* (2012). These authors also recovered a monophyletic Mosasaurini, consisting of (*Eremiasaurus* (*Mosasaurus*, *Plotosaurus*)). This clade was recovered in most of the analyses herein, except the IWMP analyses with a *k*-value of 3.0 (Figs 7A, S7A). When recovered, this clade exhibited the same topology as indicated by LeBlanc *et al.* (2012), with *Eremiasaurus* as the most basal member.

REFERENCES

- Bell, G. L. & Polcyn, M. J.** 2005. *Dallasaurus turneri*, a new primitive mosasauroid from the Middle Turonian of Texas and comments on the phylogeny of Mosasauridae (Squamata). *Netherlands Journal of Geosciences*, **84**(3), 177–194. doi:10.1017/S0016774600020965
- Caldwell, M. W.** 2007. Ontogeny, anatomy and attachment of the dentition in mosasaurs (Mosasauridae: Squamata). *Zoological Journal of the Linnean Society*, **149**, 687–700.
- Caldwell, M. W. & Palci, A.** 2007. A new basal mosasauroid from the Cenomanian (U. Cretaceous) of Slovenia with a review of mosasauroid phylogeny and evolution. *Journal of Vertebrate Paleontology*, **27**(4), 863–880. doi:10.1671/0272-4634(2007)27[863:ANBMFT]2.0.CO;2
- Grigoriev, D. V.** 2013. Redescription of *Prognathodon lutugini* (Squamata, Mosasauridae). *Proceedings of the Zoological Institute RAS*, **317**(3), 246–261.
- Jiménez-Huidobro, P. & Caldwell, M. W.** 2016. Reassessment and reassignment of the early Maastrichtian mosasaur *Hainosaurus bernardi* Dollo, 1885, to *Tylosaurus* Marsh, 1872. *Journal of Vertebrate Paleontology*, **36**(3), e1096275. doi:10.1080/02724634.2016.1096275
- Konishi, T.** 2008. A new specimen of *Selmasaurus* sp., cf. *S. russelli* (Mosasauridae: Plioplatecarpini) from Greene County, western Alabama, USA. Pp. 95–105. *Proceedings of the Second Mosasaur Meeting*. Hays, Kansas.
- Konishi, T. & Caldwell, M. W.** 2011. Two new plioplatecarpine (Squamata, Mosasauridae) genera from the Upper Cretaceous of North America, and a global phylogenetic analysis of plioplatecarpines. *Journal of Vertebrate Paleontology*, **31**(4), 754–783. doi:10.1080/02724634.2011.579023
- LeBlanc, A. R. H., Caldwell, M. W. & Bardet, N.** 2012. A new mosasaurine from the Maastrichtian (Upper Cretaceous) phosphates of Morocco and its implications for mosasaurine systematics. *Journal of Vertebrate Paleontology*, **32**(1), 82–104. doi:10.1080/02724634.2012.624145
- LeBlanc, A. R. H., Mohr, S. R. & Caldwell, M. W.** 2019. Insights into the anatomy and functional morphology of durophagous mosasaurines (Squamata: Mosasauridae) from a new species of *Globidens* from Morocco. *Zoological Journal of the Linnean Society*, **10**, 1–27. doi:10.1093/zoolinlean/zlz008/540165
- Palci, A., Caldwell, M. W. & Papazzoni, C. A.** 2013. A new genus and subfamily of mosasaurs from the Upper Cretaceous of northern Italy. *Journal of Vertebrate Paleontology*, **33**(3), 599–612. doi:10.1080/02724634.2013.731024
- Polcyn, M. J. & Bell, G. L.** 2005. *Russellosaurus coheni* n. gen., n. sp., a 92 million-year-old mosasaur from Texas (USA), and the definition of the parafamily Russellosaurina. *Netherlands Journal of Geosciences*, **84**(3), 321–333. doi:10.1017/S0016774600021107

Simões, T. R., Caldwell, M. W., Palci, A. & Nydam, R. L. 2017a. Giant taxon-character matrices: Quality of character constructions remains critical regardless of size. *Cladistics*, **33**, 198–219. doi:10.1111/cla.12163

Simões, T. R., Vernygora, O., Paparella, I., Jimenez-Huidobro, P. & Caldwell, M. W. 2017b. Mosasauroid phylogeny under multiple phylogenetic methods provides new insights on the evolution of aquatic adaptations in the group. *PLoS ONE*, **12**(5), e0176773. doi:10.1371/journal.pone.0176773